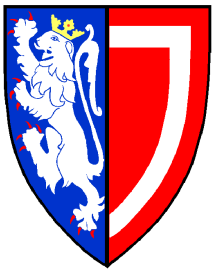
Intensity Modulated Proton Therapy in Lung Cancer



Suliana Teoh

Balliol College

University of Oxford

Supervisors:

Prof Frank Van den Heuvel

and

Prof Katherine A Vallis

A thesis submitted for the degree of

Doctor of Philosophy

Hilary 2020

Declaration

I, Suliana Teoh, declare that the work presented in this thesis is my own, unless stated otherwise, and is in accordance with the University of Oxford's regulations for the degree of Doctor of Philosophy.

February 2020

Acknowlegements

My sincerest thanks to my supervisors, Prof. Frank Van den Heuvel and Prof. Katherine A Vallis, for the guidance throughout the doctorate and encouragement to maintain high standards.

I thank all past and present members of Prof. Van den Heuvel's group for allowing me to learn from and work alongside them. I, especially thank Francesca Fiorini, who has become a very supportive friend and colleague.

Completing this doctorate has been one of the most challenging times of my life. I am grateful for the loving encouragement and understanding that my husband, Eugene, has provided over the past four years and especially in the last year. I thank our wonderful children- Nathanael, Naomi and Neave who have given me much joy. Also to Mummy and Daddy for their loving support throughout.

Finally, most importantly, I am grateful to God. It is only by His grace that I was able to see this dissertation to completion.

To him who is able to keep us from stumbling and to present us before His glorious presence without fault and with great joy, to the only God our Savior be glory, majesty, power and authority, through Jesus Christ our Lord, before all ages, now and forevermore!

Publications

Journal Articles

Proton vs photon: A model-based approach to patient selection for reduction of cardiac toxicity in locally advanced lung cancer

Radiotherapy and Oncology, August 2019 (in press)

S Teoh, F Fiorini, B George, KA Vallis, and F Van den Heuvel

Is an analytical dose engine sufficient for IMPT in lung cancer?

The British Journal of Radiology, 93(1107):20190583, 2020.

S Teoh, F Fiorini, B George, KA Vallis, and F Van den Heuvel

Assessment of robustness against setup uncertainties using probabilistic scenarios in lung cancer: a comparison of proton with photon therapy

The British Journal of Radiology, 93(1107):20190584, 2020.

S Teoh, B George, F Fiorini, KA Vallis, and F Van den Heuvel

Conference Proceedings

Robustness assessment using probabilistic scenarios of intensity modulated proton therapy and volumetric arc therapy in non-small-cell lung cancer: an in-silico radiotherapy planning study.
The Lancet, 389, Supplement 1:S94, 2017.
S Teoh, B George, F Fiorini, KA Vallis, F Van den Heuvel

Robustness assessment using probabilistic scenarios of IMPT and VMAT in SABR for NSCLC : an in-silico planning study.
S Teoh, B George, F Fiorini, KA Vallis, F Van den Heuvel
Poster presentation at PTCOG 56th Annual Conference, Japan, May 2017.

Comparison of IMPT plans robustness against VMAT in locally advanced non-small cell lung cancer against setup uncertainties and tumour motion
S Teoh, B George, F Fiorini, KA Vallis, F Van den Heuvel
Oral presentation at ESTRO Physics workshop, Glasgow, UK, Nov 2017.

P3.17-18 Towards Individualizing Patient Selection in Proton Therapy for Lung Cancer Using the Model-Based Approach
Journal of Thoracic Oncology, 2018; 13, Issue 10, S1027.
S Teoh, F Fiorini, B George, KA Vallis, F Van den Heuvel

EP-2062: Probabilistic scenarios for assessing setup uncertainty in VMAT and IMPT plans for lung cancer.
Radiotherapy and Oncology, 127:S1130, 2018.
S Teoh, F Fiorini, B George, KA Vallis, F Van den Heuvel

Sensitivity of intensity modulated proton therapy (IMPT) and volumetric modulated arc therapy (VMAT) plans to breathing motion in thoracic tumours

S Teoh, F Fiorini, B George, KA Vallis, F Van den Heuvel

Poster presentation at PTCOG 2018, Cincinnati, USA, May 2018

Ep-1931: Photon vs proton therapy for reduction of cardiac toxicities in locally advanced lung cancer.

Radiotherapy and Oncology, 133:S1051, 2019.

S Teoh, F Fiorini, B George, KA Vallis, F Van den Heuvel

Photon vs proton therapy for reduction of cardiac toxicity in locally advanced lung cancer using the model-based approach.

S Teoh, F Fiorini, B George, KA Vallis, F Van den Heuvel

Poster presentation at PTCOG 2019, Manchester, UK, June 2019.

An evaluation of radiotherapy plan sensitivity against breathing motion in lung cancer: intensity modulated proton therapy (IMPT) versus volumetric modulated arc therapy (VMAT).

S Teoh, F Fiorini, B George, KA Vallis, F Van den Heuvel

Oral presentation at ICCR 2019, Manchester, UK, Aug 2019.

Abstract

Proton beam therapy (PBT) has the potential to improve outcome in locally advanced non-small cell lung cancer (NSCLC). However, the technology associated with its delivery is still evolving. Treatment planning for PBT needs to account for various uncertainties to ensure accuracy of dose delivery. Multiple plan comparison studies have now shown that PBT is able to reduce dose to critical organs compared to photon therapy. However, dosimetric benefit does not necessarily translate to clinically meaningful outcome. The initial part of the thesis focused on the treatment planning aspect of intensity modulated proton therapy (IMPT) in conventionally fractionated radiotherapy for NSCLC. The subsequent parts that followed aimed at identifying patient groups where PBT is likely to be of highest clinical benefit. Therefore, the aims of this project were: [1] to evaluate and compare the robustness of IMPT and volumetric modulated arc therapy (VMAT) plans against setup uncertainties using the probabilistic scenarios method. [2] To evaluate the accuracy of the Raystation TPS analytical dose calculation (ADC) algorithm against Raystation Monte-Carlo (MC) algorithm. [3] To identify a sub-group of lung clinical cases where the Raystation TPS analytical algorithm may be clinically acceptable. [4] To identify a sub-group of patients who would benefit most from IMPT over VMAT with respect to cardiac sparing. The probabilistic analysis provides a fast and practical method for evaluating VMAT and IMPT plans sensitivity against setup uncertainty in locally advanced NSCLC. Although target robustness was achieved over the whole course

of treatment, fraction doses were sub-optimal when plans were optimised based on the planning target volume. However, fraction VMAT and robust-optimised IMPT doses were comparable. In the presence of mediastinal involvement and absence of range shifters use of the Raystation ADC may be clinically acceptable for treatment planning in lung IMPT. Otherwise, the MC algorithm would be recommended to ensure accuracy of treatment plans. Finally, using the model-based approach, patients with both pre-existing heart disease and disease overlapping with or inferior to T7 vertebrae are likely to benefit most from proton over photon therapy to reduce risk of cardiac toxicity.

Acronyms

ADC	Analytical dose calculation
Ave-CT	Average-intensity computed tomography
Adj	adjuvant
BED	Biologically effective dose
CI	confidence interval
CRT	concurent chemoradiotherapy
CT	Computed tomography
CTRG	Clinical Trials and Research Governance, University of Oxford
CTV	Clinical target volume
Dx%	Dose covering x% of structure's volume
DFS	Disease free survival
Dmax	Maximum dose to a structure
DIR	Deformable image registration
DTA	distance-to-agreement
DT	dose tolerance
DVH	Dose volume histogram
EBUS	endobronchial ultrasound
ECG	electrocardiogram
EUS	endoscopic ultrasound
GTV	Gross tumour volme
HR	Hazard ratio
HU	Hounsfield units
IASLC	The International Association for the Study of Lung Cancer
IMPT	Intensity modulated proton therapy
IMRT	Intensity modulated radiotherapy

ITV	Internal target volume
KV	Kilo voltage
LA	Left atrium
LC	Local control
LCA	Left coronary artery
LF	Local failure
LoA	Limits of agreement
LV	Left ventricle
MC	Monte Carlo
MC-MC	Plan with Monte Carlo optimisation and final dose calculation
MHD	Mean heart dose
MFO	Multi-field optimisation
MLD	Mean lung dose
MTD	Maximum tolerate dose
MM-IMPT	Mini-max Intensity modulated proton therapy
MV	mega voltage
NA	Neo-adjuvant
NHS	National Health Service
NR	Not reported
NSCLC	Non-small cell lung cancer
NTCP	Normal tissue complication probability
OAR	Organs at risk
OS	Overall survival
PB-PB	Plan with pencil beam optimisation and final dose calculation
PB-MC	Plan with pencil beam optimisation and Monte Carlo final dose calculation
PB-MC (s)	Plan with pencil beam optimisation and Monte Carlo final dose calculation scaled to prescribed dose

PBS	Pencil beam scanning
PBT	Proton beam therapy
PCE	Pericardial effusion
PCG	Proton Collaborative Group
PFS	Progression free survival
PET	Positron emission tomography
PFT	Pulmonary function test
PSPT	Passive scattering proton therapy
PBT	Proton beam therapy
PTV	Planning target volume
QALY	Quality of life years
QOL	Quality of life
RA	Right atrium
RBE	Relative biological effectiveness
RCA	Right coronary artery
RIHD	Radiation-induced heart disease
RV	Right ventricle
SABR	Stereotactic ablative body radiotherapy
SA node	Sino-atrial node
SBPT	Stereotactic body proton therapy
SFO	Single-field optimisation
SIB	Simultanous integrated boost
SPECT	Single-photon emission computed tomography
SVC	Superior vena cava
SCE	symptomatic cardiac event
TCIA	The cancer imaging archive
TNM	Tumour node metastasis

TPS	Treatment planning system
VxGy	Normalized volume of structure receiving xGy
VMAT	Volumetric arc therapy
3DCRT	3D conformal radiotherapy
4DCT	Four-dimensional computed tomography

Contents

1 Introduction **1**

1.1 Lung cancer . . . 3

1.1.1 Initial diagnosis and staging . . . 3

1.2 Early-stage NSCLC . . . 4

1.3 Locally advanced NSCLC . . . 8

1.3.1 Radiation-induced heart disease (RIHD) . . . 8

1.4 Proton beam therapy . . . 12

1.4.1 Technical challenges in proton beam therapy . . . 13

1.4.1.1 Range and set-up uncertainties . . . 13

1.4.1.2 Interplay effects . . . 14

1.4.1.3 Dose calculation engine . . . 15

1.4.1.4 Other technical challenges . . . 16

1.4.2 Model-based approach for estimation of toxicity . . . 17

1.4.3 PBT in early stage NSCLC . . . 18

1.4.4 PBT in locally advanced NSCLC . . . 18

1.4.4.1 Current proton clinical trial landscape . . . 20

1.5 Hypothesis . . . 21

1.6 Aims . . . 23

2 Materials and Methods **29**

2.1 In-silico comparison planning study 31
2.1.1 Assessment of robustness against setup uncertainties using probabilistic scenarios in lung cancer: a comparison of proton with photon therapy 34
2.1.1.1 Setup uncertainty 34
2.1.1.2 Tumour motion 39
2.1.1.3 Analysis 40
2.1.2 Is an analytical dose engine sufficient for IMPT in lung cancer? 40
2.1.2.1 Dosimetric evaluation 41
2.1.3 Statistical Analysis 42
2.1.4 Photon vs proton for reduction of cardiac toxicity in locally advanced lung cancer: the model based approach 43

3 Assessment of robustness against setup uncertainties using probabilistic scenarios in lung cancer: a comparison of proton with photon therapy 47

3.1 Abstract 49
3.2 Introduction 51
3.3 Results 54
3.3.1 Nominal plans 54
3.3.2 4D dose evaluation 54
3.3.3 Summed dose distributions 55
3.3.4 Fraction dose distributions 55
3.3.5 Simulation repeatability 58
3.4 Discussion 59

4 Is an analytical dose engine sufficient for IMPT in lung cancer? 71

4.1 Abstract 73

4.2 Introduction . . . 75
4.3 Results . . . 77
4.3.1 Patient and plan characteristics . . . 77
4.3.2 Dose to target . . . 78
4.3.3 Dose to OAR . . . 80
4.3.4 Predictors of high γ pass rates . . . 81
4.4 Discussion . . . 82

5 Proton vs photon: A model-based approach to patient selection for reduction of cardiac toxicity in locally advanced lung cancer 95
5.1 Abstract . . . 97
5.2 Introduction . . . 99
5.3 Results . . . 100
5.3.1 Heart dose . . . 100
5.3.2 Risk of toxicities . . . 103
5.4 Discussion . . . 105

6 Conclusions 117
6.1 Overview . . . 119
6.2 Treatment planning in PBT . . . 119
6.3 PBT to improve outcome in locally advanced NSCLC . . . 120
6.4 Future directions . . . 121

7 Appendix 123

References 129

List of Figures

1.1 Loco-regional staging pathway. 6

3.1 Summary of tumour motion, GTV and 4D dose plan robustness . . . 55
3.2 Summary of target coverage and adherence to OAR constraints . . . 56
3.3 Boxplots of all fraction CTV D98% and V95% 64
3.4 Dose volume histograms of a representative patient 65
3.5 Coronal views of dose colour maps of a nominal VMAT and IMPT plans from a representative patient 66
3.6 Coronal dose colour maps of patient 4 showing the nominal plan, summed and fraction dose distributions for a PTV-IMPT plan 67
3.7 Comparison of OARs dose metrics in VMAT and IMPT D_{sum} 69
3.8 Bland-Altman plots comparing CTV voxel dose between simulations . 70

4.1 Boxplots of CTV coverage 88
4.2 Axial dose colour map and DVH of PB-PB vs PB-MC plan of patient 14 91
4.3 Boxplots of γ analyses pass rates showing higher pass rates in plans with mediastinal involvement and absence of range shifter 92
4.4 Coronal dose colour map and DVH of PB-PB vs PB-MC plan of patient 2 94

5.1 Coronal view of disease location of cases included in study 102
5.2 Difference in dose to the heart between VMAT and IMPT according disease extension with reference to the thoracic vertebrae. 110

5.3 Difference in doses to OAR between VMAT and IMPT 111
5.4 Absolute doses to the heart and substructures 112
5.5 Relative risk reduction based on presence or absence of pre-existing heart disease and dose metrics 115
5.6 Risk of grade ≥3 cardiac toxicities based on MHD 116

List of Tables

1.1 TNM 8^{th} Edition for Lung Cancer 4

1.2 Lung cancer staging - 8^{th} edition 5

1.3 Lung cancer outcomes and cardiac doses studies 2009-2017 24

1.4 Summary of clinical experience in locally advanced lung cancer 25

1.5 RT planning and image-guidance strategies in identified studies . . . 26

1.6 Control and grade $\geq$3 toxicity rates in identified studies 27

1.7 Currently recruiting proton clinical trials 28

2.1 RTOG 1308 OAR dose constraints 33

2.2 Summary of beam arrangements and range shifter use for robustness evaluation (deg-degree, RS- range shifter in water equivalent thickness) 35

2.3 Summary of plan design 36

3.1 Tumour characteristics 54

3.2 Nominal plan and summed dose distribution dose metrics of patient 4). 58

3.3 Summary of Pearson correlation coefficient statistics of voxel-wise summed CTV dose 59

4.1 Summary of tumour characteristics, use of range shifter and γ analyses pass rates 77

4.2 CTV coverage of all plans with ADC compared to MC. 78

4.3 Absolute and relative difference in dose to target between PB-PB and PB-MC, and PB-MC scaled plans. 79
4.4 OAR doses with ADC compared to MC 89
4.5 Absolute difference in dose to OAR between PB-PB and PB-MC, and PB-MC scaled plans. 90
4.6 Univariate and multivariate analysis for γ pass rates with D20 and D99 dose at DT/DTA 3%/3mm 90
4.7 CTV coverage with ADC compared to MC stratified according to presence of predictors 93

5.1 Details of the twenty proxy cases 101
5.2 Summary of Spearman's correlation between heart dose and thoracic vertebrae level 103
5.3 Median dose indices of OAR for VMAT and IMPT plans to and below T7 vertebrae 104
5.4 Median dose indices of OAR for VMAT and IMPT plans above T7 vertebrae 113
5.5 Risk estimates of grade $\geq$3 cardiac toxicities 114

7.1 Comparison of mean heart dose stratified according to dose calculation algorithms 124
7.2 Comparison of maximum dose to the spinal cord stratified according to dose calculation algorithms 125
7.3 Comparison of mean lung dose stratified according to dose calculation algorithms 126
7.4 Comparison of lung V5 stratified according to dose calculation algorithms 127
7.5 Comparison of lung V20 stratified according to dose calculation algorithms 128

Chapter 1

Introduction

1.1 Lung cancer

Lung cancer is the leading cause of cancer-related deaths in the UK [1]. In 2016, there were around 36 000 lung cancer deaths in the UK. This accounted for over 20% of all cancer deaths. Non-small cell lung cancer (NSCLC) accounts for over 85% of cases. Unfortunately, despite advances in treatment techniques, outcome remains poor. In the UK, five- and ten-year survival is less than 15% and 5% respectively with little improvement in the last 4 decades [2].

1.1.1 Initial diagnosis and staging

In non-metastatic disease, the pathological diagnosis of lung cancer is usually obtained by forceps biopsy, bronchial brushing or washing during bronchoscopy [3]. Following this, locoregional staging is crucial to differentiate between early stage disease (stage I/II) from potentially resectable stage IIIA and unresectable stage III. Staging is performed according to the eighth tumour node metastasis (TNM) staging system [4]. This is done using imaging (computed tomography (CT) or positron emission tomography (PET)-CT), endoscopic and surgical techniques. In the absence of any evidence of mediastinal lymphadenopathy on PET-CT, patients generally proceed to surgery. Further investigations are required in patients with mediastinal lymph nodes to confirm disease in the form of endobronchial ultrasound (EBUS), endoscopic ultrasound (EUS) or mediastinoscopy. In the presence of N2/N3 disease or centrally located tumour, multimodality treatment is usually offerred. Figure 1.1 shows a schematic diagram of locoregional lymph node staging in patients with non-metastatic disease.

T_x	Tumour in sputum/bronchial washings but cannot be assessed on imaging or bronchoscopy
T_0	No evidence of tumour
T_{is}	Carcinoma-in-situ
T_1	**$\leq$ 3 cm surrounded by lung/visceral pleural, not involving main bronchus**
$T_{1a(mi)}$	Minimally invasive carcinoma
T_{1a}	$\leq$ 1 cm
T_{1b}	$>$ 1 cm $\leq$ 2 cm
T_{1c}	$>$ 2 cm $\leq$ 3 cm
T_2	**$>$ 3 cm $\leq$ 5 cm *or* involvement of the main bronchus without carina,*or* involvement of visceral pleural *or* atelactasis *or* post obstructive pneumonitis extending to hilum**
T_{2a}	$>$ 3 cm $\leq$ 4 cm
T_{2b}	$>$ 4 cm $\leq$ 5 cm
T_3	**$>$ 5 cm $\leq$ 7 cm *or* tumour of any size that involves chest wall, pericardium, phrenic nerve or satellite nodules in the same lobe**
T_4	**$>$ 7 cm *or* tumour invasion into any of the following: diaphragm, mediastinum, heart, great vessels, trachea, recurrent laryngeal nerve, oesophagus, vertebral body, carina; *or* separate tumour nodule(s) in a different ipsilateral lobe to the primary**
N_1	**Ipsilateral peribronchial and/or hilar nodes and intrapulmonary nodes**
N_2	**Ipsilateral mediastinal and/or subcarinal nodes**
N_3	**Contralateral mediastinal or hilar; ipsilateral / contralateral scalene / supraclavicular**
M_1	**Distant metastasis**
M_{1a}	Tumour in contralateral lung or pleural/pericardial nodule/malignant effusion
M_{1b}	Single extrathoracic metastasis, including single non-regional lymph node
M_{1b}	Multiple extrathoracic metastasis, in one or more organs

Table 1.1: TNM 8^{th} Edition for Lung Cancer

1.2 Early-stage NSCLC

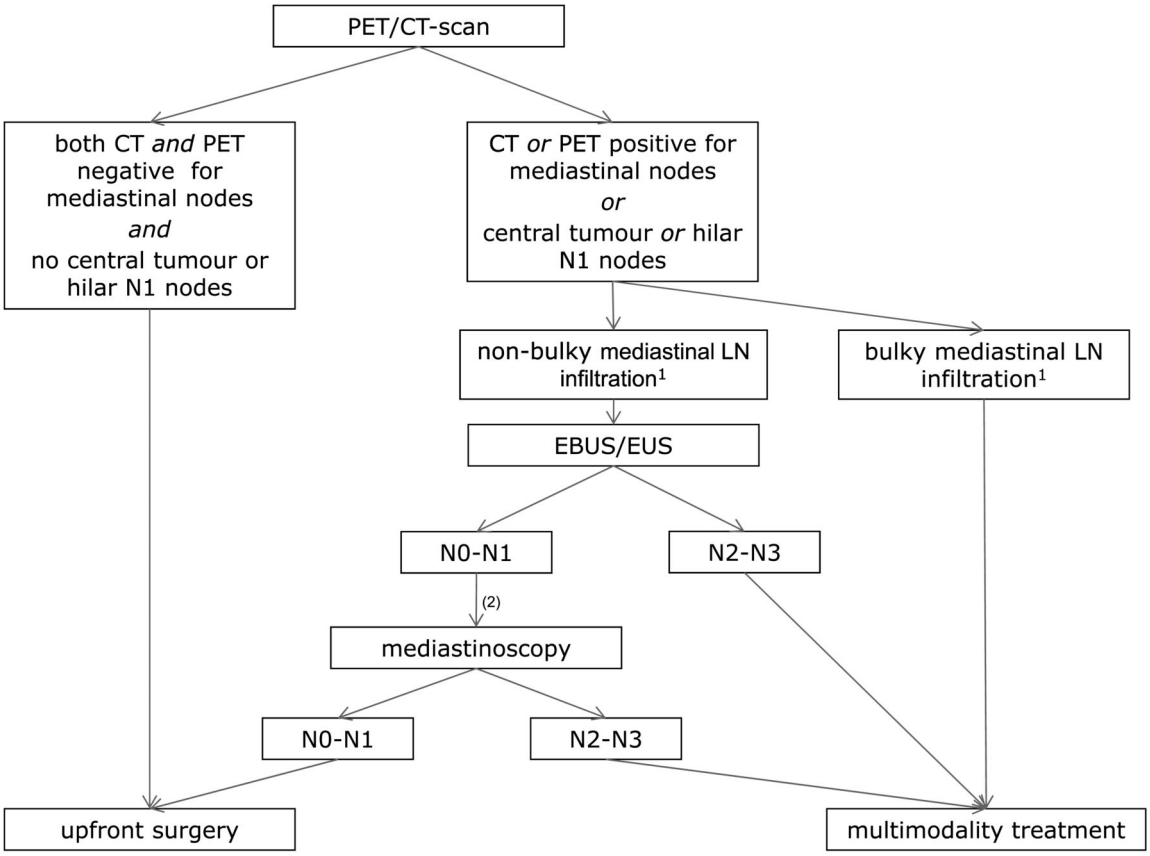
In patients with early-stage lung cancer, 5-year survival for NSCLC can be as high as 80% [5]. The current standard of treatment is surgical resection. However, approximately 20% of patients with Stage I disease are medically inoperable due to co-morbidities [6]. Stereotactic ablative body radiotherapy (SABR) allows for dose escalation with local control rates of more than 90% and minimal toxicity [5]. With image-guided radiotherapy (IGRT) and 4DCT, precise delivery of a high biological dose is possible.

T/M	Subcategory	N_0	N_1	N_2	N_3
T_1	T_{1a}	IA1	IIB	IIIA	IIIB
	T_{1b}	IA2	IIB	IIIA	IIIB
	T_{1c}	IA3	IIB	IIIA	IIIB
T_2	T_{2a}	IB	IIB	IIIA	IIIB
	T_{2b}	IIA	IIB	IIIA	IIIB
T_3	T_3	IIB	IIIA	IIIB	IIIC
T_4	T_4	IIIA	IIIA	IIIB	IIIC
M_1	M_{1a}	IVA	IVA	IVA	IVA
	M_{1b}	IVA	IVA	IVA	IVA
	M_{1c}	IVB	IVB	IVB	IVB

Table 1.2: Lung cancer staging - 8^{th} edition

These excellent results are mainly derived from small peripherally located thoracic lesions, whereby the tumours are mainly surrounded by lung tissue. The potential toxicities of SABR in centrally located NSCLC have been recognised for more than a decade now [7]. SABR for central lung tumours could lead to severe, life-threatening and lethal radiation-induced toxicity due to the proximity of OAR such as the main airways and vessels, heart, oesophagus and brachial plexus. A phase II study by Timmerman et al. of 70 patients treated with 60-66 Gy in 3 fractions (54 Gy in 3 fractions with heterogeneity correction, BED α/β_{10} = 151 Gy, α/β_3 = 378 Gy) showed a 2-year freedom from severe toxicity of 54% in patients with central tumours, compared to 83% with peripheral lung tumours [7]. There were 6 deaths: 1 fatal haemoptysis, 4 with infectious pneumonia and 1 with complications from pericardial effusion. Patients with central tumours were 11 times more likely to experience grade 3-5 adverse events compared to peripheral tumours (p=0.004). The incidence of grade 3+ toxicities were 17% and 46% in peripheral and central tumours respectively. Since then, there have been other studies confirming higher toxicities in centrally located tumours [8, 9].

Given this understanding, various dose-fractionations have been tested and more acceptable toxicity rates have been observed with gentler dose-fractionation. There is also improved understanding that even within centrally located tumours, some



[1] Category description according to CT (and PET) imaging as in ACCP staging document [Chest 143 Suppl 5:211S-250S, 2013], see text for more details.
[2] A negative result of EBUS/EUS is usually confirmed by mediastinoscopy, as the latter has the highest negative predictive value.

Figure 1.1: Loco-regional staging pathway. (adapted from De Leyn P, Lardinois D, Van Schil PE, et al. ESTS guidelines for preoperative lymph node staging for non-small cell lung cancer. Eur J Cardiothorac Surg 2007; 32(1): 1–8. By permission of Oxford University Press for the European Association for Cardio-Thoracic Surgery).

locations are at higher risk compared to others - the highest risk being those tumours touching the proximal bronchial tree [10]. Recently, the landmark RTOG 0813 Phase I/II dose-escalation study published its result [11]. The primary objective of the study was to investigate the MTD of a 5-fractions SABR protocol for centrally located stage I NSCLC tumours. The trial included patients with 'ultra-central' tumours - immediately adjacent to the trachea, bronchus, oesophagus and heart. At the highest dose level (60 Gy in 5 fractions), the risk of dose limiting toxicity was 7.2% with local control of 87.9% (median follow-up 38 months).

On the other hand in Europe, the EORTC Phase II LungTech trial has recently

reported its initial results in abstract form [12]. The trial investigated the safety of delivering a medium hypofractionated dose of 60 Gy in 8 fractions (BED $\alpha/\beta_{10} = 105$ Gy, $\alpha/\beta_3 = 210$ Gy). The trial excluded patients with very central tumours, such as those directly adjacent to the proximal bronchial tree or oesophagus, as the proximity of the tumour would not allow planning without exceeding dose constraints. Initial results from the trial reported two potentially treatment-related deaths out of 39 patients. The investigators concluded that safety of SBRT in centrally located lung tumours remained unclear.

The HILUS trial, a phase II study of SBRT in centrally located lung tumours has also reported its results in abstract form [13]. Patients were prescribed a dose of 56 Gy in 8 fractions to 65-70% isodose line. Patients with centrally located tumour, defined as within 1 cm of the proximal bronchial tree, were eligible. Grade 5 toxicity rates of 9% (7/74). Most of these occurred when the target was close to a mainstem bronchus as supposed to a lobar bronchus (grade 5 toxicity rate 14% vs 3%). Another trial that is currently recruiting is the SUNSET trial (Stereotactic Radiation for Ultra-central Non-Small-Cell Lung Cancer — A Safety and Efficacy Trial - NCT03306680). It is a phase I trial with a starting dose of 60 Gy in 8 fractions.

There are a number of theoretical benefits of stereotactic proton beam therapy (SBPT). Similar to the case in locally advanced NSCLC, multiple planning studies have shown that proton beam therapy is able to reduce dose to OAR [14, 15]. The benefit was reportedly more apparent in patients with central and larger tumours. Register et al. conducted a virtual planning study comparing photon SABR versus SBPT with PSPT and IMPT and found that only 6 of 15 photon plans satisfied the PTV coverage and OAR constraints, compared to 12 with PSPT and 14 with IMPT [16].

1.3 Locally advanced NSCLC

Radiotherapy forms an essential component of the treatment of patients with inoperable disease. Dose escalation from 40 to 60 Gy has been showed to reduce in-field failure rate from 58% to 35% [17]. Similarly, an analysis of 11 RTOG trials showed higher radiotherapy doses up to 69.6 Gy (BED $\alpha/\beta_{10} = 78$ Gy, $\alpha/\beta_3 = 97$ Gy) improved survival and local-regional control [18]. Current standard-of-care of patients with inoperable locally advanced lung cancer is concurrent chemoradiotherapy to a radiotherapy dose of at least 60 Gy in 2 Gy fractions [3]. Concurrent chemoradiotherapy appears to confer better local-regional control and consequently overall survival at the cost of increased reversible oesophagitis [19].

However, further efforts to improve outcome through dose escalation have been unsuccessful. The phase III RTOG 0617 compared the use of 60 Gy versus 74 Gy using photon with concurrent chemotherapy [20]. Disappointingly, the 74 Gy arm of the trial were closed early following a planned interim analysis. Higher treatment-related mortality was observed in the high-dose arm (at median follow-up 22.9 months, median overall survival (OS) 60 Gy vs 74 Gy arms: 28.7 vs 20.3 months). On secondary analysis, it was reported that dose delivered to the heart was an independent predictor of survival, in particular heart V5 and V30.

1.3.1 Radiation-induced heart disease (RIHD)

The association between radiation and cardiac toxicity is well established following radiotherapy for breast cancer and lymphoma [21, 22]. In a landmark study, Darby et al. showed that for every Gray of mean heart dose (MHD), there was 7.4% increase in major cardiac events (i.e. myocardial infarctions, coronary revascularization or death from ischaemic heart disease), without apparent threshold in irradiated breast cancer patients [21]. However, in both lymphoma and breast cancer patients, because of

lower doses of radiation, clinical presentations normally do not occur for many years.

In lung cancer, concerns of RIHD emerged since the publication of RTOG 0617 trial where excess mortality was associated with heart irradiation within the first years of radiotherapy [20]. The survival curves showed an absolute decline of approximately 10% in survival within the first year after radiotherapy for patients treated in the high-dose arm. On multivariable analysis of the RTOG 0617 trial, higher radiation dose to the heart (heart V5 and V30) was independently associated with worse survival [20]. A subsequent secondary analysis of RTOG 0617 found heart V40 was most associated with overall survival (HR 1.01/%) [23]. Multiple retrospective studies have also confirmed the association with high dose to the heart and reduction in overall survival [24]. Unfortunately, the data is heterogenous and mostly derived from retrospective single-institution series. Nevertheless, many showed an association between heart dose and overall survival and cardiac events. These include studies from William Beaumont (Detroit, MI) and Washington University (St. Louis, MO) which identified associations between overall survival and heart V30 and V50 respectively [25, 26].

It is also apparent that pre-existing risk factors for heart disease is an independent factor associated with RIHD. In a retrospective study by Dess et al., the association between cardiac events and radiation dose to the heart was evaluated in four prospective radiotherapy trials in NSCLC. They showed that pre-exisiting cardiac disease and higher heart dose were significantly associated with grade $\geq$3 cardiac events, with 10% and 15% risk of grade $\geq$3 cardiac events reported with MHD of 5 and 12 Gy respectively [27]. They reported a relative increase in grade 3-5 cardiac toxicity of 7% per Gy MHD. Similar findings were reported by Wang et al, showing that whole heart and left ventricle doses, and baseline cardiac risk were independently associated with symptomatic cardiac events [28]. Overall, 23% of patients experienced symptomatic cardiac events at a median of 26 months with the most common complication be-

ing arrhythmia (11%). In their cohort of patients, there was 21% risk of cardiac complication when the MHD exceeded 20 Gy.

One study by Tembhekar et al., found no clear association between cardiac dose and overall survival or symptomatic cardiac events. However, the number of patients included in the study was relatively small and correlation with cardiac substructures were not done [29]. Furthermore, most of the patients included in the study had significant co-morbidities. As such, competing causes of death may have obscured the survival effect.

As it is not usually possible to avoid the whole heart during radiotherapy for locally advanced lung cancer, understanding the mechanism of damage would be important. At present the exact pathophysiology of early cardiac toxicity is unknown but likely to be multifactorial. RIHD usually manifests itself pathologically as coronary artery disease (CAD), pericarditis, pericardial fibrosis, myocardial fibrosis, valvular disease and arrhythmia [30, 31]. Furthermore, the optimal dose constraint and location of dose-sensitive regions within the heart is currently unclear. Wang et al., investigated the pathophysiology of RIHD in lung cancer patients by correlating dose to multiple cardiac sub-volumes against three cardiac events (pericardial, ischaemia and arrhythmia [31]. They observed pericardial events were correlated with global heart, right and left atria doses but not left ventricular dose. The following dosimetric parameters had the strongest associations with pericardial events: left atrium (LA) V30 (p=0.001, HR 1.03/%), LA mean (p=0.002, HR 1.04/Gy), Heart V60 (p=0.004, HR 1.04/%), and right atrium (RA) V60 (p=0.005, HR 1.02/%. On the other hand, ischaemic events were correlated with left ventricular (LV) (LV V5 p=0.008, HR 1.03/%, LV V30 p=0.012, HR 1.03/%, LV mean (p-0.014, HR 1.05/Gy) and whole heart dose (heart V5, p=0.014, HR 1.03/%). The dosimetric parameters with the strongest associations with arrhythmia were heart V5 (p=0.042, HR 1.02/%) and right atrium V60 (p=0.047, HR 1.02/%).

In a post-hoc analysis of prospective data from IDEAL-CRT trial [32], Vivekanandan et al., reported an association between increased death rate and left atrial wall irradiation to ≥ 63 Gy [33]. They used a dose volume histogram-wide analysis approach based on principal component analysis. Based on 53 patients (out of 78 patients), they also found 38% had ECG changes at 6 months following radiotherapy. On the other hand, McWilliam et al, found that radiation dose as low as 8.5 Gy (using conventional fractionation) to the base of the heart was associated with excess mortality in lung cancer patients (HR 1.25, 95% CI 1.01-1.56) [34]. They evaluated a total of 1190 lung cancer patients treated at the Christie Hospital, Manchester between 2010 and 2013 to a dose of 55 Gy in 20 fractions (N=1101) and a validation cohort of SBRT patients treated to 60 Gy in 5 fractions (N=89). The heart was segmented using deformable registration and was validated against 386 cases previously contoured by the treating oncologist. Difference in mean dose distributions for patients who survived against those who died between 3-36 months from the end of treatment was calculated. The area of the heart with the highest statistically significant difference was found to correspond to the region where the atria, origins of coronary arteries, sinoatrial node, and proximal superior vena cava, aorta and pulmonary vessels were.

In summary, current evidence seems to suggest that high dose to a small volume and low dose to a large volume of heart are important in causing RIHD. Anatomically, doses to the base of the heart and left ventricle have been associated with survival. The mechanism of disease is likely to be different depending on the cardiac substructure exposed.

A summary of studies reporting dose-toxicity relationship in lung cancer published from 2008-2017 can be found in Table 1.6.

1.4 Proton beam therapy

Proton beam therapy (PBT), through the characteristic Bragg peak, holds the promise of improving cure without increasing treatment-related toxicity in patients with lung cancer. The physical characteristic of proton beam is such that dose deposition is highly localised at the distal edge of the Bragg peak [41]. The finite range of proton beam means that there is an integral dose reduction to surrounding normal tissue.

Broadly, there are 2 main methods of delivering PBT; one is through the use of passive scattering (passive scattering proton therapy, PSPT) and the other pencil beam scanning (PBS). In PSPT, a broad beam is scattered to create a spread-out Bragg peak. Patient-specific collimators and compensators are used to produce a conformal treatment beam. The compensator would shape the distal edge of the beam, whilst the collimators would conform the dose orthogonal to the beam direction. PBS on the other hand uses magnets to scan a mono-energetic proton beam across the target volume [42]. The depth of the scan is adjusted by varying the energy of the beam. This method does not require compensators or collimators. PBS allows for the delivery of intensity modulated proton therapy (IMPT), which is analogous to intensity modulated radiotherapy (IMRT). A further advantage of IMPT is the ability to vary the energy of each pencil beam. The result is that IMPT is able to deliver a highly conformal dose distribution with steeper dose gradient and a lower integral dose compared to PSPT. IMPT can be delivered in 2 ways: each field can be optimised individually, single-field optimisation (SFO) or, in combination, multi-field optimisation (MFO). Both methods require inverse planning to optimise the spot placements and intensity of the beams.

1.4.1 Technical challenges in proton beam therapy

1.4.1.1 Range and set-up uncertainties

The distinctive attribute of PBT, which allows for precision in dose delivery, also means that it is more sensitive to errors pertaining to changes in density of the material the beam traverses through and motion. Hence, accurate placement of the most distal edge of the Bragg peak is important in order not to underdose the target volume or overdose an OAR. The main sources of error in proton therapy are range and setup uncertainties. Range uncertainty may arise from the conversion from Hounsfield units (HU) to stopping power and inaccuracies arising from CT imaging [43]. Setup uncertainties arise from systematic and random errors in patient positioning as well as mechanical inaccuracies in the delivery unit.

Conventionally, these errors are accounted for by adding a margin to the treatment volume to produce a planning target volume (PTV) [44]. Such a method is inadequate in PBT as it does not take into account changes in density along the beam path, of which protons are highly dependent upon, resulting in a distorted dose distribution. This situation is particularly worse in IMPT whereby non-uniform fields are used to produce the desired dose distribution. Despite this, many comparative studies between proton and photons have used the same CTV and PTV margin for both modalities. In PSPT, Moyers et al. suggested a method to incorporate motion and set-up uncertainties, with the use of beam-specific distal and proximal margin [45]. A similar approach can be applied to SFO IMPT [46]. However, the same concept cannot be applied in MFO IMPT due to the non-uniform fields produced. Margins could improve target coverage at the edges of the target volume but not within the target itself. Unfortunately, they have little effect on the robustness of a plan where steep dose gradients exist within the clinical target volume (CTV) [47].

Recently, robust optimisation techniques have been developed to take into account

setup and range uncertainty within the IMPT optimisation algorithm. Using this method, a planning target volume (PTV) is not generated. Unkelbach et al. suggested two methods in solving this issue; one is a probabilistic approach whereby a prior knowledge of the probability distribution of the uncertainty is assumed [48]. In the probabilistic approach, the plan is optimised based on the likelihood of how likely each and every scenario is likely to occur. The second is a worst-case distribution approach, which optimises based only on the worst case that could occur. In both cases, in order to account for the uncertainties, there is an expansion of the high dose region and the distal dose gradient is smoothed.

Most methods for assessing plan robustness against uncertainties are based on the worst case scenarios [43, 47, 49]. However, such methods may be overly pessimistic in predicting robustness of a plan and most of them only take into account a single fraction of treatment. Furthermore, it relies on the assumption that by modelling a small number of worst case error scenarios, the maximum error dose distributions could be predicted. Unfortunately, in areas of high tissue heterogeneity, such assumption tends to breaks down [50].

1.4.1.2 Interplay effects

For the treatment of lung cancer with dynamic scanned proton beam, tumour motion adds a further dimension to the complexity of treatment. As tumour motion occurs on a similar time scale as spot scanning, the interplay effect could potentially cause large deviations between planned and delivered dose. The margin solution for compensating intrafractional organ motion is again inadequate. Various strategies have been suggested to mitigate the interplay effect such as volumetric and layer repainting and fractionation [51, 52]. Other methods of motion management include deep inspiration breath hold, tracking and gated delivery [53].

1.4.1.3 Dose calculation engine

The simplified analytical dose calculation algorithm (ADC) known as the pencil beam algorithm is currently used in most proton therapy centres around the world. It has the advantage of being fast, but its accuracy is questionable in highly heterogenous tissue [54, 55]. It uses a double Gaussian approach to model the lateral scattering of a proton beam [56]. The lateral distribution is mainly caused by multiple Coulomb scattering of protons which is represented by the first Gaussian and forms the central component of the beam. The second Gaussian, represents the low-dose, large angle component caused by inelastic nuclear scattering, also referred to as 'nuclear halo' [57]. This simplified lateral scattering algorithm in the TPS does not characterise the 'nuclear halo' well [58, 59]. In many clinical sites such as head and neck and breast, oblique beams with range shifters are used to spare OAR. The PB analytical algorithm is unable to accurately model obliquity. At oblique angle incidence, protons will travel through different thickness of material within each pencil beam. Pencil beam algorithms are mostly based on the so-called infinite slab approximation which assumes a constant thickness of material at the central axis of the pencil beam. This limitation has been observed to result in over- and under-estimation of dose in the following situations: presence of tissue heterogeneity, range shifters, large air gaps, and small fields [60].

Monte Carlo (MC) dose calculation algorithm simulates transfer of particle through materials by random sampling of the various interactions. Provided that the physics process modelling is accurate and there is adequate number of particles simulated, MC should provide a more accurate dose estimation. Therefore, MC is be useful in verifying the accuracy of the TPS analytical dose calculation algorithm [61, 62]. The main disadvantage of MC simulations is its speed and complexity to implement. However, fast treatment planning system (TPS)-based MC algorithms have recently become available commercially. Compared to the general-purposed MC, not all phys-

ical interactions are considered [63]. It has been specifically optimised for speed but at the same time maintaining sufficient accuracy to the relevant physics processes.

For lung cancer IMPT, tissue heterogeneity is inherent and use of range shifters are commonplace for optimal conformality and target coverage as well as sparing of OAR. A few studies have recently highlighted the difference between analytical and MC algorithms [64, 65, 66]. In a comparison between the PB dose distribution and MC in lung, Taylor et al. found an average overestimation of 7% (up to 46%) with PB dose calculations [65]. Doses delivered to heterogenous anthropomorphic lung phantoms were compared against doses calculated in the treatment plans. There was better agreement between lung phantom measurements with MC (mean 4%, maximum difference 12%). Saini et al, validated the Raystation PB and MC code against GATE MC code. With a range shifter and >30 cm air gap a difference of up to 10% in dose at the entrance for the beam was observed. Similar findings were reported by Liang et al in breast cancer, where a mean overestimation of $\sim 4\%$ was reported compared to MC-recalculated doses [66].

1.4.1.4 Other technical challenges

Unfortunately, implementation of on-board volumetric imaging in proton therapy lags behind the photon therapy world. Hence, most proton beam therapy facilities worldwide still rely on orthogonal imaging for setup verification (see Table 1.5). Due to this, the risk of poor target coverage secondary to daily tumour positioning uncertainty is higher in proton therapy. This could potentially impact tumour control probability. In the era of IGRT, this presents a challenge, as it may obscure the advantages of PBT especially in head-to-head comparison.

1.4.2 Model-based approach for estimation of toxicity

Poor local control rates following radical radiotherapy indicate that the current radiation dose is insufficient to eradicate the tumour. Yet, RTOG 0617 suggests that dose escalation may in fact be harmful due to excess dose to the OAR in particular the heart [20]. Dosimetrically, proton beam therapy has the potential to improve the therapeutic index of radiotherapy treatment in locally advanced NSCLC over photon therapy. There are two main methods where the physical properties of proton beams could be expected to result in clinical benefit in lung cancer- improvement in local tumour control and reduction of radiation-induced toxicities. Multiple comparison planning studies have shown better sparing of OAR, in particular to the lungs, spinal cord, oesophagus and heart, with proton beam therapy compared to photon therapy [67, 68, 69]. Zhang et al. compared IMPT with PSPT and IMRT and showed that at the same prescription dose, IMPT was able to spare more OAR while allowing for dose escalation up to 83.5 Gy relative biological effectiveness (RBE) [67].

PBT is a promising technology that could improve outcome in these patients by reducing radiation induced toxicity compared to photon therapy. However, patient selection is key in exploiting this technology. PBT is unlikely to improve outcome in cases where doses to the normal tissue and target are similar in both treatment modalities. Furthermore, even when dosimetric advantages are observed [70, 71, 72, 73], these do not necessarily translate into clinically meaningful benefit as observed in the recently published randomised-control trial in lung cancer [74]. Patient-, disease- and treatment-related factors play a role in determining the outcome.

Model-based patient selection is one method of inferring which sub-group of patients would receive the largest gain from PBT [75]. The model-based approach relies on the availability of a normal tissue complication probability (NTCP) model. A comparative study is then performed between photon and proton therapy to allow for

the potential benefit of proton therapy to be predicted based on the model. Nevertheless, choosing the appropriate model is crucial. Most NTCP models rely only on dose parameters alone in estimating complication probabilities [76]. Unfortunately, the predictive power of these models is limited [77]. Incorporating patient risk factors into these models has been shown to improve their performance [78, 77].

1.4.3 PBT in early stage NSCLC

Use of PBT in lung cancer is relatively new. Current clinical experience with PBT in NSCLC is mainly limited to using PSPT. Clinically, Loma Linda University has the longest experience with the use of SBPT in early stage NSCLC. Bush et al. reported outcomes of 111 patients (33 patients had centrally located tumours) with biopsy-proven T1 and T2 NSCLC treated with PSPT with doses from 50 to 70Gy RBE in 10 fractions [79]. Patients were either medically inoperable or refused surgery. Local control at 4 years for T1 tumours was 96%. There were no cases of radiation pneumonitis. No increased toxicities were observed in patients with centrally located tumours. Similarly Hata et al. reported good outcomes on 21 patients treated with PSPT (doses from 50 to 60Gy RBE in 10 fractions) [80]. Only one local recurrence was reported at 2 years (95% local control).

1.4.4 PBT in locally advanced NSCLC

Generally, PBT in locally advanced lung cancer was well tolerated. Data from phase I/II studies reported median overall survival (OS) and local relapse rates of between 26.7 - 33 months and 20.5 - 40% respectively (see Table 1.4. Although, these are studies with small number of patients, reassuringly, this is comparable to the OS of patients in RTOG 0617 of 28.7 months[20]. The only randomised control trial in lung cancer between PSPT and IMRT reported similar median survival of 26.1 months

in the PSPT arm vs 29.5 months in the IMRT arm (p= 0.297) [74]. Recently, the PACIFIC trial demonstrated the benefit of adjuvant PD-L1 inhibitor, durvalumab [81]. Planned interim analysis showed a significant improvement in both median and 18-month PFS rate in the durvalumab arm compared to placebo (16.8 months (95% CI: 13.0–18.1) versus 5.6 months (95% CI: 4.6–7.8), and 44.2% (95% CI: 37.7–50.5%) versus 27% (95% CI: 19.9–34.5%) respectively). However, the control arm had poorer than expected outcomes with a median PFS of only 5.6 months for stage III NSCLC following concurrent chemoradiotherapy. The result of this landmark trial made the addition of adjuvant durvalumab the new standard-of-care following radical chemoradiation. It remains to be seen how the immunogenic effects of PBT may enhance response to immunotherapy. Table 1.4 summarises current PBT clinical experience in locally advanced lung cancer published since 2010.

Unfortunately, there are a number of limitations in the current published data. There is limited data on the use of PBS in lung cancer. Most clinical studies were in the setting of a single arm phase 2 or retrospective studies. Furthermore, where photon comparison was performed, the photon radiotherapy was delivered mainly using 3D-CRT or IMRT and not VMAT. Only one randomised control study has been carried out comparing IMRT versus PSPT in locally advanced NSCLC (up to 74 Gy (RBE)) [74] where a total of 147 patients were randomised (IMRT- 90, PSPT–57). The primary endpoint of the trial was grade $\geq$3 radiation pneumonitis and local failure. The trial reported considerable fewer adverse events compared to historical experience in both arms. However, there was no significant difference in the rate of grade 3 pneumonitis or local failure between IMRT and PSPT. Despite this, it should be noted that comparison between IMRT and PSPT, which is a 3D conformal therapy as opposed to IMPT, may not be reasonable. Furthermore, a learning curve was observed in the quality of proton plans of patients enrolled in the trial. During the course of the trial, improvements in the primary endpoints of pneumonitis and

local failure were observed, in particular for the proton arm.

Other limitations of the current published literature include heterogeneity of the patient group with regards to staging, chemotherapy used and dose/fractionation. In terms of radiotherapy planning, most published data reported use of 4DCT for treatment planning with some centres using gated delivery for motion management. As discussed above, unfortunately on-board CBCT was not available until recently. Therefore, not surprisingly, none of the publications reported the use of CBCT at iso-centre. Either 2D image guidance or none were used for online set-up.

1.4.4.1 Current proton clinical trial landscape

There are currently 6 proton clinical trials registered in clinicaltrials.gov website in the treatment of stage II/III NSCLC lung cancer. Details of trials currently recruiting in the primary chemoradiotherapy setting can be found in Table 1.7. There are 3 dose escalation studies (NCT01629498, NCT03132532 and NCT01770418) looking at maximum tolerated dose. A German trial looking at toxicities randomising between photon and proton with Grade ≥ 2 pneumonitis and oesophagitis as primary objectives (NCT02731001). The largest trial currently open is a phase III RTOG 1308 trial (NCT01993810) which randomises between proton and photon. Its primary objective is overall survival. Finally, there is another trial that is currently recruiting in USA within the setting of recurrence disease and consolidation with Pembrolizumab following concurrent chemotherapy (NCT03087760).

1.5 Hypothesis

PBT has the potential to improve the therapeutic ratio of radiation therapy by reducing radiation exposure of normal tissue. This could lead to reduction in toxicity rates as well as allow for dose escalation to the target. However, there are a number of issues with clinical utilisation of SBPT. Firstly, as discussed above, very good local control with low toxicity rates is currently achieved with photon SBRT for patients with small peripheral lung tumours [5]. This therefore means that there is limited room for PBT to improve outcome in this group of patients. Due to the characteristic of the Bragg peak, the main advantage of PBT is the reduction of the medium to low dose bath. However, as previously mentioned, this very characteristic means that a PBT plan is more prone to dose perturbations due to various uncertainties. Although planning studies have highlighted that SBPT is likely to be advantageous in larger or centrally located tumours, assessment of plan robustness were not performed in these studies [14, 15, 16]. As plan robustness need to be accounted for, it would be anticipated that the high dose volume is likely to be similar if not higher in PBT compared to IMRT/VMAT. Therefore, in centrally located tumours, where the optimum dose-fractionation is unclear and toxicity is associated with the maximum dose constraints, it would be a challenge for PSPT/IMPT to achieve better dose distribution compared to IMRT/VMAT. In addition to this is the issue of higher RBE at the distal edge of the Bragg peak [94]. Although clinically, centres worldwide work on the assumption of an average RBE of 1.1, this potentially poses an additional risk especially when the tumour is abutting central structures. Finally, in hypofractionated treatments, plan robustness is all the more crucial as any random errors associated with various uncertainties (whether to do with setup errors, anatomical changes, interplay effect, etc) would be amplified.

With these issues in mind, the focus of this thesis would be to explore the use

of IMPT in locally advanced NSCLC where despite improvements in technology over the past few decades, survival of these patients remain poor. Radiotherapy forms the backbone of radical treatment in these patients. Unfortunately, efforts in improving outcome through dose-escalation has been unsuccessful. In fact, dose-escalation appears to be detrimental and reduces survival [20] Due to the sharp dose fall-off, PBT may have the potential to improve outcome in locally advanced lung cancer through reduction of OAR toxicity as well as dose escalation. A number of in-silico planning studies have shown dosimetric advantages when compared to photon therapy [70, 71, 72, 73]. However, multiple technical challenges exist in delivering this technology. Furthermore, observed dosimetric advantages do not necessarily translate to clinically meaningful benefit. Added to all these challenges is the cost of the technology, which means that access to PBT is limited. Therefore, appropriate patient selection is key in exploiting this technology.

To this end, the hypothesis of this thesis are:-

- Robust-optimisation of IMPT plans could reduce proton plan sensitivity against setup uncertainty and tumour motion such that its robustness would be comparable to that of VMAT plans.

- Monte-Carlo dose algorithm would improve accuracy of IMPT treatment plans compared to the pencil beam analytical algorithm. However, given the disadvantages of MC dose calculation (mainly speed and limited availability of a commercial solution) and improvement in ADC algorithms and understanding of the limitations of ADC algorithms, there may be a sub-group of patients where the ADC algorithm is clinically acceptable for treatment planning in lung cancer.

- PBT is able to reduce the risk of developing cardiac toxicity over photon therapy. This risk reduction is based on the dosimetric advantages of PBT and is higher in a sub-group of patients.

1.6 Aims

Therefore, this aims of this thesis are:-

- To evaluate and compare the robustness of IMPT and VMAT plans against setup uncertainties and tumour motion in locally advanced lung cancer using probabilistic scenarios in lung cancer.
- To evaluate the accuracy of the Raystation TPS analytical algorithm. against Raystation Monte-Carlo algorithm
- To identify a sub-group of clinical cases where the Raystation TPS analytical algorithm may be clinically acceptable.
- To identify a sub-group of patients who would benefit most from IMPT over VMAT with respect to cardiac sparing.

Reference	N	Follow-up	Age at RT	Study design	RT techniques	RT prescriptions	Chemo	Endpoints	Major findings
Gayed et al., 2009 [35]	44	1 yr^{+}	65.8 yrs*	Retrospective	3D-CRT (80%) IMRT (20%)	56.6 Gy*	91% CRT	MPI abnormalities	Abnormal segments 39.6 Gy* Normal segments 11.4 Gy*
Lee et al., 2009 [36]	88	7.5 yrs^{+}	58.5^{+}	Prospective	3D-CRT	74 Gy^{+}	84% CRT	MI PCE Constrictive pericarditis	Prescription dose $\geq$66Gy increases late toxicity - commonly cardiac
Schytte et al., 2010 [37]	250	7.9 yrs^{+}	NR	Retrospective	3D-CRT	60-80 Gy	NA	OS	LV mean $\geq$14.5 Gy trend to $\downarrow$OS (p=0.06)
RTOG 0617 Bradley et al., 2015 [20]	544	1.9 yrs^{+}	64 yrs^{+}	Prospective	3D-CRT (52%) IMRT (49%)	60 Gy (58%) 74 Gy (43%)	100% CRT	OS	$\downarrow$OS - heart V5 (HR 1.007/%) $\downarrow$OS - heart V30
RTOG 0617 Chun et al., 2017 [23]	482	1.8 yrs^{+}	64 yrs^{+}	Prospective	3D-CRT (53%) IMRT (47%)	60 Gy (58%) 74 Gy (42%)	100% CRT	OS	$\downarrow$OS - heart V40 (HR 1.01/%)
Dess et al., 2017 [27]	125	4.3 yrs^{+}	66 yrs^{+}	Retrospective	3D-CRT (97%) IMRT (3%)	70 Gy^{+}	84% CRT	Cardiac toxicity (CTCAE $\geq$ G3)	MHD - $\uparrow$ cardiac toxicity HR 1.07/Gy CI cardiac toxicity at 24 mos: MHD >11Gy - 11% MHD $\leq$11Gy - 2% Heart V5 >40% - 14% Heart V5 $\leq$40% - 2% Heart V30 >12% - 20% Heart V30 $\leq$12% - 4%
Johnson et al., 2017 [25]	178	1.4 yrs^{+}	72 yrs^{+}	Retrospective	3D-CRT (38%) IMRT (62%)	64 Gy^{+}	100% CRT	OS	Heart V30 - $\downarrow$ OS HR 1.013/%
McWilliam et al., 2017 [34]	1200	3-36 mos	73 yrs^{+}	Retrospective	3D-CRT IMRT SBRT (7%)	55 Gy in 20 frac 60 Gy in 5 frac	23% NA	OS	Mean to base of heart: >16.3 Gy - $\downarrow$OS HR 1.25/% (non-SBRT) >8.5 Gy vs <8.5 Gy - $\downarrow$OS (non-SBRT) > 6.5 Gy - $\downarrow$OS HR 2.11/% (SBRT)
Ning et al., 2017 [38]	201	2 yrs^{+}	NR	Prospective	IMRT (63%) PBT (37%)	74 Gy^{+}	99% CRT	PCE	Heart V35 >10% vs $\leq$10%- PCE HR 2.14 ($\geq$ CTCAE G2) Heart V35 $\leq$10% no grade $\geq$3 PCE)
Speirs et al., 2017 [26]	322	1.2 yrs^{+}	64 yrs^{+}	Retrospective	3D-CRT (60%) IMRT (40%)	66 Gy^{+}	18% NA 48% CRT 31% CRT + Adj 6% Adj	OS Cardiac toxicity (CTCAE)	Heart V50 - $\downarrow$OS HR 1.23/% Heart V55 - $\downarrow$OS HR 1.85/% (CRT subgroup) No cardiac toxicity- heart V50 13.8%$^{+}$ Cardiac toxicity- heart V50 20.8%$^{+}$
Vivekanandan et al., 2017 [33]	78	NR	66 yrs^{+}	Prospective	3D-CRT (96%)	67.7 Gy*	CRT (96%) IMRT (4%)	all-cause death rate (DR)	38% ECG changes at 6 months $\uparrow$DR with ECG changes at 6 months Heart and LA receiving 63-69 Gy - $\uparrow$DR
Wang et al., 2017 [28]	112	8.8 yrs^{+}	58 yrs^{+}	Retrospective	3D-CRT	74 Gy^{+}	100% chemo -90% CRT	SCE	MHD $\geq$20 Gy vs < 10 Gy - $\uparrow$SCE HR 5.47 MHD $\geq$20 Gy vs 10-20 Gy - $\uparrow$SCE HR 2.76 MHD - $\uparrow$SCE HR 1.03/Gy Heart V5 - $\uparrow$SCE HR 1.02/% Heart V30 - $\uparrow$SCE HR 1.02/% LV mean - $\uparrow$SCE HR 1.03/% LV V5 - $\uparrow$SCE HR 1.02/% LV V30 - $\uparrow$SCE HR 1.03/%
Wang et al., 2017 [31]	112	8.8 yrs^{+}	58 yrs^{+}	Retrospective	3D-CRT	74 Gy^{+}	100% chemo -90% CRT	MI Pericardial disease (PD) Arrhythmia	Heart V5 - $\uparrow$MI HR 1.03/% LV mean - $\uparrow$MI HR 1.05/Gy LV V5 - $\uparrow$MI HR 1.03/% LV V30 - $\uparrow$MI HR 1.03/% Heart V60 - $\uparrow$PD HR 1.04/% LV mean - $\uparrow$PD HR 1.04/Gy LV V30 - $\uparrow$PD HR 1.03/% RA V60 - $\uparrow$PD HR 1.02/% Heart V5 - $\uparrow$arrhythmia HR 1.02/% RA V50 - $\uparrow$arrhythmia HR 1.02/%
Stam et al., 2017 [39]	803	2.9 yrs^{+}	74.8 yrs^{+}	Retrospective	SBRT	54 Gy in 3 fx^{+}	none	Non-cancer death	LA max - $\uparrow$ non-cancer death HR 1.005/Gy SVC D90 - $\uparrow$ non-cancer death HR 1.025/Gy
Tembhekar et al., 2017 [29]	102	2.3 yrs^{+}	76.3 yrs^{+}	Retrospective	SBRT	50 Gy in 4 fx^{+}	none	OS SCE	No clear association between dose and OS or SCE (Heart DMax, V5, V10, 20, 30)

Table 1.3: Summary of lung cancer studies 2009-2017 comparing outcomes and cardiac doses (adapted from Niska JR, Thorpe CS, Allen SM, et al. Radiation and the heart: systematic review of dosimetry and cardiac endpoints. Expert Rev Cardiovasc Ther 2018; 16(12): 931-50 [40]. N- no of patients treated with proton, Gy - Gray, 3DCRT - 3D conformal radiotherapy, IMRT - intensity modulated radiotherapy, SBRT- stereotactic body radiotherapy, PBT - proton beam therapy, NR - not reported, NA- neo-adjuvant, CRT - concurrent chemoradiotherapy, adj - adjuvant, CI - cumulative incidence, MHD- mean heart dose, PCE- pericardial effusion, SCE- symptomatic cardiac event, HR- hazard ratio, OS- overall survival, Vx - volume receiving x Gy, frac- fractions, $^{+}$ - median, $^{+}*$ - mean)

Reference	N	Inclusion	Chemo	Disease stage	Trial design	Dose (RBE)	
						Photon	Proton
Higgins et al., 2017 [82]	348	2004 - 2012	some	I-IV	Retrospective	C, 3DCRT, IMRT 59.4 Gy*	PSPT 60 Gy*
Chang et al., 2018 [83]	64	2009 - 2011	CRT	III	Ph 2	-	PSPT 74 Gy
Liao et al., 2018 [74]	57	2009 - 2014	NA/CRT	IIB-IV	Ph 2	IMRT 66 or 74 Gy	PSPT 66 or 74 Gy
Ono et al., 2018 [84]	35	2009 - 2015	no	I-III	Retrospective	-	PSPT 87.5 Gy
Hoppe et al., 2012 [85]	19	2008 - 2010	NA+CRT	IIB-IIIB	Ph 2	-	PSPT 74 Gy*
Change et al., 2011 [86]	44	2006-2009	CRT	III	Ph 2	-	PSPT 74Gy
Hoppe et al., 2016 [87]	14	2009-2013	CRT	III	Ph 2	-	PSPT 74 Gy# or 60 Gy
Nguyen et al., 2015 [88]	134	2006-2010	CRT	II-III	Observational	-	PSPT 60Gy-74Gy
Tang et al., 2014 [89]	85	NR	NA/CRT/adj/comb	I-III	Retrospective	3DCRT, IMRT $\geq$ 60 Gy	NR,likely PSPT $\geq$ 60 Gy
Harada et al., 2016 [90]	9	2011-2013	CRT	III	Ph 1	-	NR, likely PSPT arm 1- 66 Gy arm 2- 74 Gy
Oshiro et al., 2014 [91]	15	2010-2013	CRT	III	Ph 2	-	NR, likely PSPT 74 Gy
Oshiro et al., 2012 [92]	57	2001-2010	NA/none	III	Retrospective	-	NR, likely PSPT 74 Gy*
Hatayama et al., 2015 [93]	27	2009-2013	NA/none	III	Retrospective	-	NR, likely PSPT 74 Gy*

Table 1.4: Summary of clinical experience in locally advanced lung cancer published since 2010 (N- no of patients treated with proton, RBE - relative biological effectiveness, Gy - Gray, C - conventional, 3DCRT - 3D conformal radiotherapy, IMRT - intensity modulated radiotherapy, ph - phase, PSPT - passive scatter proton therapy, IMPT - intensity modulated proton therapy, NR - not reported, NA- neo-adjuvant, CRT - concurrent chemoradiotherapy, adj - adjuvant, comb- combination, * - median dose, # - dose prescription changed to improve recruitment- initially 80 Gy or 60 Gy with elective nodes - 40 Gy in 2 Gy fractions)

Reference	Use of 4DCT	Robustness evaluation	Motion management	On-board imaging	Adapative planning
[82]	NR	NR	NR	NR	NR
[83]	Y	NR	NR	daily ortho KV	weekly 4dCT or week2-3
[74]	Y	NR	NR	NR	weekly CT
[84]	3DCT	NR	Gated delivery	daily ortho KV	NR
[85]	Y	NR	NR	daily ortho KV	weekly/biweekly 4dCT
[86]	Y	NR	NR	daily ortho KV	repeat 4dCT week3/4 or earlier
[87]	Y	NR	NR	daily ortho KV	weekly CT
[88]	Y	NR	NR	NR	NR
[89]	NR	NR	NR	NR	NR
[90]	3DCT	NR	Gated delivery	NR	NR
[91]	3DCT	NR	Gated delivery	fluoroscopy	NR
[92]	3DCT	NR	Gated delivery	NR	NR
[93]	3DCT	NR	NR	NR	NR

Table 1.5: Radiotherapy planning and image-guidance strategies in identified studies (NR - not reported, ortho KV - orthogonal kilo volatage imaging)

Reference	Control rates	grade ≥3 Toxicities, %	Median f/u, (months)
[82]	OS - overall, worse survival with photon (HR 1.21 (95%CI 1.06-1.39) no significant difference found between proton vs IMRT	NR	Photon -59.5 PBT - 39.6
[83]	5yr OS - 29% 5yr PFS - 22% MS - 26.5 months	late pulmonary - 3%	27.3
[74]	LF - IMRT 10.9%, PSPT- 10.5% MS - IMRT 29.5 months , PSPT - 26.1 months	1 yr RP: IMRT-6.5%; PSPT-10.5%	24.1
[84]	3yr OS - 67.2% 3yr LC - 86.5%	Dermatitis - 2.8%	34
[85]	2yr OS - 57% 2yr PFS - 25%	Acute toxicities - weight loss 5%, dyspnoea 5%*, haematologic- 21% Late toxicities - dyspnoea 13% haematologic - 6%	15
[86]	1yr OS - 86% 1yr PFS - 63% MS - 29.4 months	dermatitis 11%, oesophagitis 11%, dehydration 7%, pneumonitis 2%, , pulmonary fistula 2%, cough 2%, dyspnoea 7%, fever 2%, pain 2%, haematologic - 23%	19.7 months NR NR
[87]	2yr OS 57% 2yr PFS 25% Median OS 33 months Median PFS 14 months	No acute toxicities Late - GI and pulmonary 7% each	30 months
[88]	Median OS: Stage II - 40.4 months, Stage III - 30.4 months PFS: Stage II - 17.3%, Stage III - 18%	Oesophagitis 5%, Pneumonitis 1%, Dermatitis 6%	4.7 years
[89]	NR	#	
[90]	Median PFS 15 months	Oesophagitis 33%$^{+}$	43 months ^{x}
[91]	2yr OS 51% 2yr PFS 16.1%	Leukopaenia 67%, neutropenia 47%, thrombocytopenia 7%	
[92]	2yr OS 39.4% 2yr PFS 24.9% 2yr LC 64.1%	Acute- Pneumonitis 6% Late- Dyspnoea 4%, haemoptysis 2%	16.2 months
[93]	2yr OS 51.1% 2yr PFS 21.1% 2yr LC 36.4%	Pneumonitis 7%, dermatitis 11%, Oesophagitis 4%, neutropenia 4%, thrombocytopenia 4%	15.4 months

Table 1.6: Control and grade ≥3 toxicity rates in identified studies (OS- overall survival, PFS - progression free survival, LC- local control, NR- not reported, *− occurred in the same patient, patient subsequently died within 90 days of treatment, #− toxicities not stratified between proton and photon therapy, $^{+}$− 1 of 3 patients in 74 Gy arm, $^{x-}$ for surviving patients)

Trial	Location	Phase	Dose/Fractions (Gy(RBE))	Primary Objectives	Secondary Objectives	CCT
NCT02731001	Heidleberg, Germany	II, randomised	66/30*	Grade $\geq$ 2 pneumonitis and or oesophagitis	QOL, survival loco-regional control, and late toxicity	yes
NCT01629498	MD Anderson USA	I, randomised II, randomised	60/30 with SIB to 72 - 84 Gy	MTD PFS	- -	yes yes
NCT03132532	Mayo Clinic, USA	II, proton only	60, 66, or 72 Gy in 2 Gy fractions	PFS	-	yes
NCT01993810 RTOG 1308	multicentre, USA	III, randomised	70/35	OS	PFS Toxicity, QOL, cost-effectiveness and PFT changes	yes
NCT01770418	multi-centre, USA	I, single arm II, single arm	Dose level 1: 60/24 Dose level 2: 60/20 Dose level 3: 60.01/17 Dose level 4: 60/15	MTD - - - OS	- - - -	yes yes

Table 1.7: Currently recruiting proton clinical trials (CCT - concurrent chemotherapy, QOL - quality of life, SIB - simultaneous integrated boost, MTD- maximum tolerated dose, PFS- progression free survival, PFT- pulmonary function test, PCG- Proton Collaborative Group)

Chapter 2

Materials and Methods

2.1 In-silico comparison planning study

Patients

Twenty patients with locally advanced NSCLC previously treated with photon radiotherapy were selected based on varying tumour sizes and locations (10/20 patients had left sided primary tumour, 11 had middle/lower lobe primary tumours). Most cases had nodal/mediastinal involvement as the main cohort of patients receiving radical chemoradiotherapy are stage III NSCLC (16/20). Of twenty cases, fourteen were previously treated with photon radiotherapy at the Oxford Cancer Centre between August 2013 to March 2017. The in-silico planning study was registered and approved by the NHS Health Research Agency and conducted under the auspices of Oxford University Clinical Trials and Research Governance (research ethics committee reference: 16/LO/1324). The other six patients were provided by Hugo et al [95] through the cancer imaging archive (TCIA) [96].

Four-dimensional (4D) CT simulation (Optima CT580RT, GE Healthcare, WI) were acquired for all patients. Each 4DCT dataset was acquired under free breathing conditions and recorded using the Real-Time Position Management system (Varian Medical Systems, Palo Alto, CA). The entire thorax and upper abdomen were scanned with 2.5mm slice thickness. Each breathing period was phase-binned into ten bins. Unweighted averaged-intensity projection (Ave-CT) datasets were generated for treatment planning.

Contouring

Target and normal anatomy delineation were done by a Radiation Oncologist (ST) following the RTOG 1308 trial protocol [97, 98].

To account for tumour motion, the gross tumour volume (GTV) was contoured in the maximum and minimum inhalation phases and combined to form the internal

target volume (ITV). The ITV was verified in all 4DCT phases. An 8mm isotropic expansion of the ITV, edited to anatomical boundaries, formed the CTV. The CTV-PTV margins were calculated using $2.5\Sigma + 0.7\alpha$, where Σ is the population setup mean systematic error and α is the corresponding population mean random error [99]. Our institution's mean population systematic errors, Σ, were 1.0 mm, 1.3 mm, and 0.8 mm and random errors, α, were 2.3 mm, 2.7 mm, and 2.3 mm in the x-, y- and z- directions respectively. This is calculated from recorded daily on-line shifts of patients who underwent radical radiotherapy for lung cancer at our institution. The maximum calculated distance defined the CTV-PTV isotropic margin (5 mm).

The heart and the the following substructures were delineated according to RTOG 1106 [100]: right and left: atria (RA, LA), ventricles (RV, LV) and coronary arteries (RCA, LCA), and sino-atrial node (SA node). To account for contouring variability, an additional 3mm margin was added to the coronary arteries. SA node which is typically found in the right atrium on the border of the opening of the superior vena cava (SVC), was defined as the superior 0.5 cm part of the right atrium plus an additional 0.5 cm of the inferior part of the SVC.

Dose specifications and constraints

The target prescription was 70 Gy (relative biological effectiveness (RBE)) in 35 fractions. RTOG 1308 trial dose specifications and constraints were used [15]. Proton RBE was assumed to be 1.1. In PTV-optimised plans, plans were normalised such that the prescribed dose covered 95% of the PTV. In CTV-optimised plans, plans were normalised such that the prescribed dose covered 99% of the CTV. In all treatment modalities, the prescription dose had to cover at least 99% of CTV. The RTOG 1308 OAR constraints can be found in Table 2.1.

OAR	Per protocol	Acceptable variation
Non-GTV lungs	V20 $\leq$ 37% V5 $\leq$ 60% MLD $\leq$ 20 Gy (RBE)	V20 $\leq$ 40% or MLD $\leq$ 22 Gy V5 $\leq$ 65%
Oesophagus	Dmax 74 Gy (RBE) $\leq$ 1cc of partial circumference	Dmax 74 Gy (RBE) $\leq$ 1.5cc of partial circumference
Brachial plexus	V70 $\leq$ 3cc V74 $\leq$ 1.00 cc V75 $\leq$ 0.50 cc	V75 $\leq$0.5cc
Spinal cord	v50 $\leq$ 0.03 cc	v52 $\leq$ 0.03 cc
Heart	v30 $\leq$ 50% v45 $\leq$ 35%	v30 $\leq$ 55% v45 $\leq$ 40%

Table 2.1: RTOG 1308 OAR dose constraints

Robust optimisation parameters

A minimax robust optimisation method was used for robust-optimised IMPT plans [101]. The minimax optimisation minimised the objective function in the worst-case scenario. An estimate of the effects of the errors was obtained by recalculating a set of dose distributions based on the scenarios. The TPS would then expand the CTV based on this. The optimisation parameters for setup error was 3 mm based on the institution's threshold for online shifts and 3.5% for range uncertainty as recommended by Paganetti [62]. The range uncertainty component is attributed to CT imaging and conversion to stopping power which is considered to be a systemic error with a constant value for a specific patient throughout the treatment course [62].

Plan design

All plans used coplanar beams. A summary of the beam arrangements and whether range shifters were used for each plan could be found in Tables 2.2 and 2.3. In all treatment modalities, when constraints were met, plans were optimised to reduce dose

to the OAR to as low as achievable while maintaining target coverage.

2.1.1 Assessment of robustness against setup uncertainties using probabilistic scenarios in lung cancer: a comparison of proton with photon therapy

Treatment plans

Only ten out of twenty patients were included in the study, all of whom were previously treated at our institution (see Table 3.1). For every patient, a nominal plan (Dnom) was created for each optimisation technique: VMAT, PTV-optimised IMPT (PTV-IMPT) and two MFO robustly-optimised IMPT (MM-IMPT). VMAT plans were designed with two 360° arcs using 6 MV beams.

Unlike photon plans, IMPT plans need to account for both setup and range errors. The robust-optimiser expand the CTV for both of these errors to varying degrees. Therefore, for fair comparison, MM-IMPT plans optimised with only setup parameter (MM-IMPT(S)) were created. The second plan was optimised with both setup and range uncertainties parameters (MM-IMPT(S+R)). IMPT plans used two to three beams. The same beam angels were used for PTV- and MM-IMPT plans. The beam data used was based on an IBA cyclotron at Provision Proton Therapy Centre, Knoxville, TN (98 - 230 MeV) [59]. The dose calculation grid resolution was 2x2x2mm^3. All treatment planning and dose calculations were performed on Raystation 5.0.2 TPS (Pencil beam dose engine v3.5) using a two-core Intel® Xeon® 3.4 Ghz processor (RaySearch Laboratories, Stockholm).

2.1.1.1 Setup uncertainty

For every plan, a set of 35 shifts, representing a treatment course of 35 fractions, in the x, y and z directions were generated. A fraction dose is generated by recalculating

Plan	Gantry angle (deg)	RS (cm)
1	30	none
	110	none
	155	none
2	180	none
	210	none
	245	none
3	90	4
	135	4
	180	4
4	45	4
	90	none
	135	none
5	180	4
	215	4
	260	none
6	190	none
	235	none
	280	none
7	40	7.5
	220	7.5
	300	7.5
8	180	none
	180	4
	220	none
	270	none
9	0	none
	90	none
	180	none
10	45	none
	100	none
	315	none

Table 2.2: Summary of beam arrangements and range shifter use for robustness evaluation (deg-degree, RS- range shifter in water equivalent thickness)

Plan	Gantry angle (deg)	RS (cm)	Plan	Gantry angle (deg)	RS (cm)
1	30	none	11	90	4.0
	110	none		135	4.0
	155	none		180	4.0
2	0	none	12	180	none
	90	none		215	none
	180	none		250	none
3	40	7.5	13	90	4.0
	220	7.5		135	4.0
	300	7.5		180	4.0
4	180	none	14	180	4.0
	210	none		215	4.0
	245	none		260	none
5	45	none	15	180	none
	100	none		180	4.0
	315	none		220	none
6	190	none		270	none
	235	none	16	90	4.0
	280	none		140	4.0
7	225	none		180	4.0
	270	none	17	180	4.0
	305	none		225	4.0
8	45	4.0		270	4.0
	90	none	18	90	4.0
	135	none		135	4.0
9	180	4.0		180	4.0
	200	4.0	19	270	none
	245	none		230	none
10	45	7.5	20	90	none
	120	7.5		135	none
	180	7.5		180	4.0

Table 2.3: Summary of beam arrangements and range shifter use for comparison of ADC vs MC algorithms and estimation of cardiac toxicity. (deg- degree, RS - range shifter in water equivalent thickness)

the nominal plan following a shift in the isocentre in the x, y and z direction. In total 30 sets of shifts were generated (3 simulations for 10 patients). The maximum shift was limited to ±3mm.

Shifts were generated as follows: Using the calculated mean and standard deviation of the population systematic and random errors, we first defined the patient-specific systematic error by sampling from a normal distribution, denoted as follows:

$$\Sigma_s \in N(\mu_s, \alpha_s^2) \tag{2.1}$$

where μ_s is the institution's population mean systematic error and α_s is the standard deviation of the systematic error. Secondly, we defined the patient-specific random error by sampling from a normal distribution:

$$\Sigma_r \in N(\mu_r, \alpha_r^2) \tag{2.2}$$

where μ_r is the institution's population mean random error and α_r is standard deviation of the random error.

Finally, for each simulation, 35 shifts were obtained by sampling from a normal distribution with mean, Σ_s, and standard deviation, Σ_r, determined as follows:

$$Shifts \in N(\Sigma_s, \Sigma_r) \tag{2.3}$$

The arithmetic sum of the voxel doses from each of the fractions represent a treatment course (D_{sum}). Three treatment-course simulations were performed for each plan (35 x 3 = 105 dose calculations). The simulations were performed in RayStation using the scripting application programming interface accessed with IronPython.

Fraction dose analysis

Each fraction dose was evaluated against the target robustness criteria and OAR constraints.

Robustness Criteria

Each D_{sum} was compared to its respective nominal plan. In all cases, dose constraints to the OAR should be met. Target robustness criteria were:

- Dose deviation of $\leq$5% to CTV D98% as recommended by the Particle Therapy Co-operative Group consensus guidelines [102].
- CTV V95% $\geq$99.9% to mirror the target coverage criterion from which the PTV margin was derived [103].

Each fraction dose was also evaluated against the target robustness criteria and OAR constraints. To do this, D_{nom} was scaled down ($\frac{1}{35}$ D_{nom}) and compared to each fraction dose.

Simulation repeatability

We evaluated the reliability of a single simulation in predicting target robustness by comparing the voxel doses within the CTV of D_{sum} using Bland-Altman plots [104] and Pearson correlation coefficient. A single simulation would be considered representative of many if the difference in dose for a given voxel between simulations were no more than 1.4 Gy (RBE) (limits of agreement (LoA) = 2% of the prescription dose).

2.1.1.2 Tumour motion

Deformable image registration (DIR)

Intensity-based hybrid DIR algorithm was used within Raystation 5.0.2 TPS (RaySearch Laboratories AB, Stockholm) [105]. DIR was validated subjectively by visual inspection using split screen, checkerboard, image overlay, difference image and contour mapping displays. Objective validation was done by computing the Jacobian determinant [106].

Tumour motion

Tumour motion was summarised by calculating the Euclidean distance (d) between the maximum inhalation and exhalation of the centre of the GTV (Equation: 2.4).

$$d(I, E) = \sqrt{(I_x - E_x)^2 + (I_y - E_y)^2 + (I_z - E_z)^2} \tag{2.4}$$

where I and E are the position of the centre of the GTV in x-, y- and z- directions.

4D dose

4D dose evaluation was done by recalculating the nominal plan in each of the 4DCT phases. The doses from each phase were accumulated with and without weighting according to the interval recorded on the Real-time Position Management^{TM} system and compared to the robustness criteria.

Robustness Criteria

4D dose were compared to its respective nominal plan. In all cases, dose constraints to the OAR should be met. Target robustness criteria were the same as previously described in Section 2.1.1.1.

2.1.1.3 Analysis

The generation of shifts and statistical analysis was done in MATLAB (R2017a, Mathworks, MA). Conformity indices (95% isodose volume/ CTV volume) were calculated. Conformity indices and dose metrics were compared using Wilcoxon signed-rank test. The variance ($\frac{1}{N-1}\sum_{i-1}^{N}(\mu_i - \bar{\mu})^2$, N-total number of voxels, μ_i-dose in each voxel, $\bar{\mu}$-mean voxel dose) of the difference in voxel doses between D_{nom} and D_{sum} were calculated for the 3 treatment modalities. In all the statistical analyses, a P value of $<.05$ was considered to be statistically significant.

2.1.2 Is an analytical dose engine sufficient for IMPT in lung cancer?

Raystation MC algorithm

We considered the Raystation MC algorithm to be the gold-standard. The Raystation TPS ADC and MC algorithms have been validated in water and lung phantoms [64, 65]. Saini et al compared the Raystation ADC vs MC algorithms vs GATE as well as Raystation MC vs measurements in homogenous, heterogenous and anthropomorphic phantoms [64]. Taylor et al compared ADC vs MC vs measurements in heterogeneous anthropomorphic moving lung phantom. In both studies, the Raystation MC algorithm was observed to have higher accuracy over the Raystation pencil beam algorithm [65]. Saini et al reported γ pass rates of greater than 90% in six of seven planes using the Raystation MC algorithm (dose tolerance (DT)=3%, distance-to-agreement (DTA) =3mm) [64]. When Raystation MC algorithm was validated against GATE in a water phantom, the Raystation MC and GATE MC were always within 3% of the measurements. In addition, FLUKA (Fiorini et al, unpublished work) MC software packages. When Raystation MC algorithm was compared against FLUKA in different tumour sites (thoracic, CNS, pelvic tumours), the gamma analy-

sis passing rates were all above 85% (global 3%-3mm, median: 98%, range: 87-100%)). However, when the Raystation ADC was compared against FLUKA, the median pass rate was 79% (57-100%).

Treatment plans

All twenty cases were included in this study. Robust-optimised IMPT plans which took into account both range and setup uncertainty were generated in this study. The optimisation parameters for setup and range uncertainty used were as described above. Four plans were generated for each case. Optimisation of treatment plans were executed using the analytical pencil beam algorithm within Raystation TPS (v6.99, Raysearch Laboratories, Stockholm). Following this, three final dose calculations were performed to generate three different plans:

- Pencil beam algorithm (PB-PB). *Pencil-beam dose engine (v4.2).*
- Monte Carlo algorithm (PB-MC). *MC dose engine (v4.1) with 1% statistical uncertainty.*
- MC algorithm normalised to prescription dose (PB-MC scaled).

A fourth plan was generated for each plan where MC optimisation (10,000 ions/spot) and final dose calculations with 1% statistical uncertainty were performed within Raystation.

2.1.2.1 Dosimetric evaluation

For each plan, the hot spot dose received by 2% of the volume (D2%), the minimum dose received by 99% of the volume (D99%) and the mean dose (D_{mean}) to the CTV were recorded. Doses to OAR were evaluated for the oesophagus, heart, lungs and spinal cord.

Gamma-analysis

Dose distributions from PB-PB (reference dose) were compared to PB-MC through a global gamma index analysis [107] with a dose tolerance (DT) of 3% and distance-to-agreement (DTA) of 3 mm. Gamma analyses were performed in MATLAB (R2017a, Mathworks, MA). Two low-dose threshold were chosen: 20% (D20) and 99% (D99) of the prescribed dose. The former to evaluate the dose agreement of the entire treatment plan and the latter to evaluate the dose agreement within the CTV.

2.1.3 Statistical Analysis

Wilcoxon sign-rank test was used to compared the dose metrics. Univariate and backward elimination multivariate linear regression analysis were undertaken to evaluate if any variable was predictive of high correlation in the gamma-analysis between ADC and MC dose engines. GTV, CTV and average CTV HU were considered as continuous variable. The following variables were treated as binary variables: presence of mediastinal disease and use of range shifter. In order for plans to be categorised as no range shifter used, all beams within the plan must not utilise a range shifter. If one or more beams required a range shifter in order to achieve an optimal dose distribution, the plan would be classified as requiring range shifter. Statistical significance was defined as $P < .05$. All statistics were performed in IBM SPSS Statistics v20 (IBM Corp, Armonk, NY).

2.1.4 Photon vs proton for reduction of cardiac toxicity in locally advanced lung cancer: the model based approach

Treatment plans

All twenty cases were included in this evaluation. Dual-arc VMAT plans with 6 MV photons and robust-optimised IMPT plans were generated for each patient using the specifications mentioned above. Robust-optimised IMPT plans took into account both range and setup uncertainty (optimisation parameters: setup 3mm, range 3.5%). All treatment plans were generated in Raystation TPS (v6.99, Raysearch Laboratories, Stockholm). MC dose engine (v4.1) was used for optimisation and final dose calculations. The optimisation and final dose calculation parameters were a sampling history of 10,000 ions/spot and 1% statistical uncertainty.

For this study, we assumed an end-to-end tumour motion of less than 10 mm in all cases. Therefore, following RTOG-1308 trial protocol, an ITV approach based on the union of all the GTVs of all phases was used for planning for both VMAT and IMPT plans. The interplay effect would need to be mitigated in IMPT plans using solutions such as rescanning [51].

Estimation of clinical benefit

These dosimetric parameters were compared between VMAT and IMPT: MHD, volume of heart receiving 50 Gy (RBE), 30 Gy (RBE) and 5 Gy (RBE) (V50, V30 and V5), and mean dose to the atria, ventricles, coronary arteries and SA node.

Using an NTCP model developed by Dess et al [27], grade $\geq$3 cardiac toxicities were estimated. The model stratifies patients based on their baseline cardiac morbidities and heart dose parameters. It was developed based on 125 patients enrolled in four prospective trials within the University of Michigan. The specific cardiac complications the authors were interested in were acute coronary syndrome, cardiac

arrest, congestive heart failure (CHF), pericardial effusion, pericarditis, valvular disease and arrhythmia. Grading of cardiac complications was done retrospectively in the context of prospective trials using Common Terminology Criteria for Adverse Events (v4). The 12- and 24-month cumulative incidence of grade $\geq$3 cardiac events were 9% (95% CI, 3-12%) and 11% (5-16%) respectively. When non-cardiac death was accounted for as a competing risk.

Presence of cardiac disease prior to radiotherapy was linked to a higher cumulative incidence of cardiac events (12-month cumulative incidence: without vs with pre-existing cardiac disease (95% CI) - 15% (3-27%) vs 21% (7-35%), 24-month- 4% (0-9%) vs 7% (1-13%)). In their report, nomograms were available for predicting complications based on a number of dose metrics (MHD, V30 and V5) and presence of pre-existing cardiac disease. Baseline cardiac disease was defined as presence of any of the following disease: acute myocardial infarction, coronary artery bypass grafting procedure, angioplasty or stent placement, diagnosis coronary artery disease (CAD) or clinical diagnosis of CHF. The Framingham risk scores were used to further stratify patients according to their baseline cardiac risk [108].

For the analysis in this planning study, the predicted grade $\geq$3 toxicities were calculated for both treatment modalities in 3 different scenarios: in the presence of pre-existing cardiac disease, high risk of cardiac disease, and in the absence of pre-existing cardiac disease. High risk of cardiac disease was defined as Framingham risk score of $\geq$ 20%.

Statistical analysis

Conformity indices (95% isodose volume/CTV volume) were calculated for both treatment modalities. Spearman's rank correlation co-efficient was calculated between heart dose (MHD, V5 and V30) and the thoracic vertebral level to which the most inferior aspect of the disease (primary tumour and nodes) overlapped with. Wilcoxon

sign-rank test was used to compared the dose metrics and the absolute risk reduction between the treatment modalities. Statistical significance was defined as $P < .05$. All statistics were performed in IBM SPSS Statistics v20 (IBM Corp, Armonk, NY).

Sample size and power calculation

Based on the randomised control trial between IMRT and PSPT in lung cancer [74], a power calculation was performed. The median MHD of patients treated treated in the latter part of the trial for IMRT and PSPT were 10.4 Gy (RBE) (range 0.9 - 34.6) and 5.5 (0.5 - 17) respectively. (During the trial, it was observed that there were improvements in the treatment plans of patients enrolled in the latter part of the trial - therefore MHD of patients enrolled in the latter part of the trial were used). The minimum sample size required to achieve power of 95% and a significance level of 5% for detecting a mean of the differences of 4.9 between the pairs were 13. Based on this trial, we defined threshold of a difference of at least 5 Gy (RBE) to be clinically meaningful.

Chapter 3

Assessment of robustness against setup uncertainties using probabilistic scenarios in lung cancer: a comparison of proton with photon therapy

The British Journal of Radiology, 93(1107):20190584, 2020.

DOI: 10.1259/bjr.20190584

3.1 Abstract

Purpose

To compare the sensitivity of IMPT and VMAT plans to setup uncertainty and tumour motion in locally advanced NSCLC.

Materials and methods

Robust- and PTV-optimised IMPT and VMAT nominal plans were created with a dose of 70 Gy RBE in 35 fractions in ten patients. Robustness against setup uncertainty was assessed using probabilistic scenarios where a fractionated treatment course was simulated, summed (D_{sum}) and compared to the nominal plan. Three treatment-course simulations were done for each plan. Weighted and unweighted 4D dose distributions were evaluated. Target robustness criteria were: dose deviation of $\leq 5\%$ to CTV D98% and CTV V95% $\geq 99.9\%$. Target voxel-wise dose simulation repeatability was analysed using Bland-Altman plots. Acceptable limits of agreement (LoA) were 2% of the prescription dose.

Results

All D_{sum} met target robustness criteria. $> 99\%$ of VMAT and MM-IMPT fraction doses met both target robustness criteria. For PTV-IMPT, only 96.9 and 80.3% of fractions met CTVD98% and V95% criteria respectively. Simulation repeatability was excellent (LoA range: 0.41 - 1.1 Gy) with strong positive correlations. 4D CTV V95% coverage was poor in both photon and proton plans where tumour motion was larger 10mm.

Conclusion

Probabilistic analysis provides a fast and practical method for evaluating VMAT and IMPT plans sensitivity against setup uncertainty. Target robustness was achieved in all D_{sum}. Whilst fraction VMAT and MM-IMPT doses were comparable, simulated fraction doses in PTV-IMPT were suboptimal. In tumours with large motion there was inadequate target coverage in both treatment modalities. Weighted 4D dose sum would be recommended where tumour motions are above 6mm.

3.2 Introduction

Although PBT holds the promise of improving cure without increasing treatment-related toxicity in patients with NSCLC, it is prone to multiple uncertainties. Therefore, accurate placement of the distal edge of the Bragg peak is necessary if underdosing the target volume or overdosing OAR are to be avoided. Sources of uncertainty in PBT include setup and anatomical variations, dose calculation algorithms, organ motions and biological effects [62]. The sensitivity of a plan to various uncertainties is termed robustness.

In conventional photon-based treatment, setup errors are compensated for by adding a margin to the treatment volume to produce a PTV [103]. This method may be inadequate in PBT as the margin required is highly dependent on the changes in tissue density along the beam path. A standard PTV does not account for the non-uniform distortion of the proton dose distribution caused by a setup error. This situation is of particular concern in IMPT when MFO is used. In this technique, non-uniform fields are used to produce the desired dose distribution. Incorporating uncertainties due to tissue heterogeneity in PTV-optimised MFO plan is not straightforward. The addition of margins can improve target coverage only at the edges of the target volume and not within the target itself. Margins have little effect on the sensitivity of the plan when there is steep dose gradients within the CTV [47].

Robust optimisation is proposed as a solution for this, in which the uncertainties are taken into account during optimisation [48, 101, 109, 110]. This approach incorporates setup and range uncertainties in the optimisation algorithm and do not require a PTV to be created. One current commercially available TPS use minimax optimisation which optimises the worst-case scenario dose distribution at each iteration [101].

Once a plan has been optimised, it is necessary to quantify its sensitivity to setup

errors. Several methods have been reported for quantifying plan robustness against setup uncertainties. Unfortunately, there is no consensus on the definition of robustness or on the ideal metric for assessing robustness. A number of methods rely on simulating treatment plans under extreme conditions: worst-case dose distribution [43], error-volume histogram [47] and DVH bands [49]. Unfortunately, worst-case scenario analyses tend to overestimate errors as by definition it estimates the maximum likely error resulting in a disproportionate number of plans being unnecessarily rejected. Furthermore, it cannot be assumed that a large shift results in a worse dose error than smaller ones [50]. This is particularly true in plans with high tissue heterogeneity as in the case of thoracic IMPT. Other robustness analyses use statistical sampling where several hundred scenarios are simulated [104, 111]. These methods may be more realistic in modelling changes to the dose distribution, but may not be viable for routine clinical use.

There are two components to this part of the thesis. The first describes a fast and practical approach to assess setup uncertainty in NSCLC using probabilistic scenarios. The method uses a simple extension of a commercial treatment planning system. Here, a fractionated treatment course is simulated, summed and compared to the planned treatment plan. The initial results appear promising with robustly optimised IMPT plans having similar target robustness to VMAT [112]. The time taken to compute a-thirty-five-fraction treatment course simulation is approximately five minutes on an off-the-shelf Intel-based computer. An advantage of this technique is that it is independent of the worst-case scenario optimisation method, thereby providing an independent measure of robustness. Furthermore, the main requirement for the probabilistic method is knowledge of the facility's setup errors. This is advantageous for new proton centres or treatment of new tumour sites where retrospective robustness analysis is not possible [113]. The second component assesses the plan robustness against tumour motion. If IMPT is to be a viable alternative in the

treatment of locally advanced lung cancers, its robustness needs to be comparable to photon therapy. Therefore, we compared the robustness of IMPT to photon VMAT.

3.3 Results

3.3.1 Nominal plans

A summary of the tumour characeteristics can be found in Table 3.1. All D_{nom} plans were compliant with the OAR constraints. MM-IMPT had statistically significantly lower conformity indices compared to PTV-IMPT (P <.05).

Case	GTV (cc)	TNM 7 staging	Primary tumour location	IASLC lymph node stations
1	15	TxN2M0	-	5
2	25	TxN2M0	-	10R, 4R
3	27	T2N1M0	Left lower lobe	-
		T1N0M0	Left upper lobe	-
4	28	T1N2M0	Left upper lobe	10L, 4L
5	32	T2N0M0	Right lower lobe	-
6	50	T2N2M0	Right upper lobe	4R
7	106	T2N0M0	Right middle lobe	-
8	115	T4N1M0	Right lower lobe	10R
9	261	T4N2M0	Left upper lobe	7,10L
10	404	T4N0M0	Left upper lobe	-

Table 3.1: Tumour characteristics. (GTV - gross tumour volume, TNM - tumour node metastasis, IASLC - The International Association for the Study of Lung Cancer)

3.3.2 4D dose evaluation

Target coverage was poor in both weighted and unweighted dose distributions for patients 3 and 5 in VMAT, PTV-IMPT, and both MM-IMPT where tumour motion was >12 mm (see Figure 3.1). In all cases, CTV V95% criterion was violated. Where tumour motion was less than 6mm, there was no statistically significant difference in the V95% coverage in the weighted and unweighted 4D dose. Above 6 mm, V95% coverage was significantly lower in the weighted 4D dose distribution (p <.001).

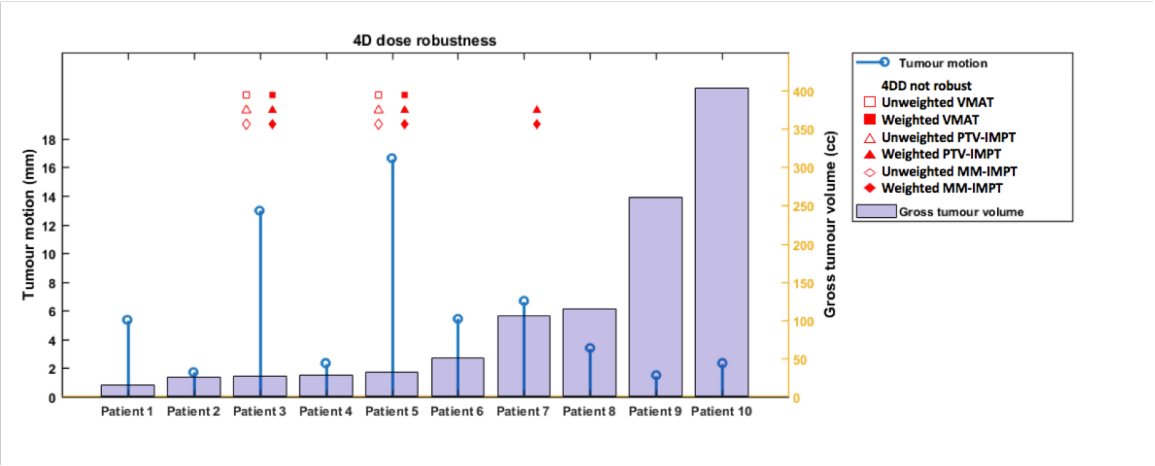


Figure 3.1: Summary of tumour motion, gross tumour volume (GTV) and 4D dose plan robustness. Tumour motion defined as Euclidean distance between the centre of GTV at maximum inhalation and exhalation. Red symbols indicate plans where 4D dose accumulation did not meet robustness criteria. In patients where tumour motion was above 10 mm (patients 3 and 5), all three plan modalities were not robust against tumour motion.

3.3.3 Summed dose distributions

For each plan, three treatment course simulations were performed. Each simulation consisted of 35 fractions (as the dose prescription for the treatment is 70 Gy (RBE) in 35 fractions). In total 4200 fractions doses were simulation (3 simulations x 35 fractions x 4 plans x 10 patients). Apart from one D_{sum} plan for PTV-IMPT (Patient 9) which exceeded the maximum dose (Dmax) constraint for the spinal cord, all other D_{sum} met OAR constraints. The Dmax to the spinal cord of patient 9 in simulation 3 was 50.2 Gy (RBE). When the target robustness was considered, all D_{sum} met target robustness criteria.

3.3.4 Fraction dose distributions

Evaluation of fraction doses showed varying plan qualities. This was especially so for PTV-IMPT plans. Almost all VMAT and both MM-IMPT fraction CTV D98% doses

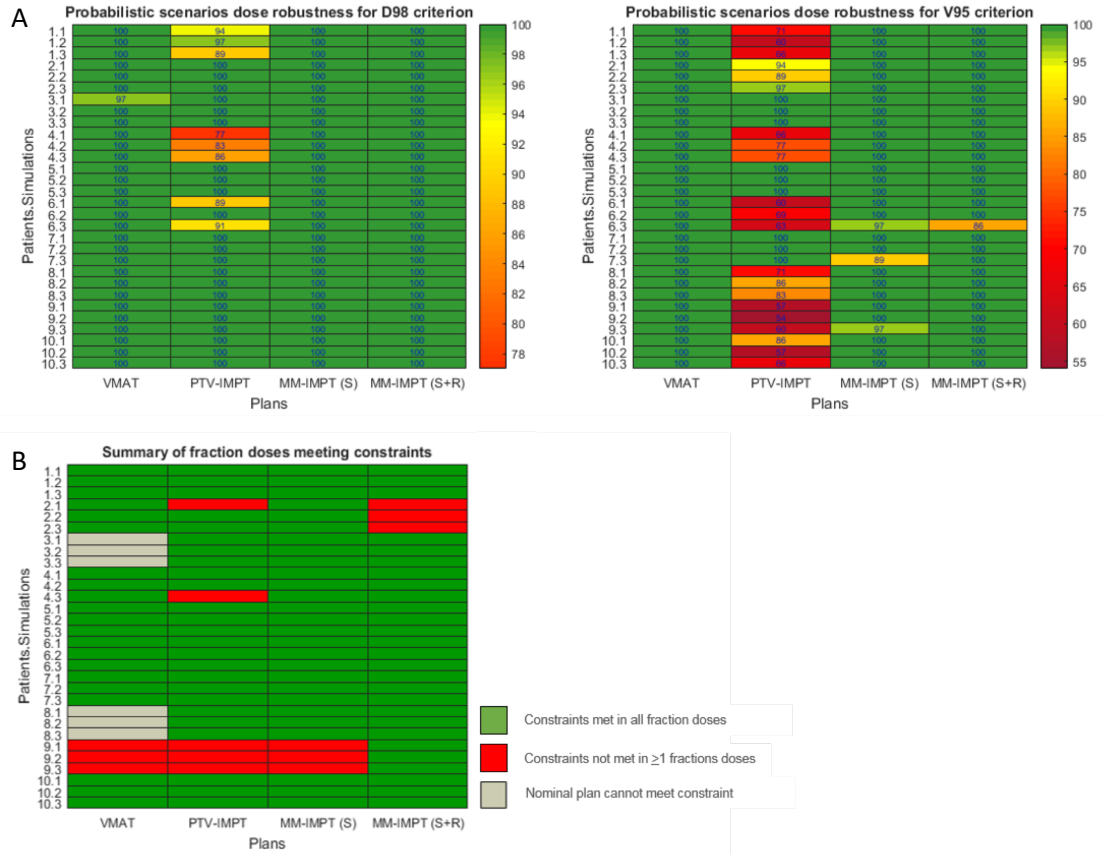


Figure 3.2: Summary of target coverage and adherence to OAR constraints. A. target coverage (number indicates percentage out of 35 fractions). B. adherence to organs-at risk (OAR) constraints for fraction doses in the different treatment modalities.

were within 5% of the respective nominal plans (VMAT - 99.9%; MM-IMPT (S) and (S+R) - 100%). Conversely, for PTV-IMPT fractions doses, only 96.9% (1017/1050 fractions) were within 5% of the nominal CTV D98%. Similar observations were seen for V95% criterion where almost all VMAT and MM-IMPT fraction doses met the criterion (VMAT - 100%; MM-IMPT (S) - 99.4%, (S+R)- 99.5%) compared to only 80.3% (843/1050) in PTV-IMPT. This result is summarised in Figure 3.2. The proportion of fraction doses per simulation meeting the minimum dose criteria varied most widely for PTV-IMPT (range 54 - 100%). Figure 3.3 shows boxplots of the spread of fraction CTV D98% and V95% for the different modalities. For each

simulation, PTV-IMPT had the largest spread of fraction doses.

Following the simulations, a proportion of fraction doses did not meet OAR constraints: three VMAT, five PTV-IMPT, three MM-IMPT (S) and three (MM-IMPT (S+R) simulation plans (see Figure 3.2). OAR doses were generally lowest with MM-IMPT (S), followed by MM-IMPT (S+R) and PTV-IMPT. The tumour was located immediately adjacent to the spinal cord in Patient 9. In all three simulations the spinal cord Dmax was exceeded in a number of fraction doses for VMAT (nominal Dmax 46.9 Gy; range, 12-19 fractions), PTV-IMPT (48.16 Gy (RBE); 14-19 fractions), MM-IMPT (S) (44.00 Gy (RBE); 5-12 fractions) and MM-IMPT (S+R) (45.30 Gy (RBE); 10 fractions each).

Dose volume histograms (DVH) and axial dose colour maps for all 4 plans of a representative patient (Patient 10) are shown in Figures 3.4 and 3.5. Figure 3.4 shows the DVH of D_{nom} versus D_{sum} and D_{nom} versus D_{frac}. Visual inspection of the DVHs shows subtle differences between the nominal and summed dose distributions in all three plans. Similarly, there is little deviation in target coverage with VMAT and MM-IMPT plans on a single fraction level. In contrast, target coverage is inferior in the PTV-IMPT plan with sub-volumes receiving over and under dosage. These areas of under- and overdosage varied with each fraction (see Figure 3.6), therefore the sum of all the fraction dose was still meeting the robustness criteria despite deviations in the fraction doses (see Table 3.2 for summary of dose metrics between D_{nom} and D_{sum}. A low dose area is noted within the CTV of the simulated PTV-IMPT plan compared to the nominal plan (Figure 3.5).

There was internal consistency in the OAR doses for each simulation. These doses show that compared to VMAT, IMPT plans deliver statistically significantly lower spinal cord Dmax, lung V5, lung V20, MLD, heart V30 and heart V5 ($P < .005$). There was no statistically significant difference between the three regimens with respect to heart V45 and oesophagus V50. A comparison of OAR dose metrics in VMAT and

Dose Metric	Nominal plan	Summed plan
CTV D98% (Gy (RBE))	70.96	70.38
MLD	10.80	10.80
Heart V5Gy (RBE) (%)	15	16
Spinal Cord Dmax (Gy (RBE))	6.25	5.98
Oesophagus V50Gy (RBE) (%)	0.44	0.43

Table 3.2: Nominal plan and summed dose distribution dose metrics of patient 4. (CTV- clinical target volume, MLD- mean lung dose, Dx - Dose to x% of volume of interest, Vx - Volume in percentage receiving x of prescribed dose

IMPT D_{sum} is shown in Figure 3.7.

3.3.5 Simulation repeatability

In terms of the difference in dose between nominal and simulated plans, VMAT had the smallest variance followed by MM-IMPT, then PTV-IMPT (VMAT - 0.78 Gy^2; MM-IMPT (S) – 0.97 Gy^2, MM-IMPT (S+R) - 1.21 Gy^2; PTV-IMPT - 2.52 Gy^2).

Using Bland-Altman plots, voxel-wise CTV dose analysis showed strong positive correlations between each simulation for VMAT and IMPT plans (range of r: 0.89 - 0.94, n = 107500, all $P < .001$) with limits of agreement (LoA) ranging from 0.41 to 1.1 Gy. Figure 3.8 shows plots with mean difference and LoA. In all cases the 95% confidence interval of the mean difference, upper and lower limit of LoA were no more than 0.02. All of the simulations met a priori criteria of LoA <1.4 Gy. VMAT and MM-IMPT had superior agreement compared to PTV-IMPT. Table 3.3 shows the correlation statistics between each simulation.

N= 107500	r	P value
VMAT		
Sim 1 vs Sim 3	0.97	
Sim 1 vs Sim 2	0.94	
Sim 2 vs Sim 3	0.98	
PTV-IMPT		
Sim 1 vs Sim 3	0.94	P <.001
Sim 1 vs Sim 2	0.89	
Sim 2 vs Sim 3	0.96	
MM-IMPT		
Sim 1 vs Sim 3	0.97	
Sim 1 vs Sim 2	0.94	
Sim 2 vs Sim 3	0.97	

Table 3.3: Summary of Pearson correlation coefficient statistics of voxel-wise summed CTV dose (r–correlation coefficient)

3.4 Discussion

The sensitivity of PBT plans to uncertainties in lung cancer is a concern due to tissue heterogeneity and the effect this has on the delivered dose distribution under expected patient setup variations. The use of MFO with inhomogeneous dose distribution within the target poses a problem. Solutions use in PSPT and uniform single-field optimised plans such as beam-specific PTV may not hold in highly modulated fields as margins only ensure coverage at the edge of a target and not within it. Use of margins alone may result in uncertainties within the target [47]. Robust optimisation techniques have been described and are one approach to overcoming this problem. Although a number of methods have been reported, consensus has yet to be reached on the ideal tool and optimal definition of robustness. Nevertheless, given that current commercially available TPSs rely on minimax robust optimisation, it is important to evaluate the sensitivity of these plans using a method independent of the optimisation algorithm.

In this study, plan robustness was evaluated using probabilistic scenarios for setup uncertainty and tumour motion in locally advanced NSCLC. All summed simulated

doses met the robustness criteria for the target for all patients in VMAT, PTV-IMPT and both MM-IMPT plans. By sampling from various normal distributions, we assumed that smaller setup errors were more likely to occur than larger ones. However, evaluation of the fraction doses revealed marked differences in plan quality. VMAT and MM-IMPT fraction doses had comparable target robustness and were superior to PTV-IMPT plans. For PTV-IMPT plans, the minimum dose coverage criteria to the CTV was only fulfilled in 80% of the simulations. A similar result has been seen in other studies which have shown that fractionation reduces the effect of setup uncertainty [114, 115].

This study showed that, the ITV method for accounting tumour motion during treatment planning could not ensure target coverage in all treatment modalities, including VMAT, where there was large tumour motion. This was particularly noticed when tumour motion was large relative to the tumour size (Patient 3 and 5, tumour motion $>$ 10mm). When 4D robust optimisation was used, target coverage improved (data not shown). Other solutions for this would be to restrict target motion using breath-hold or gating [116]. This evaluation compared the result of the 4D dose accumulated with and without weighting based on the time stamp from the RPM system on the planning CT. The results suggest that in tumours with motion larger than 6mm, performing a weighted 4D dose accumulation is recommended as target V95% coverage was reduced compared to the unweighted sum.

This analysis showed that the minimax robust optimisation algorithm is able to produce robust plans in locally advanced lung cancer. There was little variation in fraction and summed dose distribution in the MM-IMPT (S) plans. However, range uncertainty in the order of $\pm$3.5% associated with CT and conversion to stopping power exists which is unique to proton beam therapy [62]. As this error needs to be accounted for during the optimisation process, sensitivity analysis in MM-IMPT plans with setup and range parameter included in the optimisation were presented.

However, for fair comparison, we have assessed how well the minimax algorithm was at creating robust plans when only the setup parameter was used in the optimisation. The result showed that, MM-IMPT (S) plans were robust against setup uncertainty. The high dose region was larger where both setup and range parameters have been incorporated compared to when only setup uncertainty parameter was included resulting in higher doses to OAR but still significantly lower compared to VMAT.

Similar to findings published by other groups, hyperfractionation can reduce the effect of setup uncertainty [114, 115]. However, as the aim of conventional fractionation is usually to deliver a homogenous dose distribution, the biological effect of under-dosing part of the CTV for a proportion of the treatment is unknown. Simple dose accumulation of the fraction doses in 2 Gy-equivalent doses (EQD2) showed target robustness against both criteria was maintained in all treatment techniques. Conversely, robustness is likely to be an issue if PTV-optimisation is to be used for hypofractionated treatment as hyperfractionation improves plan robustness by compensating for areas that are underdosed or overdosed.

Where a simulation reveals that OAR constraints were exceeded for fraction doses, care must be taken when deciding if a nominal plan is acceptable, even if the summed dose distribution does meet the constraints. In such cases, the nominal OAR doses are usually close to the OAR constraints.

This study highlights the potential for dose escalation with IMPT. The prescription dose of 70 Gy (RBE) in 35 fractions is higher than the conventional dose-fractionation of up to 66 Gy in 33 fractions. At 70 Gy (RBE) in 35 fractions, two VMAT nominal plans did not meet dose constraints for MLD and lung V20 Gy. IMPT did meet all the constraints with potentially room for further dose escalation. As would be expected, IMPT delivered statistically significantly lower doses to OARs at low-dose levels compared to VMAT (MLD, lung V5 and V20 and heart V5 and V30). At high dose levels, there was no statistically significant difference in

oesophagus V50 and heart V45.

Comparison of summed simulated doses within the CTV at voxel level showed excellent repeatability with LoA within 2% of the prescription dose and strong positive correlations. Additionally, LoA for VMAT and MM-IMPT were within 1% of the prescription dose. High degrees of consistency were observed in the D_{sum} target voxel doses from the three simulations. This was also observed in PTV-IMPT plans despite vast differences in the fraction doses. These results indicate that performing a single simulation is predictive of multiple simulations for evaluating robustness of the target dose coverage.

This study has intentionally focused on the effect of setup uncertainty and a simple representation of tumour motion. The sensitivity analysis described has not taken into account uncertainty due to changes in patient anatomy during treatment or interplay effects. Our next work is focused on incorporating the probabilistic scenarios method with the issue of interplay. Adaptive radiotherapy with repeated volumetric imaging during the course of treatment would be necessary to account for changes in patient anatomy. Assessment of range uncertainty has not been included in this study. Range uncertainty related to CT and conversion to stopping power is considered a systemic error that is fixed and propagated throughout the whole treatment. Therefore, a population study is required to use the probabilistic method to assess the effect of range uncertainty. Evaluation of the robustness of the minimax optimisation by scaling to the maximum and minimum range uncertainty and found it to be robust [101].

Stutzer et al has recently suggested a method for assessing robustness against both setup and range uncertainty in head and neck proton plans [117]. A key difference in this method for setup uncertainty estimation is that sampling of the setup error positions is from a regular grid. A controversial aspect of the 4D dose calculation is the use of DIR. The DIR tool used within this study has been validated with uncer-

tainties of up to 2mm [105]. Finally, we recognized the limitation of the pencil beam algorithm for dose calculations. Comparison of analytic algorithm dose calculations against anthropomorphic lung phantom measurements have been reported to over-predict dose within the target by up to 40% [65]. Better agreement with physical measurements were found when Monte Carlo algorithms were used [59]. Assessment of the robustness of these plans could be validated by performing Monte Carlo dose calculations.

In conclusion, probabilistic analyses provide a fast and practical method for determining the sensitivity of VMAT and IMPT plans to setup uncertainties. In tumours with large motion relative to its size, motion mitigation techniques such as breath-hold or gating are required to ensure target coverage. Alternatively, 4D robust optimisation is a solution at the expense of increased planning time. Whilst target robustness between VMAT and MM-IMPT fraction doses were comparable, fraction doses in PTV-IMPT were sub-optimal.

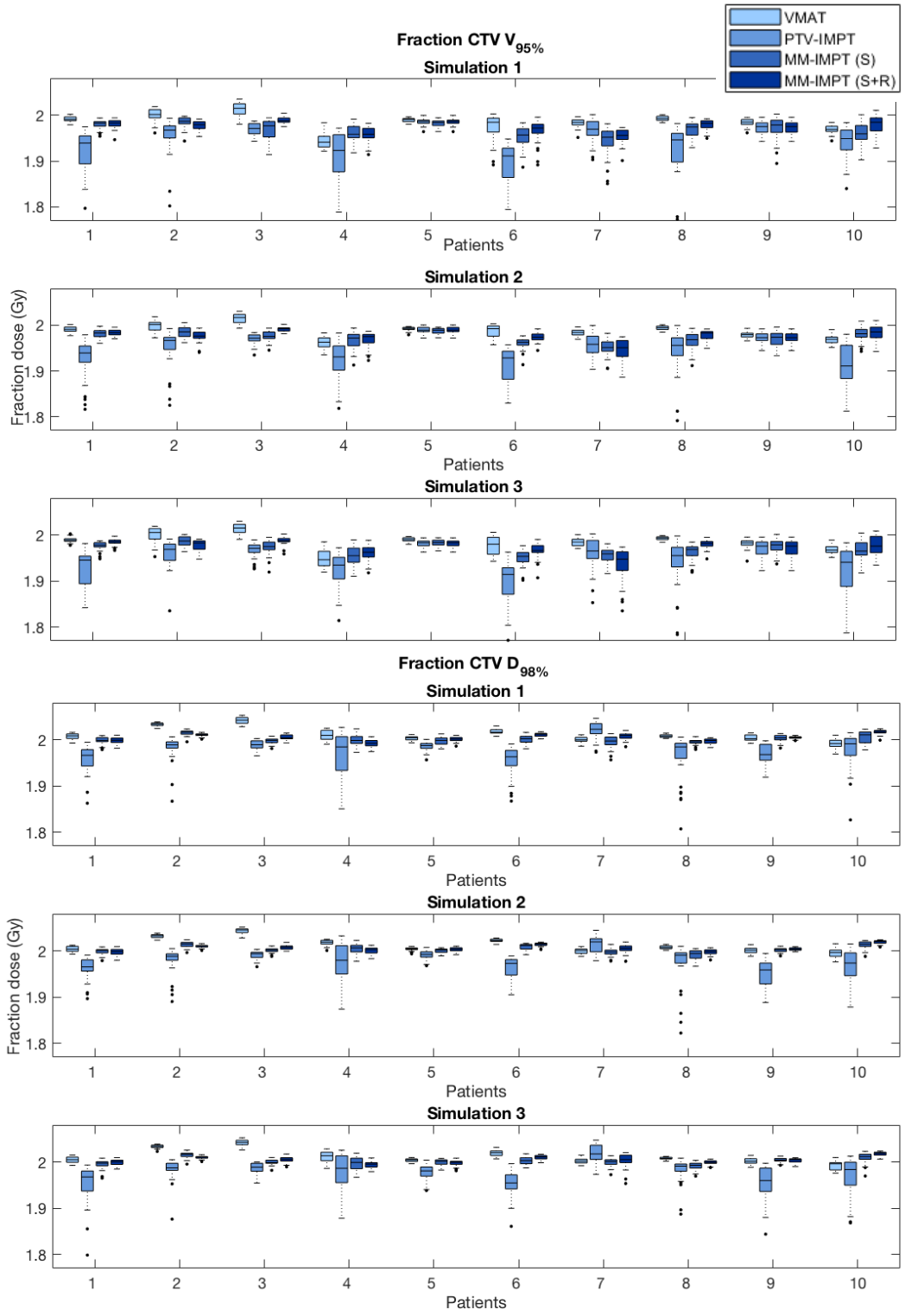


Figure 3.3: Boxplots of all fraction doses CTV D98% and V95%. PTV-IMPT has the largest spread of fraction doses compared to VMAT and both MM-IMPT plans.

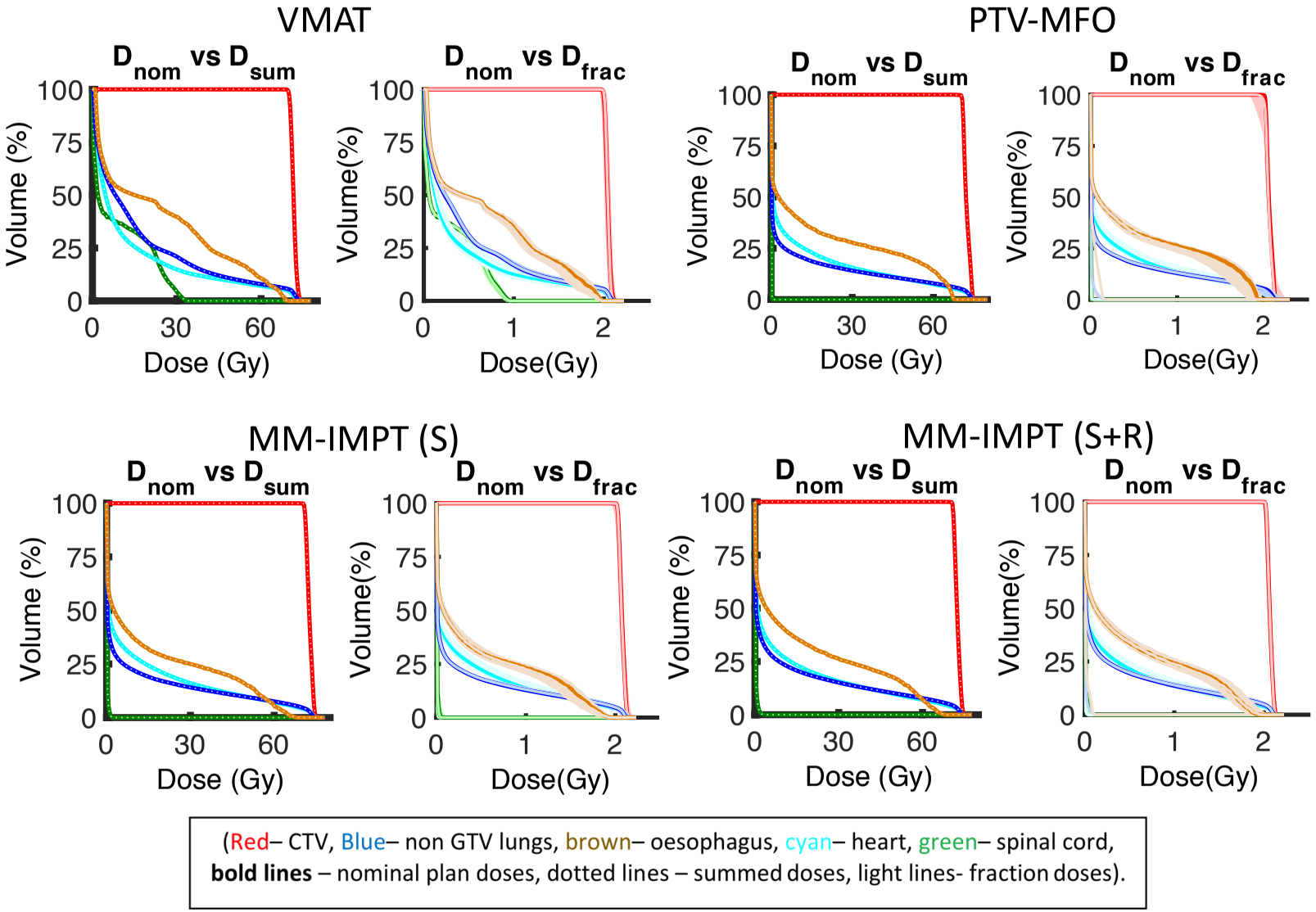


Figure 3.4: Dose volume histograms of Patient 10. Nominal versus summed dose distributions and nominal versus perturbed fraction dose distributions with different the treatment modalities.

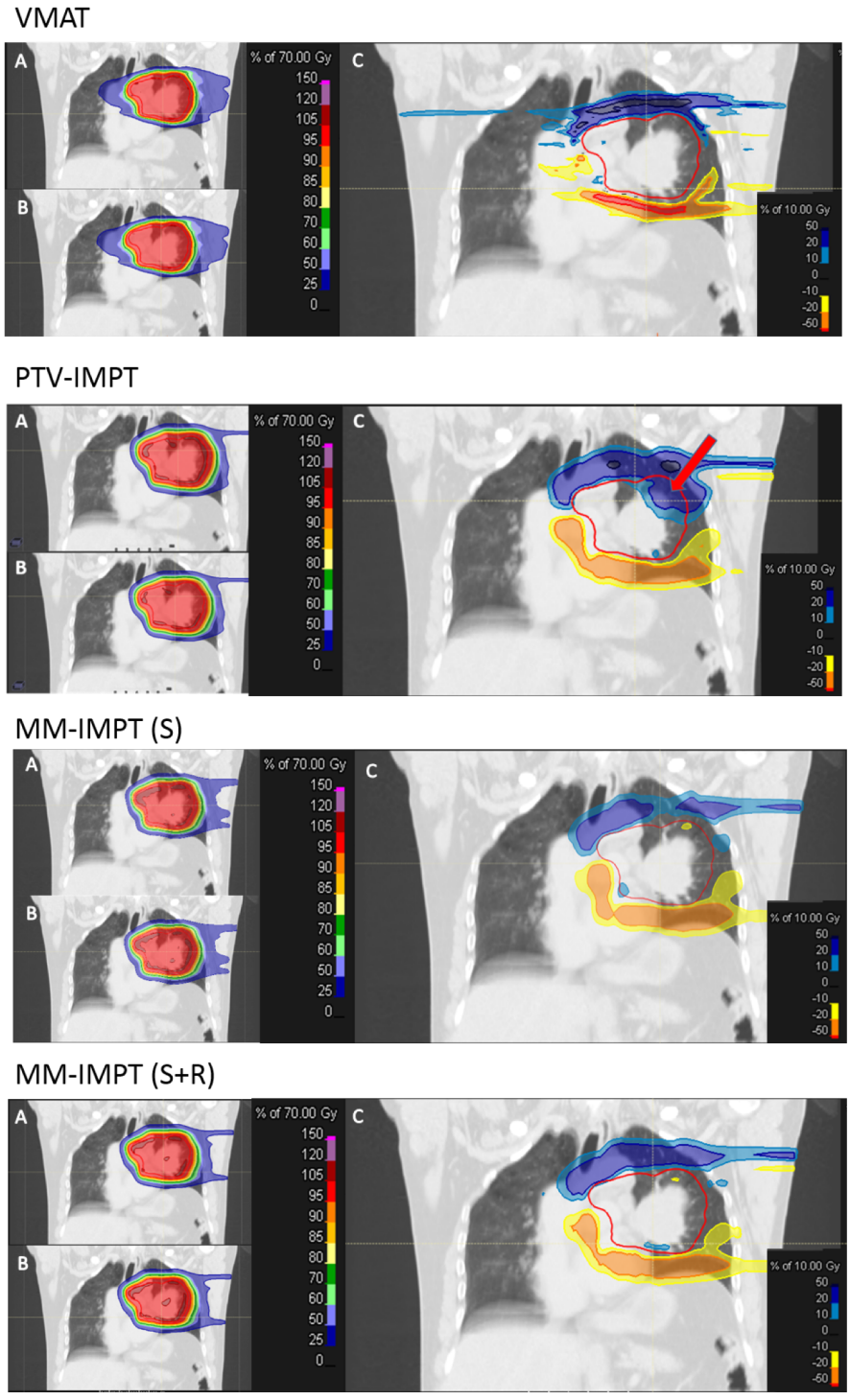


Figure 3.5: Coronal views of dose colour maps the nominal VMAT, PTV-IMPT and MM-IMPT (S) and MM-IMPT (S+R) plans of patient 10. CTV- red contour, A- nominal plan, B- summed dose distribution, C- difference in dose between nominal plan and sum dose distribution, red arrow indicates area of cold spot within CTV in PTV-IMPT plan.

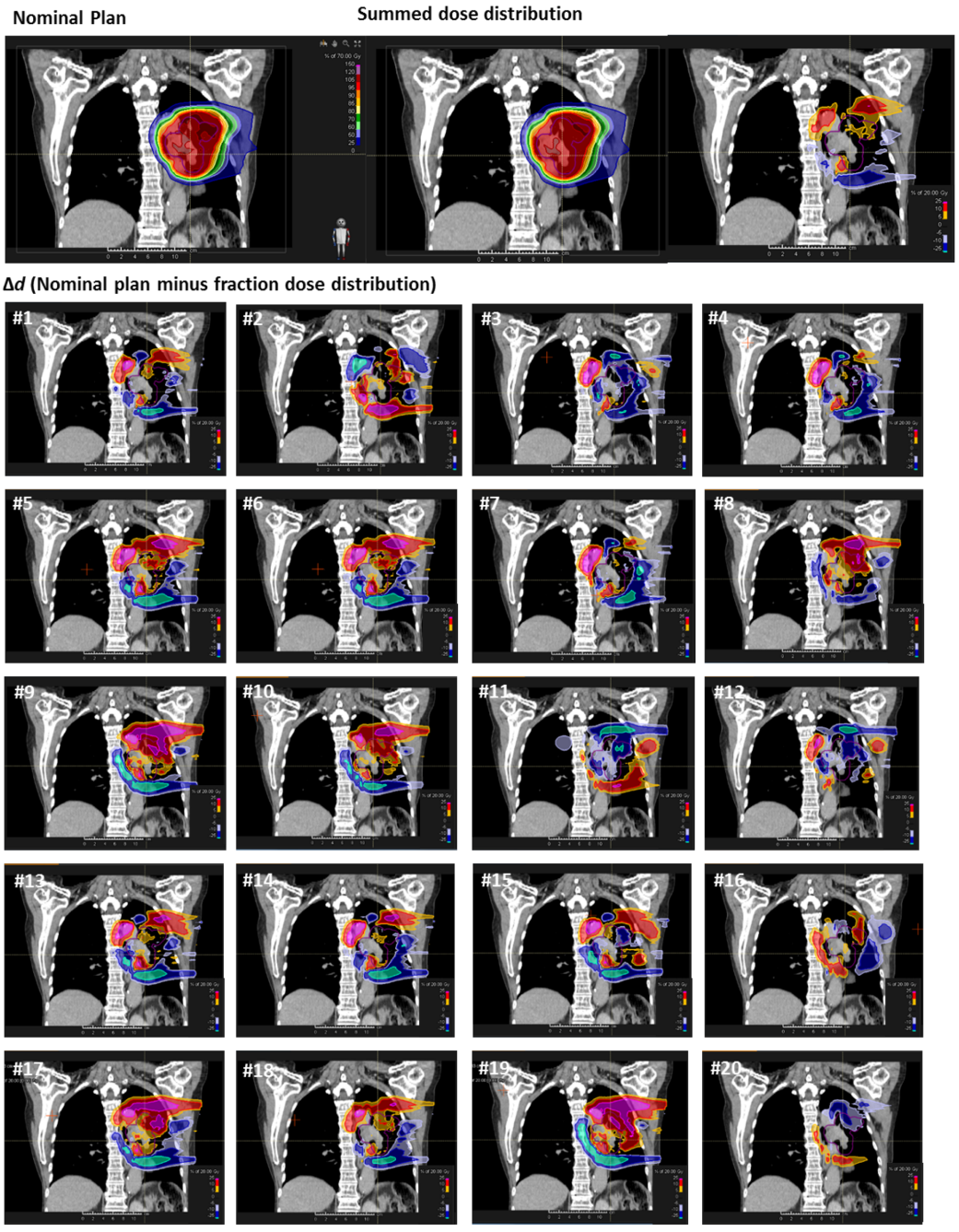


Figure 3.6: Coronal dose colour maps of patient 4 showing the nominal plan, summed and fraction dose distributions for a PTV-IMPT plan. Areas of under and over-dosage varied with each fraction such that when summed together, the summed dose distribution is similar to the nominal plan.

(cont.)

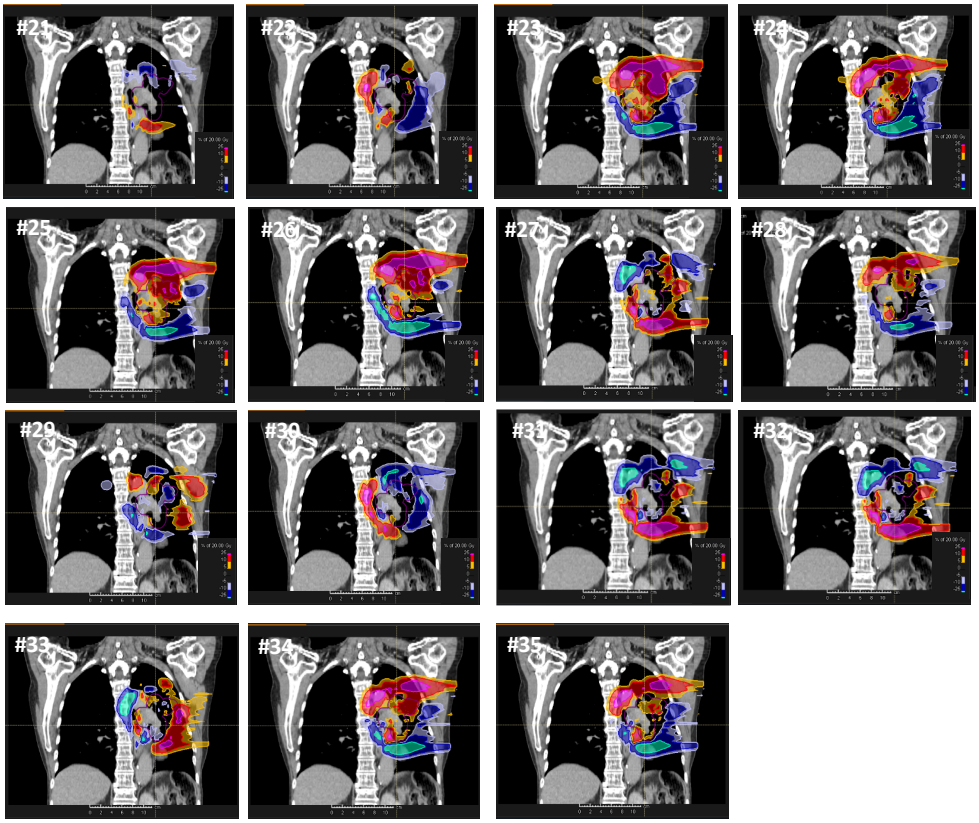


Figure 3.6: Coronal dose colour maps of a representative patient showing the nominal plan, summed and fraction dose distributions for PTV-IMPT plan. Areas of under and over-dosage varied with each fraction such that when summed together, the summed dose distribution is similar to the nominal plan.

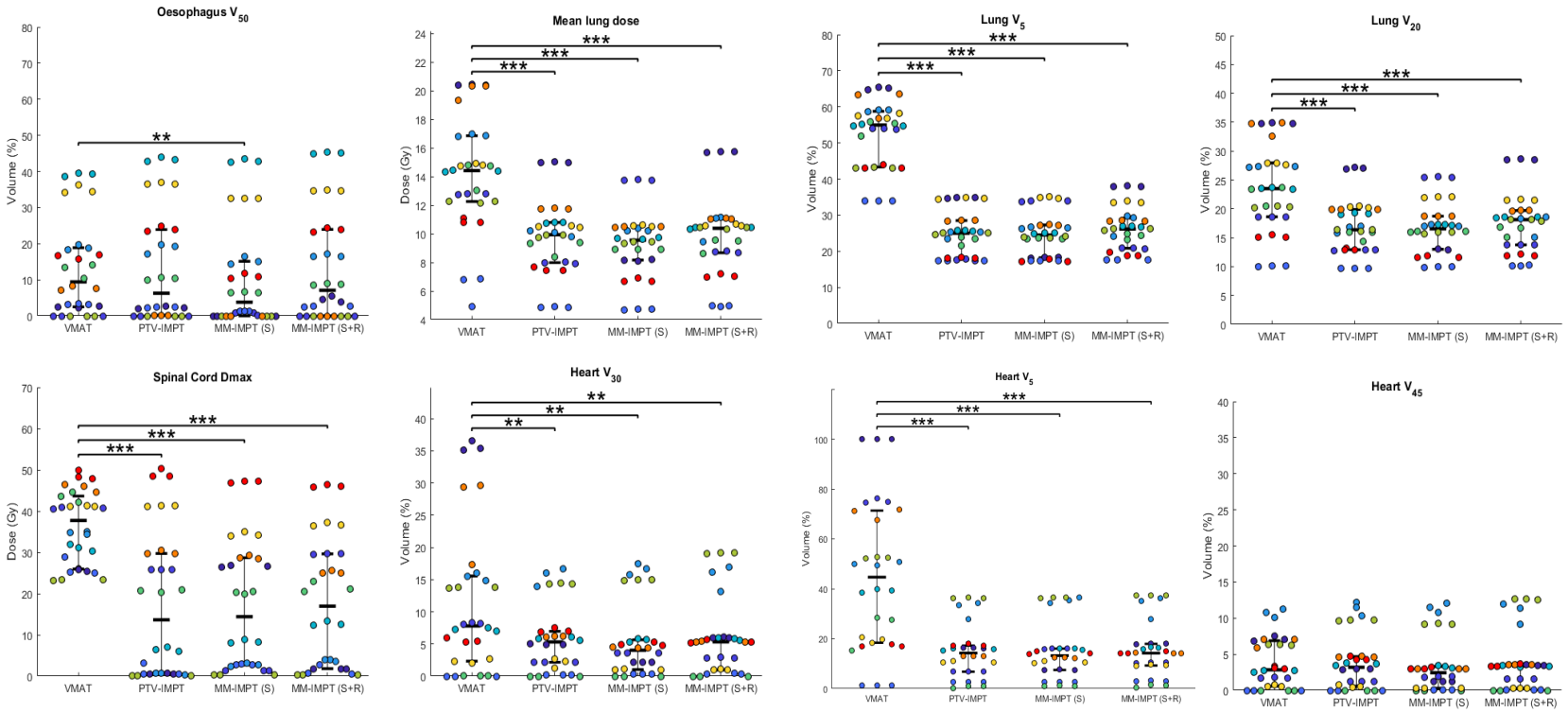


Figure 3.7: Comparison of OARs dose metrics in VMAT and IMPT D_{sum}. Each o represents a patient and the three simulations represented by a colour. The plots show that there was internal consistency in the OAR doses for each simulation.

, whiskers - 25th, 50th and 75th centiles, * - Wilcoxon signed-rank P<0.05, ***-P<0.0001)

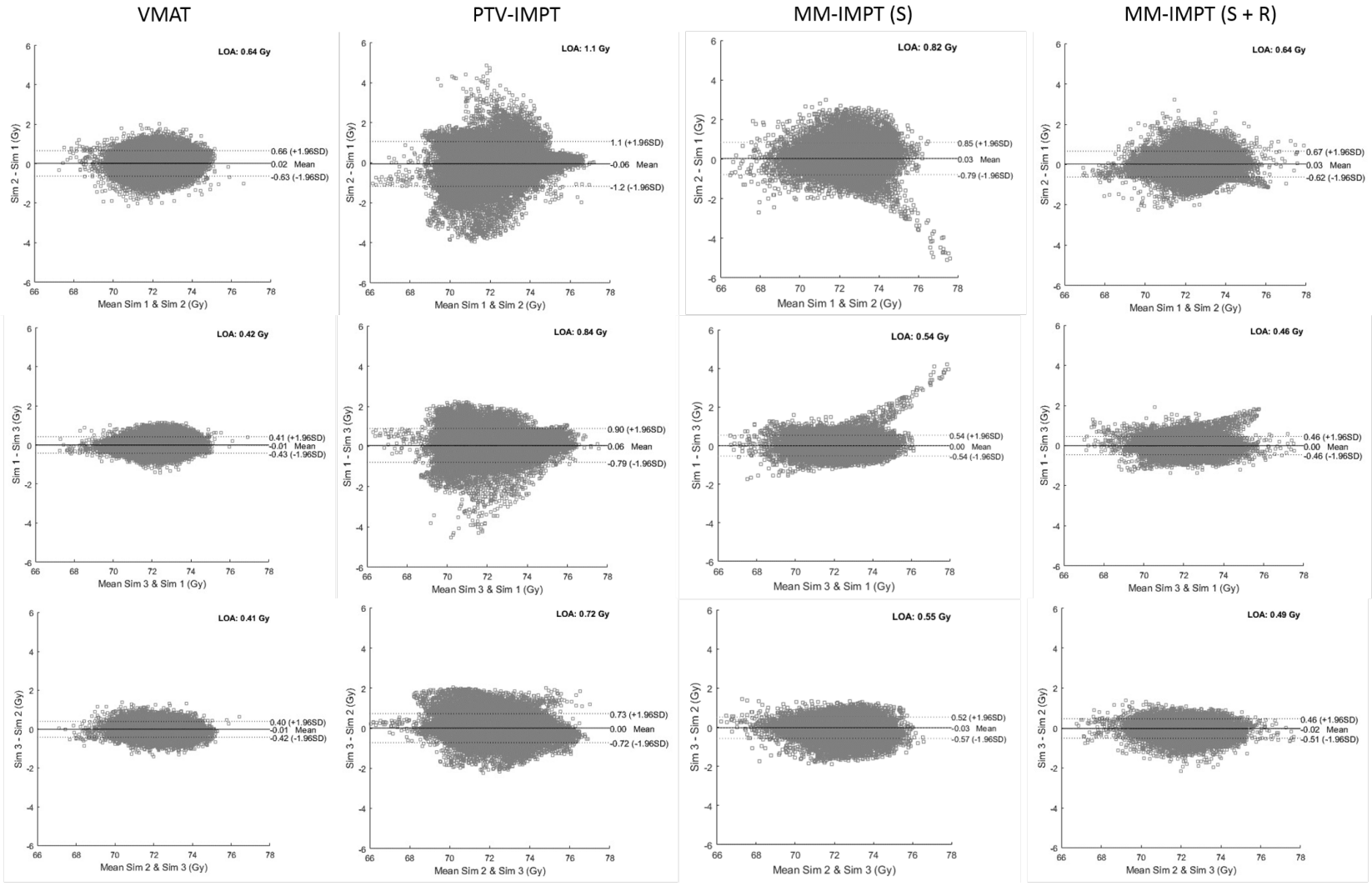


Figure 3.8: Bland-Altman plots comparing CTV voxel dose between simulations. (LoA - limits of agreement)

Chapter 4

Is an analytical dose engine sufficient for IMPT in lung cancer?

The British Journal of Radiology, 93(1107):20190583, 2020.

DOI: 10.1259/bjr.20190583

4.1 Abstract

Purpose/Objective

To identify a subgroup of lung cancer plans where the ADC algorithm may be clinically acceptable compared to MC dose calculation in IMPT.

Material/methods:

Robust-optimised IMPT plans were generated for twenty patients to a dose of 70Gy (RBE) in 35 fractions in Raystation. For each case, four plans were generated: three with ADC optimisation using the pencil beam algorithm (PB) followed by a final dose calculation with the following algorithms: PB (PB-PB), MC (PB-MC) and MC normalised to prescription dose (PB-MC scaled). A fourth plan was generated where MC optimisation and final dose calculation was performed (MC-MC). Dose comparison and gamma analysis (PB-PB vs PB-MC) at two dose thresholds were performed: 20% (D20) and 99% (D99) with PB-PB plans as reference.

Results:

Overestimation of CTVD99 and CTVmean was observed in all PB-MC compared to PB-PB plans (median: 3.7Gy (RBE) (5%) (range: 2.3 to 6.9 Gy (RBE)) and 1.8Gy (RBE) (3%) (0.5 to 4.6 Gy (RBE)). PB-MC scaled plans resulted in significantly higher CTVD2 compared to PB-PB (median difference: -4Gy (RBE) (-6%) (-5.3 to -2.4 Gy (RBE)), $p \leq 0.001$). The overall median gamma pass rates (3%-3mm) at D20 and D99 were 93.2% (range: 62.2 - 97.5%) and 71.3 (15.4 - 92.0%). On multivariate analysis, presence of mediastinal disease and absence of range shifters were significantly associated with high γ pass rates. Median D20 and D99 pass rates

with these predictors were 96.0% (range 95.3 - 97.5%) and 85.4% (75.1 - 92.0%). MC-MC plans were able to achieve similar target coverage and doses to OAR compared to PB-PB plans.

Conclusion:

In the presence of mediastinal involvement and absence of range shifters Raystation ADC may be clinically acceptable for treatment planning in lung IMPT. Otherwise, MC algorithm would be recommended to ensure accuracy of treatment plans.

4.2 Introduction

PBT is increasingly used in the treatment of a number of non-conventional tumour sites such as lung, breast and head and neck, both within and outside the context of clinical trials [118, 119]. Unfortunately, PBT is prone to multiple uncertainties [62]. One of these include the dose calculation algorithm within the treatment planning system (TPS). Currently, most proton therapy centres worldwide use a simplified ADC algorithm known as pencil beam algorithm to generate clinical plans. The analytical dose engine has the advantage of being fast. Until recently, fast commercially available MC-based TPS were not available. However, in the presence of tissue heterogeneity its accuracy is debatable [54, 55]. Unfortunately, there are limits to how the ADC algorithm model multiple Coulomb scattering [59]. Coulomb scattering describes different types of proton interactions in matter [56]. In inelastic Coulomb interaction, protons interact with atomic electrons. Most protons travel in a nearly straight line as the mass of an electron is much smaller than a proton. Here, kinetic energy is continuously loss. On the other hand, in elastic Coulomb interaction, a proton is deflected by the relatively large positively charged nucleus. This deflection causes a change in the trajectory of the proton. This interaction is responsible for determining the sharpness of the lateral penumbra. The TPS uses the so-called infinite slab approximation and therefore disregards lateral inhomogeneities for each individual ray traces. The inaccuracy is accentuated in lung cases as well as those with metal implants, bones or air cavities [120, 121]. This error tends to increase with the magnitude of air gaps, use of range shifters for shallow targets and treatment of small volumes requiring small fields [64, 122, 123].

A number of comparison studies have now been published assessing the accuracy of the ADC against MC simulations. Both Schuemann et al. and Bednarz et al. evaluated compared the ADC and MC in PBT delivered in the setting of PSPT

[121, 122]. In IMPT, a number of publications, comparing the Raystation ADC and MC have been published in homogenous, heterogenous and anthropomorphic phantoms [64, 65], and in breast and lung cancer clinical cases [66, 124]. Yepes et al. evaluated the Eclipse ADC against an in-house MC for IMPT in 5 different tumour sites in over 500 cases [125]. The overall conclusion of these studies was that MC algorithm was found to be more accurate compared to ADC in particular for thoracic tumours.

Despite the availability of a fast commercial MC algorithm, ADC remains the most widely used for treatment planning in PBT. Furthermore, although the commercial MC algorithm is faster than a general purpose MC algorithms, optimisation and dose calculations time is still longer compared to ADC algorithms. Given our understanding of the limitations and advantages of ADC, we aimed to identify if there are any clinical lung cases where the ADC would be acceptable for lung IMPT.

4.3 Results

4.3.1 Patient and plan characteristics

A summary of the patient characteristics along with the result of the γ analysis can be found in Table 4.1. GTV (primary and nodes) ranged from 15-404cc. The overall median pass rates of γ analysis for D20 and D99 at DT/DTA 3%/3mm were 93.2% (range: 62.2% - 97.5%) and 71.3 (15.4% - 92.0%).

Patient	GTV (cc)	CTV (cc)	TNM 8 staging	Average HU of CTV	Range Shifter	Mediastinal disease	γ pass rates, %	
							D20	D99
1	15	82	TxN2	-142.93	no	yes	96.02	75.13
2	261	502	T4N2	-135.03	no	yes	95.81	92.00
3	106	296	T2N0	-522.8	yes	no	62.16	15.40
4	25	96	TxN2	-319.72	no	yes	93.15	48.39
5	404	715	T4N0	-518.43	no	yes	95.26	91.42
6	50	194	T2N2	-378.6	no	yes	96.89	85.39
7	21	78	T4N0	-169.25	no	no	91.20	41.56
8	28	152	T1N2	-344.52	yes	yes	90.41	75.22
9	127	335	T2N2	-33.68	yes	yes	85.51	53.57
10	56	170	T3N0	-106.04	yes	no	80.10	29.72
11	46	295	T3N2	-78.28	yes	yes	94.52	67.53
12	50	238	T3N2	-377.44	no	yes	95.56	81.19
13	48	238	T2N3	-220.04	yes	yes	92.28	60.07
14	32	159	T3N0	-279.68	yes	no	86.02	60.91
15	115	252	T3/4 N1	-212.58	yes	yes	94.15	78.13
16	33	175	T2N1	-525.07	yes	yes	87.96	27.08
17	175	542	T3N2	-443.06	yes	yes	84.40	42.84
18	27	130	T2N0* T1N0*	-294.21	yes	no	89.72	47.40
19	306	603	T4N0	-206.26	no	yes	97.50	92.00
20	68	317	T4N3	-252.29	yes	yes	97.30	87.26

Table 4.1: Summary of tumour characteristics, use of range shifter and γ analyses pass rates. (HU - hounsfield units).

Metric	PB-PB	PB-MC	PB-MC (s)	MC-MC
CTV D99				
Median, Gy (%D_{pres})	70.0 (100)	66.3 (95)	70.0 (100)	70.0 (100)
Range, Gy	70.0-70.0	63.1-67.7	70.0-70.0	70.0-70.0
CTV mean				
Median, Gy (%D_{pres})	72.2 (103)	70.3 (100)	74.4 (106)	72.4 (104)
Range, Gy	71.2-73.6	67.6-71.8	71.1-75.6	71.8-73.8
CTV D2				
Median, Gy (%D_{pres})	74.5 (106)	74.0 (106)	78.5 (112)	74.7 (107)
Range, Gy	72.4-76.3	70.5-77.0	75.9-80.7	73.4-75.9

Table 4.2: CTV coverage of all plans with ADC compared to MC. (D_{pres} - dose relative to the prescribed dose of 70 Gy (RBE), PB-MC (s) - PB-MC scaled).

4.3.2 Dose to target

Underestimation of CTV D99 and CTV mean was observed in all PB-MC compared to PB-PB plans. Both over- and under-estimation were found for CTV D2 metric when PB-PB were compared with PB-MC plans. Median and range values of CTV coverage in the different plans can be found in Table 4.2. There were highly statistically significant differences in CTV D99 coverage between PB-PB and PB-MC plans and PB-PB and PB-MC scaled plans (both $p \leq .001$, see Figure 4.1). The overall median overestimation of CTV D99 and CTV mean was 3.7 Gy(RBE) (5%) (range: 2.3 to 6.9 Gy(RBE) (3 to 10%)) and 1.8 Gy(RBE) (3.1%) (0.5 to 4.6 Gy(RBE) (1 to 7%), see Table 4.3). Simple scaling of PB-MC plans resulted in significantly higher CTVD2 compared to PB-PB or PB-MC plans (median difference: 4 Gy(RBE) (6%), range: 2.4 to 5.3 Gy(RBE) (3-8%), $p \leq .001$, see Table 4.3). When PB-PB plans were compared to MC-MC plans, no statistically significant difference was found in CTV D99 coverage. Statistically, CTVD2 and mean dose to CTV were found to be significantly higher with MC-MC plans compared to PB-PB plans (CTV mean: median: -0.5 Gy(RBE) (-1%) (-0.8 to 0.6 Gy(RBE) (-1 to 1%), CTVD2: -0.3 Gy(RBE) (0%) (-1.4 to 1.0 Gy(RBE) (-2 to 1%)).

Metric	Difference in dose		
Gy (% D_{pres})	PB-PB – PB-MC	PB-PB – PB-MC (s)	PB-PB – MC-MC
Overall			
CTV D99			
Median	3.7 (5)	0.0 (0)	0.0 (0)
Range	2.3 to 6.9 (3 to 10)	0.0 to 0.0 (0 to 0)	0.0 to 0.0 (0 to 0)
CTV mean			
Median	1.8 (3)	-2.2 (-3)	-0.5 (-1)
Range	0.5 to 4.6 (1 to 7)	-3.2 to 1.4 (-5 to 2)	-0.8 to 0.6 (-1 to 1)
CTV D2			
Median	0.3 (0.4)	-4.0 (-6)	-0.3 (0)
Range	-1.6 to 3.1 (-2 to 4)	-5.3 to -2.4 (-8 to -3)	-1.4 to 1.0 (-2 to 1)
With predictors, n=7			
CTV D99			
Median	2.9 (4)	0.0 (0)	0.0 (0)
Range	2.3 to 4.1 (3 to 6)	0.0 to 0.0 (0 to 0)	0.0 to 0.0 (0 to 0)
CTV mean			
Median	0.7 (1)	-2.1 (-3)	-0.3 (0)
Range	0.5 to 1.7 (1 to 2)	-2.9 to -1.6 (-4 to -2)	-0.7 to 0.0 (-1 to 0)
CTV D2			
Median	-0.4 (-1)	-3.5 (-5)	-0.2 (0)
Range	-1.6 to 0.8 (-2 to 1)	-5.2 to -2.4 (-7 to -3)	-1.4 to 0.4 (-2 to 1)
The rest, n=13			
CTV D99			
Median	4.4 (6)	0.0 (0)	0.0 (0)
Range	3.2 to 6.9 (5 to 10)	0.0 to 0.0 (0 to 0)	0.0 to 0.0 (0 to 0)
CTV mean			
Median	2.5 (4)	-2.1 (-3)	-0.5 (-1)
Range	1.4 to 4.6 (2 to 7)	-3.2 to 1.4 (-5 to 2)	-0.8 to 0.6 (-1 to 1)
CTV D2			
Median	0.9 (1)	-3.9 (-6)	-0.4 (1)
Range	-1.5 to 3.1 (-2 to 4)	-5.3 to -3.2 (-8 to -5)	-1.3 to 1.0 (-2 to 1)

Table 4.3: Absolute and relative difference in dose to target between PB-PB and PB-MC, and PB-MC scaled plans. ($D_{pres}-$ dose relative to the prescribed dose of 70 Gy (RBE))

4.3.3 Dose to OAR

When comparing PB-PB and PB-MC plans, similar to the target, both over and under-estimation is observed outside the target. A summary of the absolute dose to OAR and observed differences can be found in Tables 4.4 and 4.5. There were a few cases where underestimation of dose occurred immediately distal to the target. For example, in patient 14, dose to the area distal to the target (Figure 4.2, pink arrow) was underestimated by at least 15 Gy, PB-PB vs PB-MC plans point dose from 25.8 to 44.8 Gy (RBE)). A separate area (red arrow) was underestimated by 9 Gy (RBE) (point dose: 58.2 to 67.6 Gy (RBE)).

In all cases, apart from one (patient 4), the OAR dose constraints were met in all the plan modalities. In patient 4, the oesophageal D1.5cc constraint was not met (PB-PB: 69.4 Gy (RBE), PB-MC: 72.1 Gy (RBE), PB-MC scaled 75.5 Gy (RBE), RTOG 1308 dose constraint oesophagus max dose: 74 Gy (RBE) $<$ 1.5cc). In patient 8, although the spinal cord Dmax constraint was met in all the plans, PB-PB plan underestimated the Dmax dose by 9.2 Gy (RBE) compared to PB-MC plan (Cord Dmax, PB-PB: 12.0 Gy (RBE), PB-MC: 21.3 Gy (RBE), PB-MC scaled: 22.3 Gy (RBE), MC-MC: 18.5 Gy (RBE)). A table summarising the absolute dose to the OAR for each plan can be found in the appendix.

Conversely, PB-MC scaled plans had significantly higher OAR doses compared to PB-PB plans (all $p<0.05$). There were no statistically significant difference in dose to OAR between PB-PB and MC-MC plans for the following OAR dose metrics: MHD, MLD, lung V5, lung V20, oesophagus D1.5cc and maximum dose to the spinal cord. Figure 2 shows a representative axial dose colour map of the 4 different treatment plans and DVHs. Simple scaling of PB-MC plan resulted in considerable hot spots within the CTV (see Figure 4.2C).

4.3.4 Predictors of high γ pass rates

Presence of disease in the mediastinum followed by absence of a range shifter were consistently the largest predictors for good agreement in the γ analysis between PB-PB and PB-MC plans in both univariate and multivariate analysis for D20 and D99 (see Table 4.6). The average CTV HU were marginally significant in the univariate analysis for D99 (P=.059).

High collinearity was observed between GTV and CTV (Pearson correlation r= 0.95), hence only GTV was included in the multivariate model. On multivariate analysis, presence of mediastinal involvement and absence of range shifter were significantly associated with higher γ pass rates for D20 (β = 9.75, 95% CI = 2.95 to 16.55 and β= -6.48, 95% CI = -12.48 to -.47 respectively, both P<.05, see Table 4.6). Similarly for D99, presence of mediastinal involvement and absence of range shifter were significantly associated with higher γ pass rates (β = 28.24, 95% CI = 9.99 to 46.49 and β = -20.31, 95% CI = -36.45 to -4.18 respectively, both P<.05).

Figure 4.3 shows that plans with mediastinal involvement and absence of range shifters were found to have higher D20 and D99 γ pass rates compared to those without these two predictors. Median D20 and D99 pass rates with these predictors were 96.0% (range 95.3-97.5%) and 85.4% (75.1-92.0%). Similarly, CTV coverage in PB-MC plans was observed to be superior when these predictors were present in a treatment plan (see Table 4.7). A summary of the absolute differences in CTV D99, mean and D2 coverage between the different plans with and without the predictors is found in Table 4.3. For comparison between PB-PB and PB-MC plans, the median difference in CTV D99 with predictors vs the rest of the plans were 2.9 Gy (RBE) (4%), (range: 2.3 to 4.1 Gy (RBE) vs 4.4 Gy (RBE) (6%), (3.2 to 6.9 Gy (RBE) and CTV mean 0.7 Gy (RBE) (1%) (0.5 to 1.7 Gy (RBE) vs 2.5 Gy (RBE) (4%) (1.4 to 4.6 Gy (RBE)). The median difference in CTV mean between PB-PB and PB-MC

scaled plans with predictors vs the rest of the plans were -2.1 Gy (RBE) (-3%) (-2.9 to -1.6 Gy (RBE) vs -2.1 Gy (RBE) (-3%) (-3.2 to 1.4 Gy (RBE)). Figures 4.4 and 4.2 illustrate the difference between ADC and MC dose calculations depending on whether plans have the associated predictors. In the absence of both mediastinal disease and use of range shifters, larger discrepancies were observed between the two dose distributions.

4.4 Discussion

Outcome of patients with locally advanced lung cancer is poor and PBT increasingly used due to the potential clinical benefit [70, 74, 126]. However, accuracy of treatment delivery is at the heart of radiotherapy and a number of reports have recently emerged regarding the limitations of the ADC algorithm especially in thoracic cancers [64, 65, 66, 124, 127]. Comparison studies between measurements in heterogeneous and anthropomorphic phantoms showed systematic overestimation of dose to parts of the target with ADC algorithm by up to 30% [64, 65]. Both Saini et al and Taylor et al found improved agreement with MC algorithm [64, 65]. Similarly, in ten clinical lung cases, Maes et al. found a median decrease in CTV V95% of 10% when ADC plans were recalculated using MC algorithm (Raystation 6 PB v4.0, MC v6.0, 0.5% statistical uncertainty, 10,000 ions/spot) [124]. Their reported median dose discrepancy in CTV coverage was higher compared to our study. This is likely to be due to differences in the individual patient cohort included in the studies (i.e. proportion of plans where range shifters were used and patients with mediastinal disease). In our case, 15 of 20 had mediastinal disease and eight plans did not utilise a range shifter. As well as overestimation, we observed underestimation within and outside the target. Although, the degree of underestimation tended to be small, we observed in one of the cases (patient 8), an underestimation of the Dmax to the spinal cord of

up to 9 Gy (RBE).

Our analysis showed that, although overestimation was observed in all cases, there was a subgroup of lung cancer plans where the difference between PB-PB and PB-MC plans may be clinically acceptable. In this group of patients, >95% of pixels passed the γ analysis (DT/DTA 3%/3mm - D20) with an average difference in CTV D99 coverage of 3.2% (maximum 6%). At DT/DTA 2%/2mm - D20, pass rates were >85% in these six plans (data not shown). Predictors found to be significantly associated with high γ pass rates on univariate and multivariate analyses include: plans requiring no range shifter with mediastinal involvement (see Table 4.6). On univariate analysis, higher CTV HU was marginally associated with higher γ pass rates at D99%. Our findings on the dose discrepancy between ADC and MC when range shifter is used is consistent with that of Widesott et al (Raystation 6, PB v4.0, MC v6.0, 0.5% statistical uncertainty) [123].

These findings are relevant as currently most proton therapy centres around the world still rely on ADC algorithm for treatment planning. ADC has the benefit of being fast compared to MC dose engines. Although, fast commercial MC TPS are becoming available, optimisation and dose calculation times are still longer compared to ADC. When tested on different tumour sites, with 1% statistical uncertainty, the final dose calculation times with Raystation MC could take as much as four times that of the pencil beam algorithm [64]. Liang et al, reported the time taken to generate an MC robust-optimised plan with 147 scenarios for a breast and regional lymph node case was 20 hours (200 iterations with 50,000 ions/spot). The PB plan took 1/4 of the time [66]. In our case, as an example, it took 50 minutes to optimise an MCMC robust-optimised plan for patient 2 with PB-PB plans taking only half the time (200 iterations with 10,000 ions/spot, 21 scenarios). Furthermore, although this study specifically reports on lung cancer cases, the findings could be applied to other tumour sites such as oesophagus where tumours tend to be located deep within the

mediastinum and use of range shifters could be avoided.

As previously described, simple scaling of dose to correct the underestimation of dose by PB-PB plans within the target would result in significant hotspots generated within the target as well as OAR (see Figure) [66]. Of all the cohort of patients included in the study, the maximum dose constraints to the target were met with the scaled plan. For OAR, as PBT was able to significantly reduce dose to surrounding organs compared to photon [126], there was only one patient where the oesophagus D1.5cc was exceeded with the scaled plan (patient 4). If these hotspots were located in serial organs, such as the spinal cord, they could potentially be detrimental. For other organs such as the heart, there is increasing evidence to show that exposure of high doses to small volumes could contribute to cardiac toxicity [40]. As it is difficult to predict where these hotspots might occur, solving the issue of overestimation by simple scaling would not be advisable. We note that although, statistically, CTVD2 and mean dose to CTV were found to be significantly higher with MC-MC plans compared to PB-PB plans, these differences were not clinically relevant (see Table 4.2 for median and range values of CTV coverage). Doses to OAR were generally over-estimated by the ADC algorithm, however, we observed that there were a number of cases where under-estimation of dose occurred at potentially clinically relevant dose levels. Figure 4.2E showed an area of underestimation of at least 15 Gy distal to the target (pink arrow, PB-PB vs PB-MC plans point dose from 25.8 to 44.8 Gy (RBE)). The potential biological effect of the dose underestimation would need to be considered individually as it is dependent on which OAR the dose is deposited. For this particular case, dose to the right atrium was markedly underestimated which could increase risk of cardiac toxicity [126]. In view of this, caution needs to be taken when using ADC when an OAR is immediately distal to the target as the dose underestimation could then be of clinical relevance.

There are a number of limitations to our study. Firstly, only twenty cases were

evaluated. However, despite the number, we were able to identify statistical significance in both the univariate and multivariate analysis for predicting high agreement between PB-PB plans and PB-MC plans. This was due to the large effect of the predictors. These predictors are consistent with what is known to be limitations of the ADC algorithm.

Another limitation to our study is that these findings are specific to the Raystation PB algorithm investigated and as such is not generalizable to other ADC algorithms. Therefore, validation of other ADC dose engines would need to be performed. Interestingly, although overestimation of up to 10% was observed by Yepes et al., dependence on presence of range shifter was not observed when the Eclipse ADC algorithm was evaluated [125]. Similarly, Winterhalter et al. did not see dependence when using a pre-absorber when evaluating their pencil beam or ray-casting algorithms [128].

Our evaluation has specifically focused on the uncertainties based on the dose calculation algorithm. We recognize that this is only one aspect of thoracic PBT plan that needs to be considered. Careful considerations to the robustness of a lung plan against the interplay effect, setup and range uncertainties also need to be accounted for. While robust optimisation would reduce most of the plan sensitivities against setup and range uncertainties, the interplay effect would need to be mitigated by strategies such as rescanning [51]. Furthermore, it is known that the limited spatial resolution of current clinical planning CT could impact the dose predicted by the TPS especially in highly heterogenous lung tissue [129]. However, as both dose algorithms rely on the same planning CT, the magnitude of error is likely to be the same in both algorithms.

In conclusion, we have identified a sub-group of lung cases where the Raystation ADC may be clinically acceptable for treatment planing in thoracic PBT. Key to this is understanding the limitations of the ADC algorithm used. In the presence of mediastinal involvement and absence of range shifters ADC maybe clinically acceptable

for treatment planning in lung IMPT. Without these features, the Raystation MC algorithm would be recommended to ensure accuracy of treatment plans.

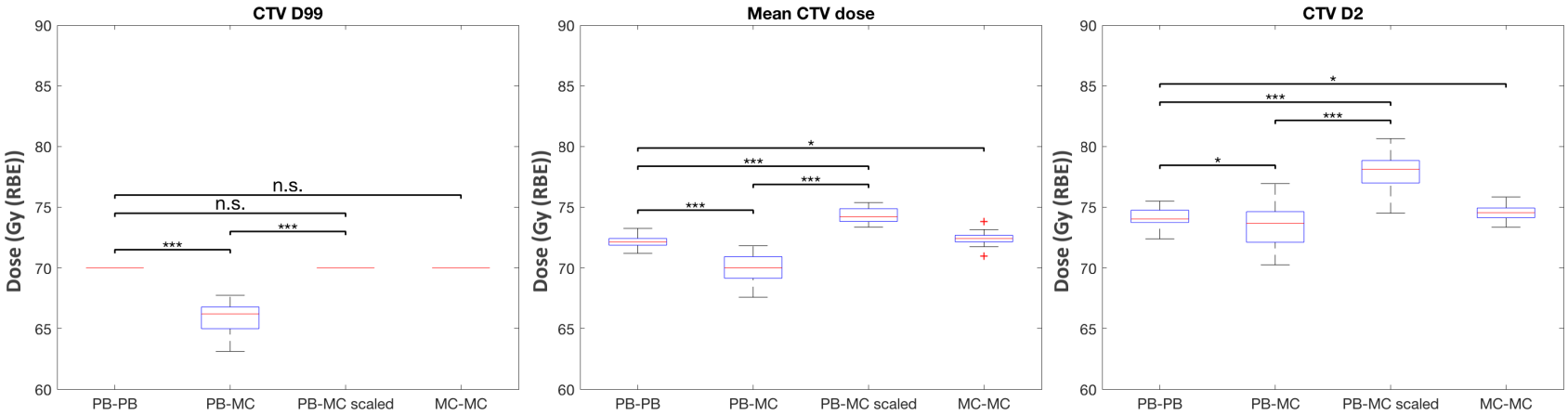


Figure 4.1: Boxplots of CTV coverage. (* - P≤.05, *** - P≤ .001, n.s.- not statistically significant)

Metric	PB-PB (range)	PB-MC (range)	PB-MC (s) (range)	MC-MC (range)	P-values			
					PB-PB vs PB-MC	PB-PB vs PB-MC (s)	PB-MC vs PB-MC (s)	PB-PB vs MC-MC
MHD (Gy (RBE))	4.5 (0.1-14.2)	4.3 (0.1-13.5)	4.6 (0.1-15.0)	4.7 (0.1-14.1)	0.001	<0.001	<0.001	0.765
MLD (Gy (RBE))	10.9 (5.1-16.6)	10.8 (5.1-16.2)	11.5 (5.4-17.7)	11.8 (5.7 - 17.9)	0.057	<0.001	<0.001	0.370
Lung V20 (%)	19.4 (10.4-29.7)	19.3 (10.5-29.4)	20.4 (10.9-30.3)	20.4 (10.5-32.5)	0.550	<0.001	<0.001	0.411
Lung V5 (%)	27.8 (17.4-45.4)	28.0 (17.6-45.9)	28.4 (17.8-46.3)	30.7 (17.8-46.3)	0.001	<0.001	<0.001	0.411
Oesophagus D1.5cc (Gy (RBE))	56.2 (0.0-71.5)	54.7 (0.0-71.7)	57.4 (0.1-75.8)	55.7 (0.1-73.6)	0.023	0.001	<0.001	0.185
Spinal cord Dmax (Gy (RBE))	22.1 (0.5-45.2)	21.3 (0.5-46.1)	22.3 (0.5-49.5)	25.9 (0.7-46.8)	0.108	<0.001	<0.001	0.737

Table 4.4: OAR doses with ADC compared to MC

Median (range)	Difference in dose		
	PB-PB – PB-MC	PB-PB – PB-MC (s)	PB-PB – MC-MC
MHD (Gy (RBE))	0.1 (-0.1 to 0.7)	-0.2 (-0.8 to 0.0)	-0.5 (-1.4 to 2.7)
MLD (Gy (RBE))	0.1 (-0.2 to 0.6)	-0.6 (-1.2 to -0.3)	-0.9 (-2.2 to 0.9)
Lung V20 (%)	0.0 (-0.3 to 0.7)	-0.5 (-1.2 to 0.0)	-1.1 (-3.1 to 2.4)
Lung V5 (%)	-0.4 (-2.0 to 0.3)	-0.7 (-2.8 to 0.0)	-1.8 (-7.3 to 0.3)
Oesophagus D1.5cc (Gy (RBE))	0.7 (-2.7 to 3.1)	-2.1 (-6.1 to 1.4)	-0.2 (-5.3 to 6.7)
Spinal cord Dmax (Gy (RBE))	-0.4 (-9.2 to 2.9)	-2.0 (-10.2 to 1.9)	-1.0 (-8.5 to 2.9)

Table 4.5: Absolute difference in dose to OAR between PB-PB and PB-MC, and PB-MC scaled plans. (PB-MC (s) - PB-MC scaled).

Variables	Co-efficient (β)	SE	95% CI	P value
Univariate analysis - D20 3%/3mm				
GTV	.01	.02	-.03 to .05	.624
CTV	.01	.01	-.02 to .03	.729
Mediastinal disease	11.47	3.48	4.17 to 18.78	.004
Range shifter	-8.51	3.34	-15.52 to -1.50	.020
Average CTV HU	.01	.01	-.15 to .04	.373
Multivariate analysis - D20 3%/3mm				
Mediastinal disease	9.75	3.22	2.95 to 16.55	.008
Range shifter	-6.48	2.85	-12.48 to -.47	.036
GTV	.08	.05	-.02 to .18	.102
CTV	.04	.03	-.02 to .10	.156
Mediastinal disease	33.66	9.72	13.24 to 54.07	.003
Range shifter	-26.20	9.21	-45.55 to -6.85	.011
Average CTV HU	.07	.03	-.00 to .138	.059
Multivariate analysis - D99 3%/3mm				
Mediastinal disease	28.24	7.65	9.99 to 46.49	.005
Range shifter	-20.31	8.65	-36.45 to -4.18	.017

Table 4.6: Univariate and multivariate analysis for γ pass rates with D99 dose at DT/DTA 3%/3mm. PB-PB plans (reference dose) were compared to PB-MC (SE-standard error of β, 95% CI - 95% confidence interval, HU - hounsfield unit)

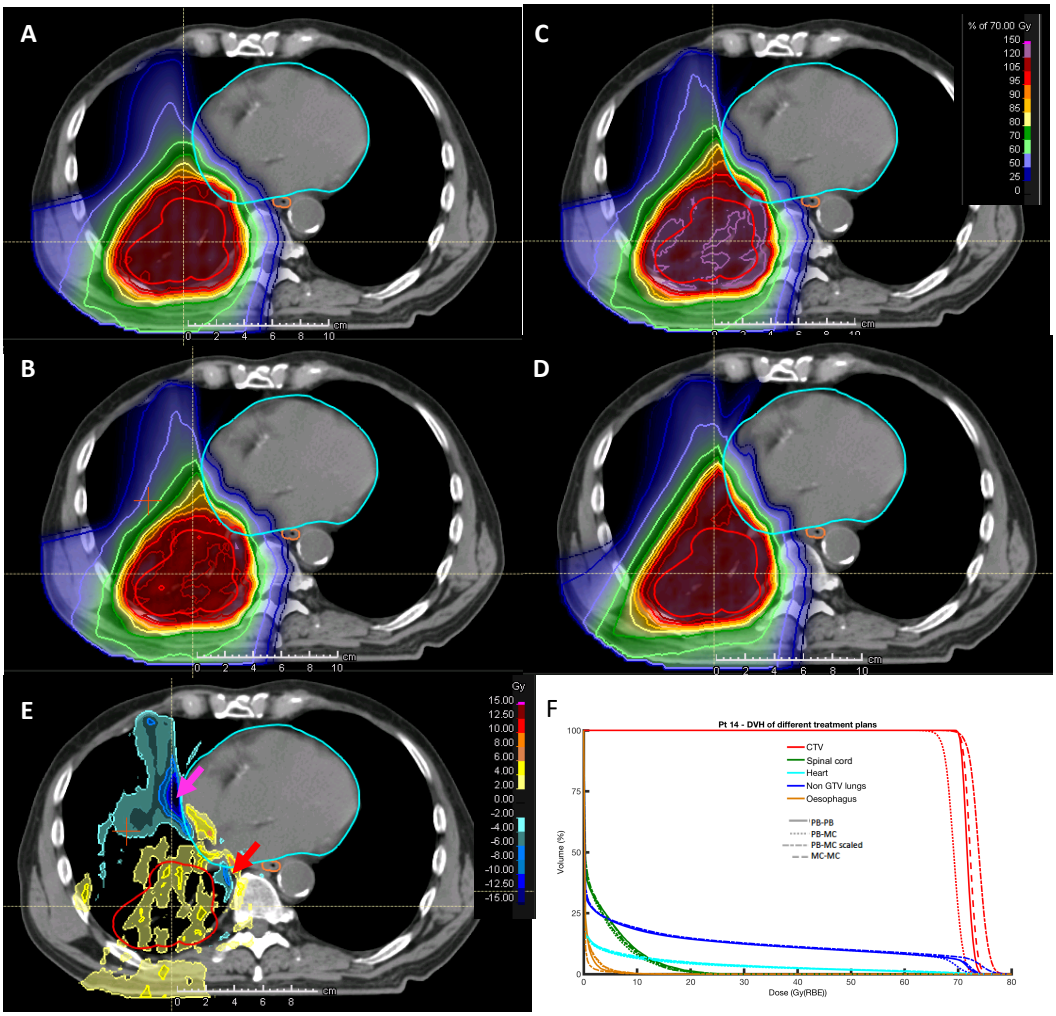


Figure 4.2: Axial dose colour map and DVH of PB-PB vs PB-MC plan of patient 14. The GTV was 32cc, stage T3N0 with range shifter used. A- PB-PB, B- PB-MC, C- PB-MC scaled, D- MC-MC plans. E- Dose difference between PB-PB and PB-MC (A minus B). In PB-MC plan, dose overestimation observed in CTV. F- DVH of all four plans. Red and pink arrows indicate area of underestimation by PB-PB plan compared to PB-MC plan. (Red region of interest (ROI) - CTV, Cyan ROI - heart, Orange ROI - oesophagus).

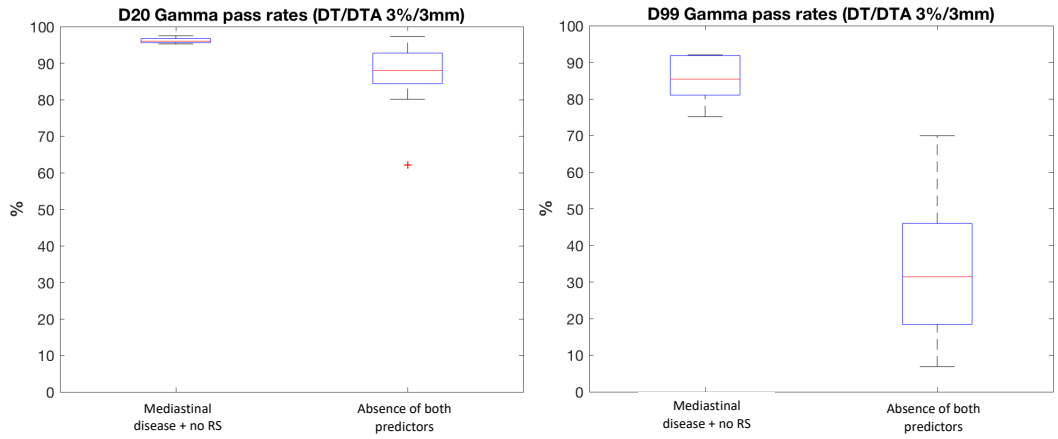


Figure 4.3: Boxplots of γ analyses pass rates showing higher pass rates in plans with mediastinal involvement and absence of range shifter.

Metric Gy (% D_{pres})	PB-PB	PB-MC	PB-MC (scaled)
Absence of RS + mediastinal disease, n=7			
CTV D99			
Median	70.0 (100)	67.1 (96)	70.0 (100)
Range	70.0 - 70.0	66.0 – 67.7	70.0 - 70.0
CTV mean			
Median	72.0 (103)	71.2 (101)	74.5 (106)
Range	71.8 – 72.4	70.4 – 71.7	73.6 – 74.7
CTV D2			
Median	74.0 (106)	74.5 (106)	78.1 (112)
Range	73.6 – 75.2	73.7 – 75.6	76.9 – 78.8
The rest, n=13			
CTV D99			
Median	70.0 (100)	65.4 (93)	70.0 (100)
Range	70.0 - 70.0	63.1 – 66.5	70.0 - 70.0
CTV mean			
Median	72.4 (103)	69.4 (99)	74.4 (106)
Range	71.2 – 73.6	67.6 – 71.1	71.1 – 75.6
CTV D2			
Median	74.7 (107)	73.0 (104)	78.8 (113)
Range	72.4 – 76.3	70.5 – 75.1	75.9 – 79.8

Table 4.7: CTV coverage with ADC compared to MC in plans stratified according to presence of predictors (associated predictors based on multivariate analysis for high γ passing rates are absence of range shifter and presence of mediastinal involvement. (D_{pres}− dose relative to the prescribed dose of 70 Gy (RBE))

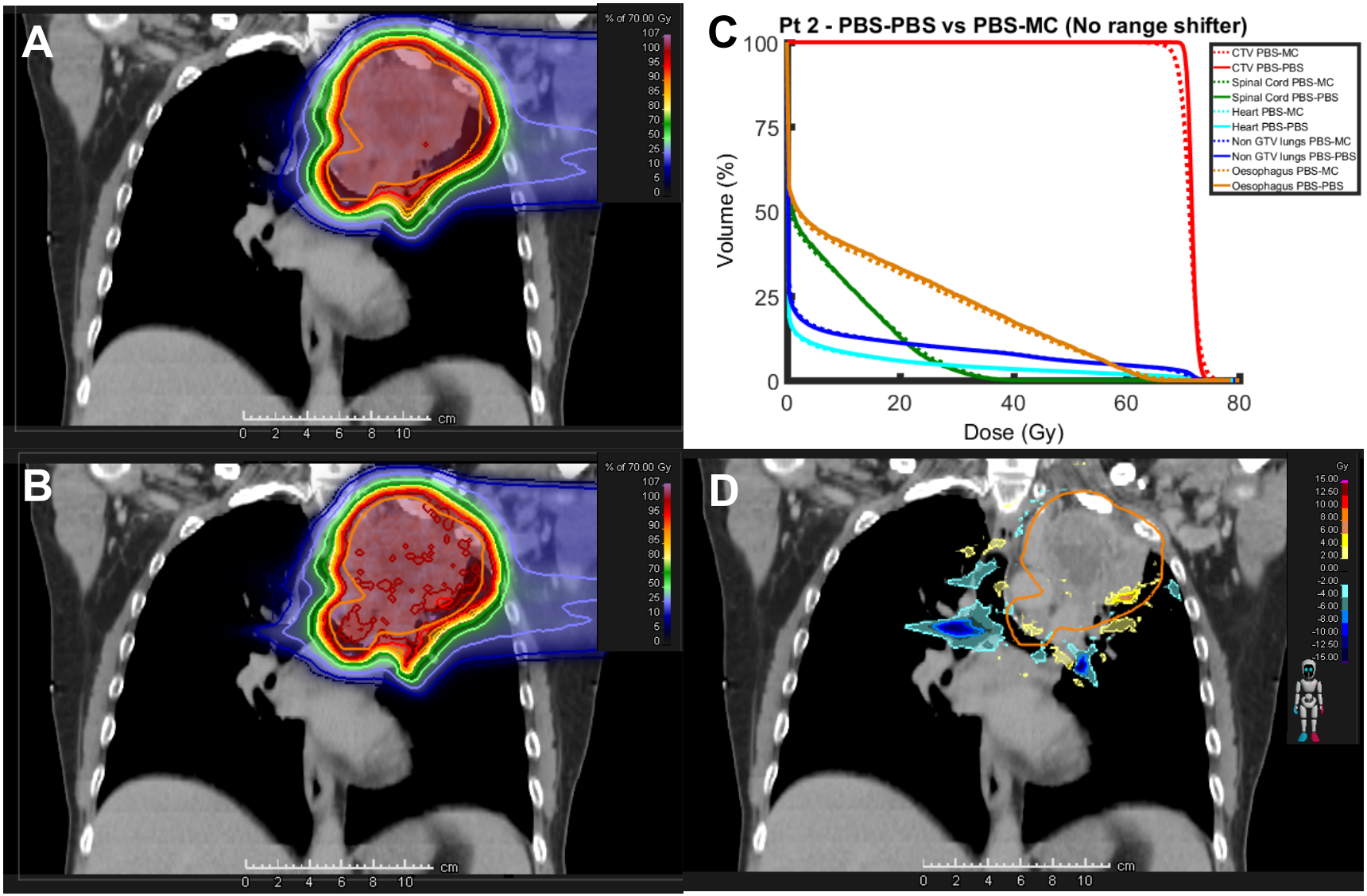


Figure 4.4: Coronal dose colour map and DVH of PB-PB vs PB-MC plan of patient 2. The GTV was 261cc, stage T4N2 and no range shifter was used. A & B coronal dose colour maps of PB-PB and PB-MC plans respectively, C - DVH of both plans, D - Difference dose colour map between PB-PB and PB-MC plans (PB-PB minus PB-MC plan).

Chapter 5

Proton vs photon: A model-based approach to patient selection for reduction of cardiac toxicity in locally advanced lung cancer

Article-in-press for publication in Radiotherapy and Oncology, August 2019

DOI: 10.1016/j.radonc.2019.06.032

5.1 Abstract

Purpose/Objective

To use a model-based approach to identify a sub-group of patients with locally advanced lung cancer who would benefit from proton therapy compared to photon therapy for reduction of cardiac toxicity.

Material/methods:

VMAT and robust-optimised IMPT plans were generated for twenty patients with locally advanced lung cancer to a physical dose of 70 Gy (RBE) in 35 fractions. Cases were selected to represent varying anatomical locations of disease. Contouring, treatment planning and organs-at-risk constraints followed RTOG-1308 protocol. Whole heart and sub-structure doses were compared. Risk estimates of grade $\geq$3 cardiac toxicities were calculated based on normal tissue complication probability (NTCP) models which incorporated dose metrics and patients' baseline risk-factors (RF) (pre-existing cardiac disease (CD)).

Results:

There was no statistically significant difference in target coverage between VMAT and IMPT. IMPT delivered lower doses to the heart and cardiac substructures (mean, heart V5 and V30, $P<.05$). In VMAT plans, there were statistically significant positive correlations between heart dose and thoracic vertebral level that coincided with the lower limit of disease. The median level at which the superior aspect of the heart contour began was T7 vertebrae. There was a statistically significant difference in dose (mean, V5 and V30) to the heart and all substructures (except mean dose to left coronary artery and V30 to sino-atrial node) when disease overlapped with or was inferior to T7 vertebrae. In the presence of pre-existing CD and disease overlapping

with or inferior to T7 vertebrae, the mean estimated relative risk reduction of grade $\geq$3 toxicities were between 24-59%.

Conclusion:

Reduction in cardiac toxicity is expected with IMPT compared to VMAT by lowering dose exposure to the heart and substructures. Patients with both pre-existing heart disease and tumour and nodal spread overlapping with or inferior to T7 vertebrae are likely to benefit most from proton over photon therapy.

5.2 Introduction

The hypothesise of this part of the thesis is that PBT could reduce dose to the heart and its substructures and therefore reduce cardiac complications without compromising tumour control in patients with locally advanced lung cancer. The study aim was to identify a sub-group of patients who would benefit from IMPT over photon VMAT with respect to cardiac sparing. Identification of this sub-group would ultimately be useful in informing future clinical trial design of proton vs photon therapy in locally advanced lung cancer.

5.3 Results

A summary of the anatomical distribution of the primary disease and the lymph node involvements along with the TNM 8 staging included in this study can be found in Table 5.1. An illustration of all the disease locations on a coronal view can be found in Figure 5.1. GTV (primary and nodes) ranged from 15 - 404 cc. The majority of patients had stage III (16/20). Out of 16, 4 had T4N0 disease. These patients do not have nodal involvement but two had large tumours with mediastinal invasion (patient 5- GTV 404 cc, patient 19- GTV 306 cc), one had pericardial invasion (patient 7) and one was classified as stage III due to the presence of two tumours in the ipsilateral lung (patient 18). There was no statistically significant difference in target coverage between VMAT and IMPT. Three of twenty patients had stage II disease (patient 3, 10 and 18). There was no statistically significant difference in conformity indices (95% isodose volume/ CTV volume) between VMAT and IMPT plans (VMAT vs IMPT, median (range): 1.92 (1.47 to 2.64) vs 2.03 (1.33 to 2.80), P= .351).

5.3.1 Heart dose

There was a statistically significant lower dose to the heart and all its substructures with IMPT compared to VMAT (P<.05). MHD increased as the disease extended further down the thoracic vertebrae levels in VMAT plans with similar observations seen with heart V5 and V30. This correlation was statistically significant in VMAT plans (MHD, V5 and V30; ρ=.67, .79, .48, P<.05), but not in IMPT plans (see Table 5.2). A similar trend was seen in VMAT plans for the atria (left and right, ρ=.65 and.58, P<.01) and ventricles (left and right, ρ=.68 and .64, P<.005). This association was not observed for cardiac structures that are immediately adjacent to the T7 thoracic vertebrae (SA node, RCA, LCA, ρ=.25, .41 and .29, P=ns).

Difference in MHD between VMAT and IMPT increased the lower the disease

Patient	GTV (cc)	CTV (cc)	TNM 8 staging	Primary tumour locations	IASLC Lymph node stations	Disease extension (thoracic vertebrae level)
1	15	82	TxN2	-	5	6
2	261	502	T4N2	LUL	7, 10L	5
3	106	296	T2N0	RML	-	10
4	25	96	TxN2	-	10R, 4R	6
5	404	715	T4N0	LUL	-	8
6	50	194	T2N2	RUL	4R	6
7	21	78	T4N0	RUL	-	7
8	28	152	T1N2	LUL	10L, 4L	7
9	127	335	T2N2	RUL	10R, 7	9
10	56	170	T3N0	LLL	-	11
11	46	295	T3N2	LLL	7, 10L	9
12	50	238	T3N2	RLL	4R	8
13	48	180	T2N3	LUL	7, 10R	8
14	32	159	T3N0	RLL	-	10
15	115	252	T3/4 N1	RLL	10R	8
16	33	175	T2N1	LLL	10L	9
17	175	542	T3N2	RLL	7, 8	11
18	27	130	T2N0* T1N0*	LLL	-	10
19	306	603	T4N0	RLL	-	10
20	68	317	T4N3	LLL	4L, 4R, 2Rx2	9

Table 5.1: Details of the twenty proxy cases. (GTV - gross tumour volume (includes primary and nodal spread), IASLC - International Association for the Study of Lung Cancer, LUL - left upper lobe, LLL - left lower lobe, RUL - right upper lobe, RML - right middle lobe, RLL - right lower lobe, * - 2 separate primary tumour nodules found in left lung

(tumour and nodal involvement) extended with reference to the thoracic vertebrae (see Figure 5.2). The absolute and difference in dose between VMAT and IMPT to the heart, its substructures and other OAR for each case are shown in Figures 5.3 and 5.4.

The median level at which the most superior aspect of the heart contour started was T7 vertebra (range: T6 - T8). The difference in MHD between VMAT and IMPT approached 5 Gy (RBE) when the inferior part of disease overlapped with T7 vertebra. In this patient group, there was a statistically significant difference in dose (mean, V5 and V30, $P<.05$) to the heart and all substructures between VMAT and

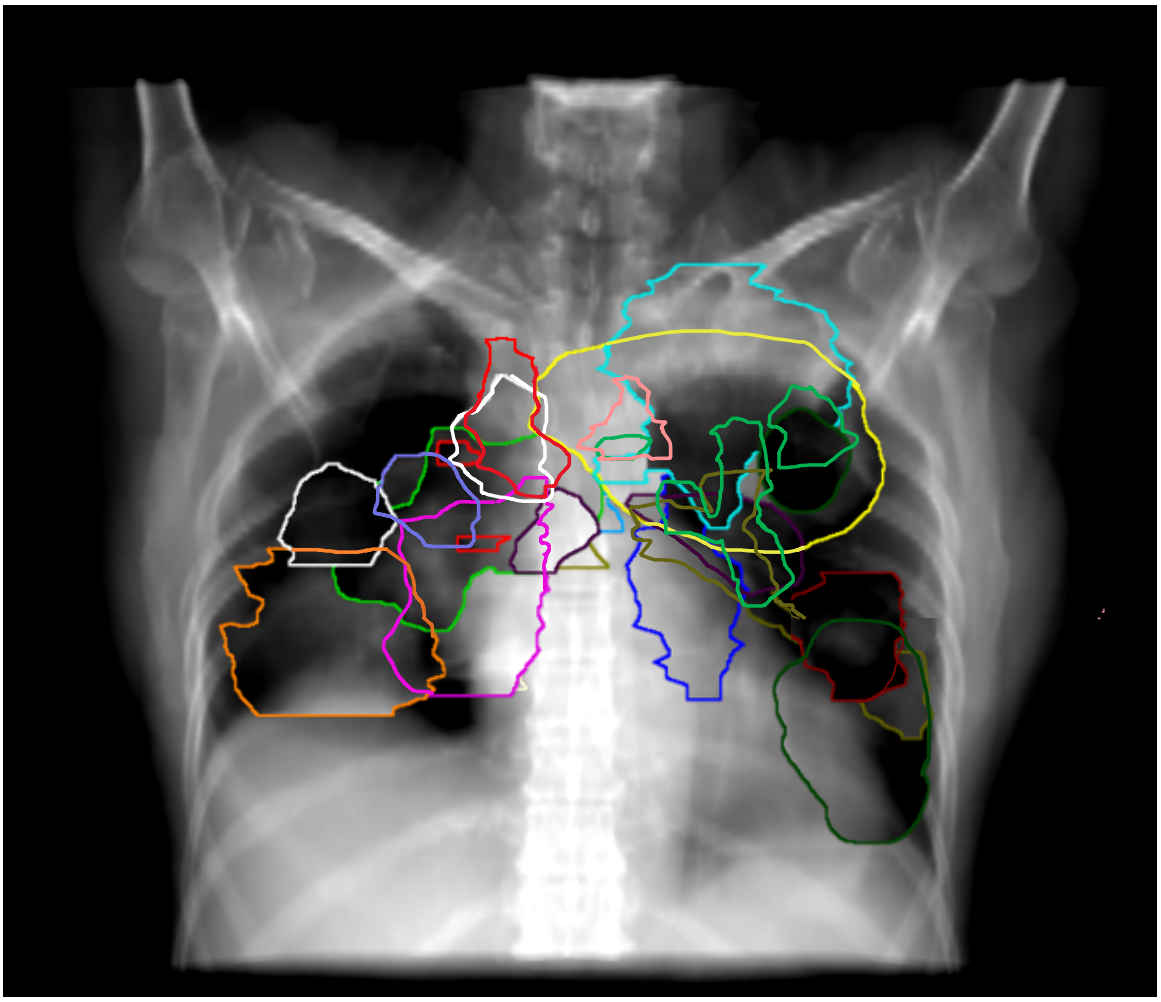


Figure 5.1: Coronal view of disease location of cases included in study

IMPT, except mean dose to LCA and V30 to SA node. There was no significant difference in V50 for this group of patients or the whole cohort of patients. There was no significant difference in dose to the whole heart or substructures for any of the dose metrics evaluated (mean, V5, V30 and V50) when the most inferior part of disease did not overlap with T7 vertebrae. Tables 5.3 and 5.4 shows a summary of the dose indices.

		VMAT		IMPT	
OAR	Metric	Spearman's ρ	P	Spearman's ρ	P
Heart	MHD	.67	.001	.40	.08
	V30	.48	.032	.40	.084
	V5	.79	<.001	.35	.131
RA	Mean	.65	.002	.25	.297
LA	Mean	.58	.007	.35	.135
RV	Mean	.68	.001	.17	.484
LV	Mean	.64	.002	.36	.115
RCA	Mean	.41	.07	-.04	.856
LCA	Mean	.29	.221	-.12	.620
SA node	Mean	.25	.298	.16	.504

Table 5.2: Summary of Spearman's correlation between heart dose and thoracic vertebrae level in VMAT and IMPT. (RA- right atrium, LA- left atrium, RV- right ventricle, LV- left ventricle, RCA- right coronary artery, LCA- left coronary artery, SA node- sino-atrial node)

5.3.2 Risk of toxicities

The risk of cardiac toxicity was highest in the presence of pre-existing CD and when the disease overlapped with or was inferior to T7 vertebrae. A summary of the absolute and relative risk reduction for the different scenarios can be found in Table 5.5. For the patients in the highest risk group, the relative risk reduction (RRR) between proton and photon therapy based on MHD, V5 and V30 were 38% (95%CI 30-46%), 59% (50-67%) and 24% (13-36%) see Figure 5.5). Similar RRR were observed in the absence of pre-existing CD. However, the absolute benefit was more than twofold lower for IMPT. There was limited RRR if the tumour did not extend below T7 vertebrae (RRR range:0-16%). Risk estimates of each individual case can be found in 5.6.

OAR	Metric	VMAT (range)	IMPT (range)	P value
To and below T7 vertebrae				
Heart	Mean (Gy (RBE))	16.7 (5.9-37.4)	6.5 (0.7-14.1)	<.001
	V50 (%)	5 (0-24)	5 (0-14)	.691 (NS)
	V30 (%)	19 (0-100)	9 (0-20)	.001
	V5 (%)	70 (39-100)	20 (5-34)	<.001
RA	Mean (Gy (RBE))	17.7 (3.2-54.0)	2.2 (0-42.0)	.001
	V50 (%)	0 (0-57)	0 (0-46)	.374 (NS)
	V30 (%)	12 (0-100)	0 (0-62)	.009
	V5 (%)	95 (1-100)	14 (0-91)	.001
LA	Mean (Gy (RBE))	24.1 (6.2-59.3)	13.8 (1.0-54.7)	.001
	V50 (%)	9 (0-75)	5 (0-60)	.308 (NS)
	V30 (%)	29 (0-98)	17 (0-83)	.005
	V5 (%)	100 (63-100)	42 (7-99)	<.001
RV	Mean (Gy (RBE))	9.5 (1.5-31.0)	0.1 (0.0-1.94)	<.001
	V50 (%)	0 (0-5)	0 (0-0)	.109 (NS)
	V30 (%)	1 (0-52)	0 (0-0)	.003
	V5 (%)	60 (7-100)	0 (0-11)	<.001
LV	Mean (Gy (RBE))	9.9 (3.2-36.9)	1.8 (0.0-14.1)	.001
	V50 (%)	0 (0-30)	0 (0-10)	.043
	V30 (%)	3 (0-72)	1 (0-19)	.013
	V5 (%)	59 (7-100)	7 (0-42)	<.001
RCA	Mean (Gy (RBE))	21.7 (16.3-27.2)	0.1 (0.0-11.9)	.001
	V50 (%)	0 (0-11)	0 (0-0)	.317 (NS)
	V30 (%)	0 (0-100)	0 (0-0)	.028
	V5 (%)	100 (0-100)	0 (0-98)	.001
LCA	Mean (Gy (RBE))	31.5 (3.2-49.5)	13.3 (0.0-72.7)	.679 (NS)
	V50 (%)	0 (0-70)	0 (0-77)	.500 (NS)
	V30 (%)	46 (0-100)	0 (0-100)	.013
	V5 (%)	100 (43-100)	26 (0-100)	.001
SA node	Mean (Gy (RBE))	37.5 (0.2-72.6)	16.5 (0.0-72.7)	.020
	V50 (%)	9 (0-100)	0 (0-100)	.735
	V30 (%)	82 (0-100)	16 (0-100)	.091 (NS)
	V5 (%)	100 (0-100)	90 (0-100)	.007
Non-GTV lungs	Mean (Gy (RBE))	16.3 (9.8-24.9)	12.7 (8.4-17.9)	<.001
	V20 (%)	28 (16-45)	22 (15-33)	<.001
	V5 (%)	55 (32-79)	32 (22-46)	<.001
Oesophagus	V50 (%)	15 (0-55)	8 (0-56)	.875 (NS)
Spinal Cord	DMax (Gy (RBE))	42.7 (18.3-48.8)	25.9 (0.7-46.8)	<.001

Table 5.3: Median dose indices of OAR for VMAT and IMPT plans to and below T7 vertebrae (OAR- organs-at-risk, CI - confidence interval, RA - right atrium, LA - left atrium, RV - right ventricle, LV - left ventricle, RCA - right coronary artery, LCA - left coronary artery, SA node - sino-atrial node, NS- not statistically significant)

5.4 Discussion

The analysis conducted here showed that IMPT could potentially reduce dose to the heart compared to VMAT. Patients with pre-existing CD and disease overlapping with or extending to the most superior aspect of the heart contour appeared to benefit most. In this cohort of patients, the median level of the superior aspect of the heart contour was T7 vertebrae. For this group of patients, the estimated RRR of grade $\geq$3 cardiac toxicities were between 24 and 60%. However, the estimated risk of complications is dependent upon the dose metric used. The estimated RRR was highest with V5 and lowest with V30.

Long-term risk of CD is known to be increased due to radiotherapy. In breast cancer [21] and lymphoma [22], this association is well-established. Since the results of RTOG-0617 trial was published, the link between cardiac toxicity and radiotherapy for lung cancer is increasingly recognised. However, the mechanism of RIHD in the context of radiotherapy to the lung is not well understood. Multiple dose-volume parameter is likely to increase the risk of cardiac toxicity. Current evidence appear to show that both low dose to a large volume and high dose to a small volume of the heart are likely to be of relevance [40]. Furthermore, not only whole heart dose is important [23, 27] but various sub-structures have been linked to survival [31, 34]. These particular sub-structures include the base-of-the-heart and left ventricle.

PBT has the potential to reduce dose to the heart. However, access to this technology is limited and therefore patient selection is crucial to maximise benefit of PBT. Trials of equivalent doses in unselected patient groups are unlikely to show an advantage for protons. In fact, one would anticipate similar local control and toxicity rates. For instance, when comparing oesophageal dose (see Table 5.3), it would not be unexpected if both IMPT and VMAT result in similar rates of oesophagitis. The benefit of PBT is likely to be related to reduction in integral dose and therefore patient selection

where this advantage can be drawn on is critical. Although, our analysis showed that IMPT could potentially reduce cardiac toxicity due to lowering of heart exposure to the medium-to-low dose, there was little reduction in the high-doses volume to the heart. Therefore, PBT may not reduce toxicity when it is associated with high dose to the heart or its substructures,

We acknowledge that there are limitations to the NTCP model. Firstly, the model that was used was to estimate cardiac toxicity was derived from retrospective data from a single institution. Furthermore, the true incidence of cardiac toxicity following radiotherapy for lung cancer is currently unknown. It is highly likely that not all cardiac complications were captured. This is particularly so for grade 5 toxicity, as accurate documentation of cause of death is challenging in these patients [130]. Secondly, the NTCP model used for the analysis was derived from a cohort of patients treated with 3D-conformal radiotherapy. We now know that pneumonitis rates are lower with IMRT as compared to 3D-conformal radiotherapy [23]. It is not known if cardiac toxicity rates are lower with IMRT as compared to 3D-conformal radiotherapy. Furthermore, the model by Dess et al, has not been validated. However, it gives a plausible explanation for the observed decrease in overall survival in RTOG 0617. Also, a number of studies have since reported a link between cardiac toxicity and lung radiotherapy [40, 24]. Unfortunately, as highlighted in a recent review by Zhang et al, there are weaknesses in the literature [24]. These studies are mainly retrospective and heterogeneous in nature with inconsistencies in terms of the specific dose parameter tested. The merit of this study is that this evaluation has identified a subgroup of patients where specific dose volume parameters for the heart and its substructures are significantly lower in IMPT compared to VMAT. Current literature shows that cardiovascular disease impacts on survival of lung cancer patients [131, 132]. Therefore, to our knowledge, this is the best complication model to date which incorporates baseline cardiac risk as well as dose metrics.

Another limitation is that, the model lacks consideration of lung dose metric. A number of reports have emerged suggesting the possible synergistic effect between heart and lung toxicity following lung cancer radiotherapy [133, 134]. Although a preclinical study has suggested the likely mechanism of action being mutual cardiopulmonary dysfunction following combined cardiac and lung irradiation compared to irradiation of the heart or lung alone [133], current clinical findings are conflicting [134, 135, 136]. Finally, with the new standard of care of the addition of an immune checkpoint inhibitor following chemoradiotherapy, an updated model is needed [81].

This evaluation has assumed an averaged proton RBE value of 1.1 relative to photons based on RBE values measured in vivo. It is recognized that microscopically this concept breaks down and that, RBE significantly increases towards the distal end of a spread out Bragg peak [94]. Unfortunately, considerable uncertainties exist in translating in vitro and in vivo data to a clinical RBE. Therefore, given the paucity of published clinical data indicating that the average RBE of 1.1 is incorrect and lack of validated RBE models for proton therapy planning [137, 138], for the purpose of the study, we have assumed an averaged relative proton of RBE of 1.1 to photon therapy.

Unfortunately, the relevance of photon NTCP models to proton therapy is not established. However, this analysis is useful in giving some indication of the likely clinical benefit of PBT in specific situations. Using an easily identifiable surrogate marker of T7 vertebrae, one could propose a randomised VMAT vs IMPT trial in locally advanced lung cancer where the primary endpoint is cardiac toxicity. Enrichment of study population could be achieved by only enrolling patients with stable pre-existing cardiac disease or at high risk of heart disease. A health economics evaluation needs to be embedded within the trial given the cost of the technology.

However, multiple challenges exist in conducting a well-designed PBT trial in lung cancer. A number of lessons are to be learnt from the published passive scatter proton therapy (PSPT) vs intensity modulated radiotherapy (IMRT) trial in lung cancer [74].

Although, there was no statistically significant difference in grade ≥3 pneumonitis rate, reduction in heart dose at all dose levels was observed. Improvements in the primary endpoints of pneumonitis and local failure as the trial progressed was seen, in particular for the proton arm. This highlights the value of experience in treatment planning. Other treatment planning considerations that need to be considered in proton therapy include: the dose calculation engine, robust planning and evaluation, and motion management. Finally, similar to photon therapy, adaptive planning and strict radiotherapy quality assurance are necessary. All of these technical issues are critical in PBT relative to photon therapy due to the sensitivity of PBT plans to dose perturbations.

In conclusion, this analysis suggests that IMPT has the potential to benefit patients with locally advanced NSCLC whose primary tumour and nodal spread overlapped with or is inferior to T7 vertebrae compared to VMAT. Patients with pre-existing heart disease are likely to receive the greatest benefit followed by those at high-risk of heart disease. In the highest risk group, the RRR of grade ≥3 cardiac complications was between 40 and 60%.

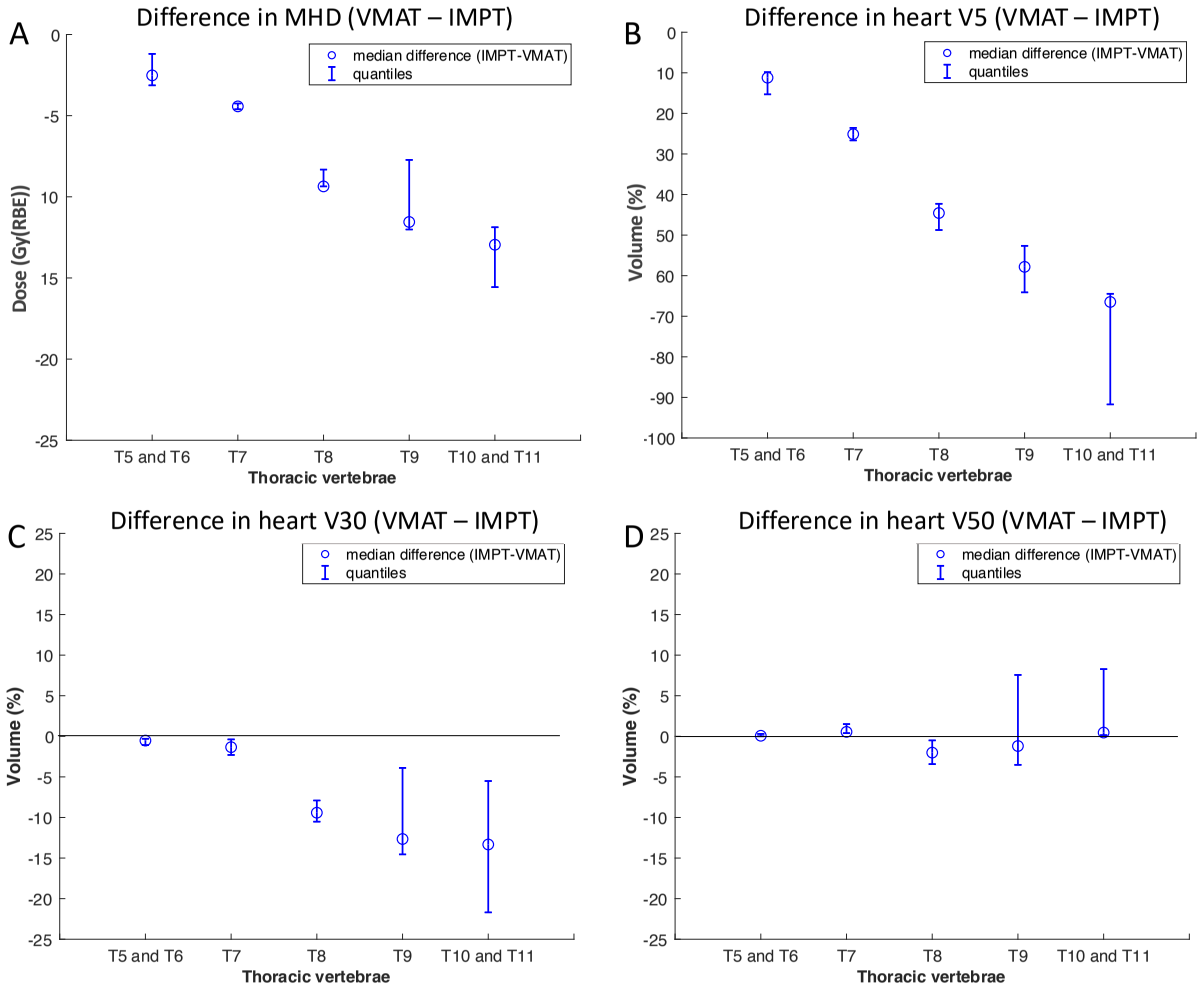


Figure 5.2: Difference in dose to the heart between VMAT and IMPT according disease extension with reference to the thoracic vertebrae.

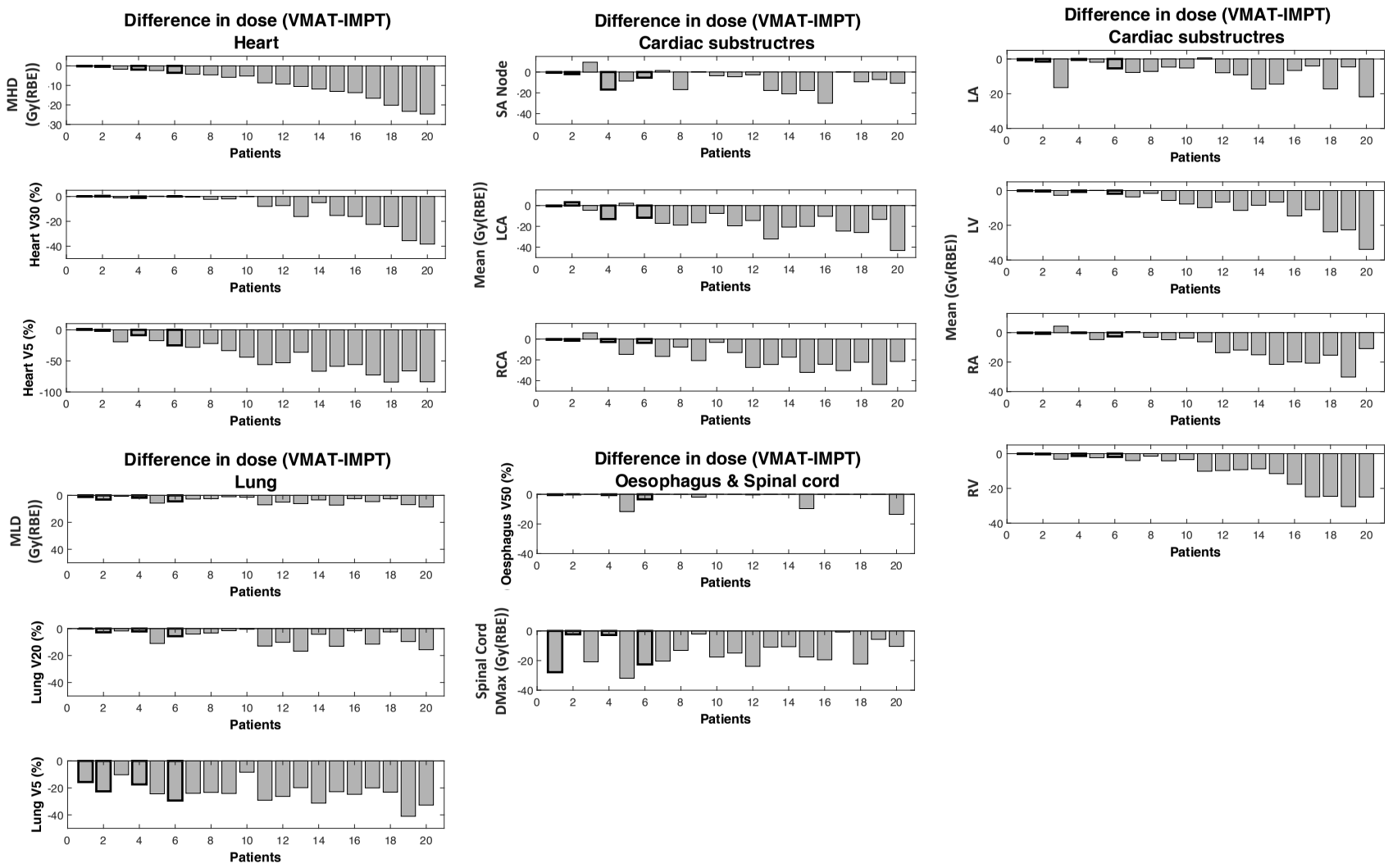


Figure 5.3: Difference in doses to OAR between VMAT and IMPT. Patients marked in bold box (pt 1, 2, 4 and 6) indicate those with tumour not extending to and below T7 vertebrae.

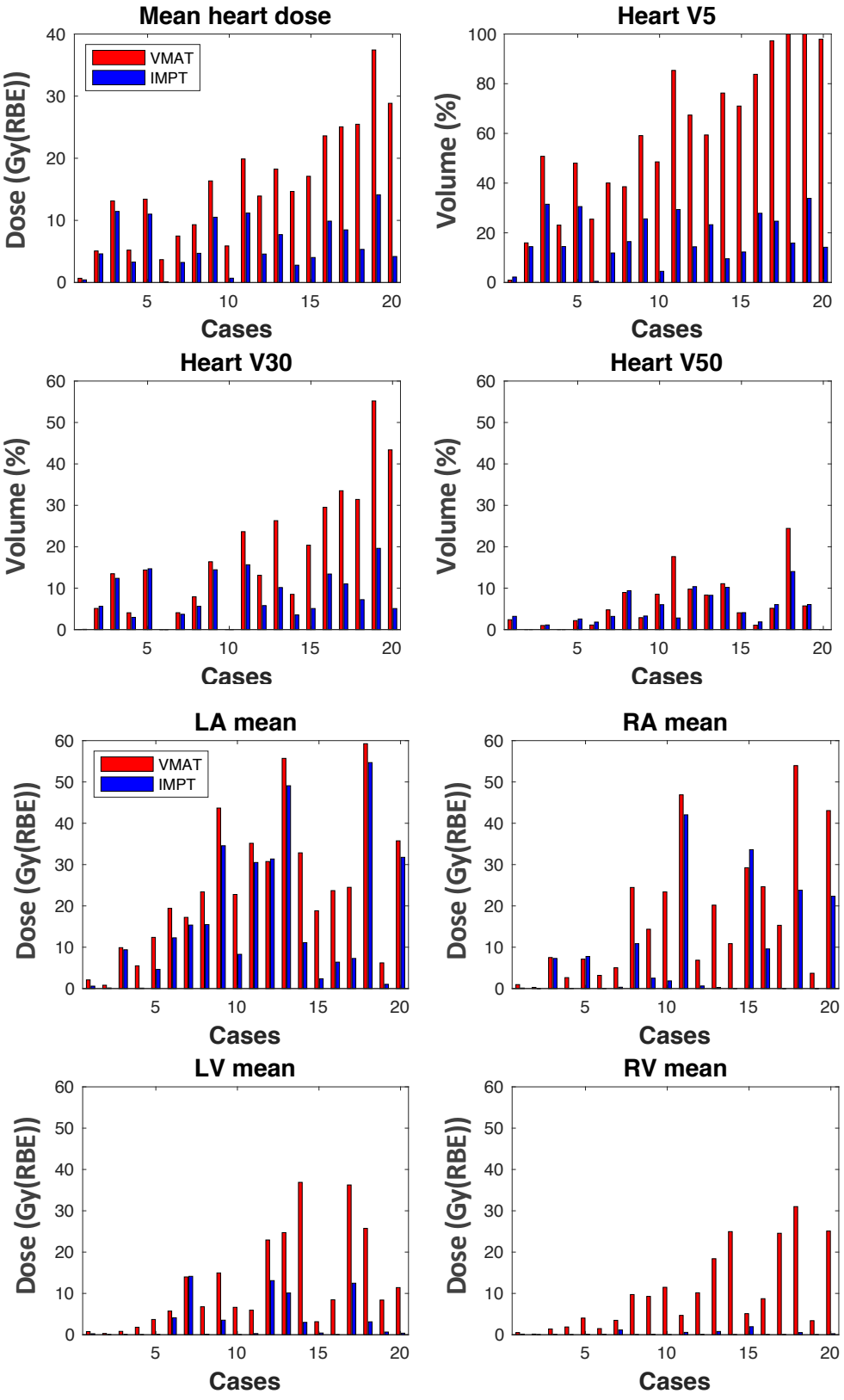


Figure 5.4: Absolute doses to the heart and substructures

OAR	Metric	VMAT (range)	IMPT (range)	P value
Above T7 vertebrae				
Heart	Mean (Gy (RBE))	4.4 (0.7-5.2)	1.9 (0.1-4.6)	.068
	V50 (%)	0 (0-2)	1 (0-3)	.180
	V30 (%)	2 (0-5)	2 (0-6)	1.000
	V5 (%)	20 (0-26)	8 (0-14)	.144
RA	Mean (Gy (RBE))	1.8 (0.3-7.5)	0.1 (0-7.2)	.068
	V50 (%)	0 (0-1)	0 (0-0)	.317
	V30 (%)	0 (0-9)	0 (0-3)	1.000
	V5 (%)	5 (0-27)	0 (0-39)	.317
LA	Mean (Gy (RBE))	3.8 (0.8-9.9)	0.4 (0.1-9.4)	.068
	V50 (%)	2 (0-7)	4 (0-9)	.109
	V30 (%)	1.9 (0-8)	0 (0-0)	.317
	V5 (%)	18 (0-51)	0 (0-36)	.285
RV	Mean (Gy (RBE))	1.0 (0.2-1.9)	0.1 (0-0.2)	.068
	V50 (%)	0 (0-0)	0 (0-0)	1.000
	V30 (%)	0 (0-0)	0 (0-0)	1.000
	V5 (%)	3 (0-13)	0 (0-0)	.180
LV	Mean (Gy (RBE))	0.8 (0.3-1.8)	0.0 (0-0.2)	.068
	V50 (%)	2 (0-11)	0 (0-1)	.655
	V30 (%)	0 (0-0)	0.0 (0-0)	1.000
	V5 (%)	0 (0-11)	0 (0-0)	.317
RCA	Mean (Gy (RBE))	2.7 (0.6-3.6)	0.2 (0-0.7)	.068
	V50 (%)	0 (0-0)	0 (0-0)	1.000
	V30 (%)	0 (0-0)	0 (0-0)	1.000
	V5 (%)	9 (0-21)	0.0 (0-0)	.180
LCA	Mean (Gy (RBE))	10.3 (2.3-15.0)	0.2 (0.0-28.3)	.715
	V50 (%)	0 (0-0)	0 (0-0)	1.000
	V30 (%)	0 (0-0)	0 (0-6)	.655
	V5 (%)	84 (0-100)	6 (0-71)	.285
SA node	Mean (Gy (RBE))	3.4 (0.7-46.7)	0.2 (0.0-25.8)	.715
	V50 (%)	0 (0-29)	0 (0-0)	.317
	V30 (%)	0 (0-99)	0 (0-26)	.317
	V5 (%)	19 (0-100)	0 (0-100)	0.317
Non-GTV lungs	Mean (Gy (RBE))	11.5 (6.9-14.7)	9.0 (5.7-10.3)	.068
	V20 (%)	19 (10-24)	15 (11-20)	.144
	V5 (%)	45 (34-55)	23 (18-29)	.068
Oesophagus	V50 (%)	15 (3-35)	14 (0-34)	.465
Spinal Cord	DMax (Gy (RBE))	42.8 (30.0-47.0)	30 (1.8-44.6)	.068

Table 5.4: Median dose indices of OAR for VMAT and IMPT plans above T7 vertebrae (OAR- organs-at-risk, CI - confidence interval, RA - right atrium, LA - left atrium, RV - right ventricle, LV - left ventricle, RCA - right coronary artery, LCA - left coronary artery, SA node - sino-atrial node).

Cardiac Risk (%)	VMAT (95% CI)	IMPT (95% CI)
To and below T7 vertebrae		
Pre-existing CD		
AR (based on MHD)	19 (16-22)	11 (10-12)
AR (based on V5)	24 (20-29)	9 (8-10)
AR (based on V30)	23 (17-32)	14 (13-15)
No pre-existing CD		
AR (based on MHD)	7 (5-10)	3 (3-4)
AR (based on V5)	10 (8-13)	3 (3-4)
AR (based on V30)	9 (5-14)	5 (4-5)
High risk of CD		
AR (based on MHD)	10 (8-12)	5 (5-6)
Above T7 vertebrae		
Pre-existing CD		
AR (based on MHD)	9 (8-10)	8 (7-9)
AR (based on V5)	8 (6-9)	7 (6-8)
AR (based on V30)	12 (11-12)	11 (11-12)
No pre-existing CD		
AR (based on MHD) .	3 (2-3)	2 (2-3)
AR (based on V5)	3 (2-3)	2 (2-3)
AR (based on V30)	4 (4-4)	4 (4-4)
High risk of CD		
AR (based on MHD)	4 (4-5)	4 (3-4)

Table 5.5: Risk estimates of grade $\geq$3 cardiac toxicities. High risk of cardiac disease defined as Framingham score of $\geq$20% (CI - confidence interval, CD - cardiac disease, AR - absolute risk, MHD - mean heart dose, RRR - relative risk reduction).

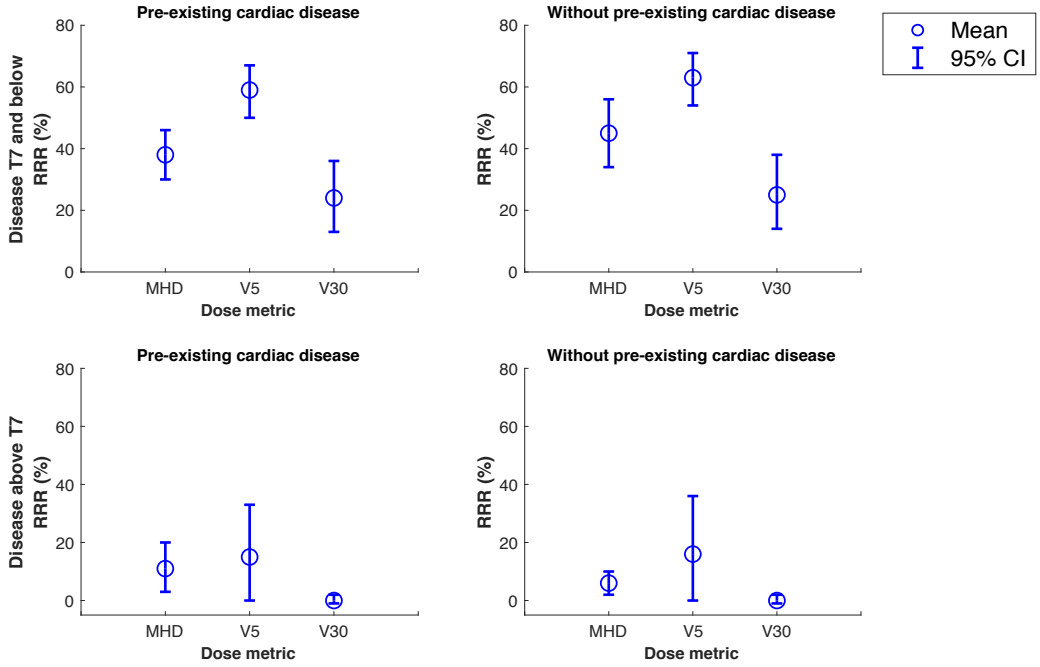


Figure 5.5: Relative risk reduction (RRR) based on presence or absence of pre-existing heart disease and dose metrics.

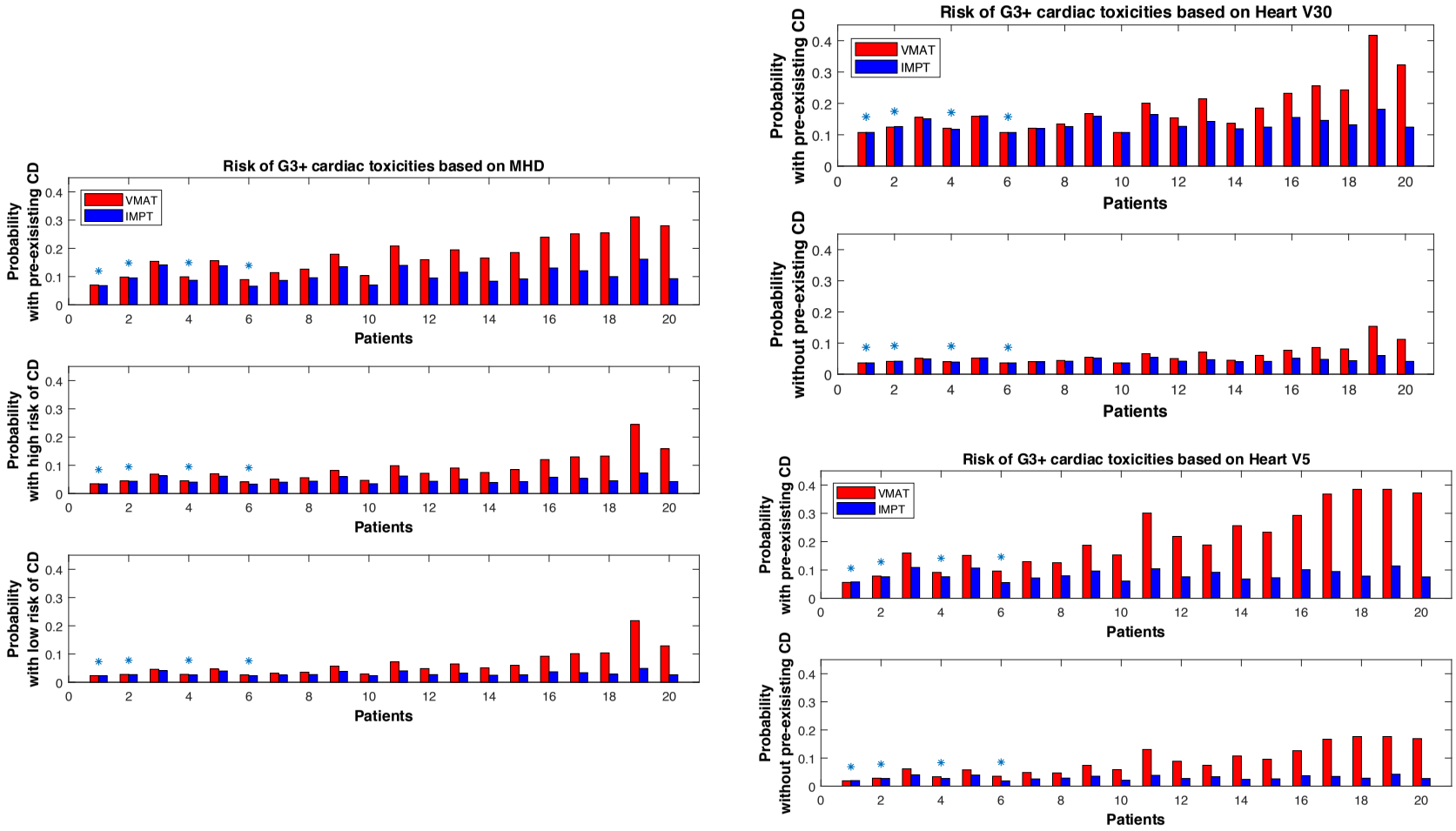


Figure 5.6: Risk of grade $\geq$3 cardiac toxicities based on MHD. Asterisks indicate patients with disease not extending to and below T7 vertebrae.

Chapter 6

Conclusions

6.1 Overview

The aims of this thesis were:-

- To evaluate and compare the robustness of IMPT and VMAT plans against setup uncertainties and tumour motion in locally advanced lung cancer using probabilistic scenarios in lung cancer.
- To evaluate the accuracy of the Raystation TPS analytical algorithm against Raystation Monte-Carlo algorithm.
- To identify a sub-group of clinical cases where the Raystation TPS analytical algorithm may be clinically acceptable.
- To identify a sub-group of patients who would benefit most from IMPT over VMAT with respect to cardiac sparing.

6.2 Treatment planning in PBT

The first part of this thesis described a fast and practical method for analysing robustness of VMAT and IMPT plans against setup uncertainty. A course of fractionated radiotherapy treatment was simulated, summed and compared against the nominal plan. The method was applied to ten conventionally fractionated NSCLC radiotherapy cases planned using VMAT, PTV-optimised IMPT, and robust-optimised IMPT. It was observed when considering the whole treatment course, setup errors did not influence robustness irrespective of planning techniques used. However, on a fraction level, VMAT and robust-optimised IMPT plans were superior compared to PTV-IMPT plans. Robustness of plan against tumour motion was also assessed by recalculating and accummulating the nominal plan in each of the 4DCT phases.

Using the ITV method to account for tumour motion did not ensure CTV V95% coverage in both photon and proton plans where tumour motion was larger 10mm.

The second part of the thesis evaluated the dose calculation algorithms in a commercial TPS. An analytical dose calculation algorithm known as the pencil-beam scanning was compared against Monte-Carlo algorithm in twenty IMPT lung cancer cases. The results showed that although Monte Carlo algorithm was more accurate compared to pencil-beam algorithm in lung IMPT, use of the analytical algorithm for optimisation and final dose calculation might be clinically acceptable where there was mediastinal involvement and absence of range shifters. Otherwise, use of MC algorithm would be recommended to ensure accuracy of treatment delivery.

6.3 PBT to improve outcome in locally advanced NSCLC

Finally, using the model-based approach, we demonstrated that dosimetric benefit of proton therapy is likely to be most beneficial in patients with locally advanced NSCLC whose disease overlapped with or is inferior to T7 vertebrae compared to photon therapy. Patients with pre-existing heart disease were likely to receive the greatest benefit followed by those at high-risk of heart disease. In the highest risk group, the relative risk reduction of grade ≥ 3 cardiac complications was between 40 and 60%. Although dosimetric advantages were observed using the most up-to-date planning techniques what remained to be established is the validity of a photon NTCP model in proton therapy.

6.4 Future directions

PBT is a promising technology that could improve outcome in patients with locally advanced NSCLC. The advantages conferred by the physical characteristics of proton is unlikely to be realised where doses to the normal tissue and target are similar compared to photon therapy. Furthermore, patient outcome is a complex interaction between patient-, disease- and treatment-related factors. Hence, dosimetric benefit alone is not expected to yield improved outcome. Given this, it is doubtful that a randomised-control trial in an unselected patient group between proton and photon would result in proton therapy showing better outcome. Stratification of patients and identifying the key clinical questions are important. Moreover, any proposed trials in this patient group would need to consider the addition of immunotherapy which has now become the new standard-of-care [81].

There are multiple other challenges in conducting a well-designed PBT trial in lung cancer. As discussed in this thesis, the technical aspects of treatment delivery are far more complex compared to photon therapy. Furthermore, given the cost of the technology, a health economics assessment is crucial. Future work based on this thesis include a pre-trial health economics evaluation of IMPT vs VMAT in this patient group. We recognised that there will be limitations to the analysis, however, the purpose of the analysis is to permit a head-to-head comparison in the absence of a randomised-control trial. This would give an indication of the likely cost-effectiveness of proton therapy.

The resulting data gathered in this thesis should hopefully serve well in increasing our understanding and informing future application of intensity modulated proton therapy in lung cancer.

Chapter 7

Appendix

Patient	Heart mean (Gy (RBE))			
	PB-PB	PB-MC	PB-MC scaled	MC-MC
1	0.48	0.5	0.53	0.43
2	4.02	4	4.26	4.62
3	14.15	13.5	14.97	11.44
4	2.65	2.72	2.91	3.3
5	10.45	10.43	10.81	11.01
6	0.1	0.12	0.12	0.13
7	2.89	2.91	3.15	3.24
8	5.04	4.9	5.14	4.7
9	9.79	9.44	10.15	10.51
10	0.63	0.54	0.59	0.7
11	10.13	9.88	10.41	11.19
12	4.04	3.9	4.09	4.59
13	6.93	6.75	7.11	7.71
14	2.66	2.48	2.64	2.79
15	3.98	3.8	4.01	4.03
16	9.42	8.91	9.64	9.88
17	7.59	7.39	7.94	8.48
18	4.87	4.56	4.99	5.33
19	12.77	12.69	13.2	14.13
20	3.95	3.89	4.1	4.19

Table 7.1: Comparison of mean heart dose stratified according to dose calculation algorithms

Patient	Spinal Cord Dmax (Gy (RBE))			
	PB-PB	PB-MC	PB-MC scaled	MC-MC
1	2.13	1.32	1.4	1.8
2	45.18	44.36	47.2	44.64
3	1.71	2.25	2.5	2.38
4	38.56	40.25	43	39.13
5	0.49	1.01	1.05	5.8
6	20.11	19.63	20.49	20.92
7	3.7	5.17	5.6	7.83
8	12.04	21.26	22.28	18.54
9	40.56	40.24	43.26	44.61
10	0.73	0.48	0.52	0.7
11	32.81	33.13	34.91	33.91
12	24.19	21.29	22.32	23.43
13	29.88	29.22	30.76	32.92
14	33.94	34.88	37.2	31.02
15	19.99	21.13	22.28	28.47
16	13.17	13.58	14.68	13.84
17	43.39	46.12	49.53	46.75
18	3.75	4.09	4.48	3.58
19	40.15	40.55	42.18	42.29
20	33.41	34.3	36.13	36.05

Table 7.2: Comparison of maximum dose to the spinal cord stratified according to dose calculation algorithms

	Lung mean (Gy (RBE))			
Patient	PB-PB	PB-MC	PB-MC scaled	MC-MC
1	5.08	5.1	5.41	5.67
2	6.96	7.12	7.58	7.79
3	12.48	11.88	13.18	11.61
4	8.86	8.79	9.39	10.27
5	9.87	9.9	10.27	10.71
6	9.59	9.58	10	10.19
7	7.44	7.36	7.97	8.4
8	11.11	11.03	11.56	11.96
9	10.75	10.62	11.42	12.99
10	7.85	7.57	8.16	8.44
11	14.26	14.24	15	15.78
12	10.24	10.32	10.82	11.16
13	13.11	13.19	13.89	14.89
14	9.11	9.06	9.66	9.44
15	11.23	11.12	11.73	12.41
16	12.92	12.58	13.61	13.6
17	12.6	12.45	13.37	14.06
18	16.55	16.18	17.71	17.86
19	15.17	15.19	15.8	15.45
20	15.86	15.86	16.7	16.27

Table 7.3: Comparison of mean lung dose stratified according to dose calculation algorithms

Patient	Lung V5 (%)			
	PB-PB	PB-MC	PB-MC scaled	MC-MC
1	17.45	17.63	17.8	17.88
2	18.76	19.75	20.15	20.5
3	29.52	29.43	30.02	32.92
4	27.46	27.76	28.07	29.31
5	23.42	24.16	24.4	30.12
6	24.06	24.73	24.93	25.44
7	23.54	23.54	23.99	24.75
8	26.08	26.36	26.6	30.69
9	28.15	28.31	28.69	30.94
10	23.07	22.81	23.06	23.63
11	35.83	36.76	37.21	39.25
12	25.99	26.87	27.15	27.41
13	38.66	40.7	41.49	45.98
14	21.87	21.95	22.26	22.28
15	28.53	29.02	29.29	30.78
16	33.11	33.42	33.81	34.33
17	34.7	35.81	36.42	38.15
18	38.74	38.68	39.02	40.62
19	32.08	32.62	32.78	32.36
20	45.41	45.88	46.29	46.22

Table 7.4: Comparison of lung V5 stratified according to dose calculation algorithms

Patient	Lung V20 (%)			
	PB-PB	PB-MC	PB-MC scaled	MC-MC
1	10.39	10.49	10.93	10.52
2	11.84	11.96	12.27	12.71
3	21.41	20.73	21.43	19.03
4	18.98	18.96	19.9	20.06
5	15.45	15.41	15.63	16.65
6	17.37	17.41	17.79	18.1
7	13.83	13.72	14.66	15.45
8	18.63	18.66	18.94	20.64
9	19.9	19.85	20.49	22.99
10	14.04	13.8	14.5	15.29
11	25.5	25.49	26.04	27.56
12	17.7	17.82	18.2	18.68
13	21.51	21.65	22.18	23.93
14	14.32	14.39	14.73	14.68
15	19.77	19.6	20.19	21.32
16	24.51	24.3	24.92	25.09
17	22	21.89	22.54	23.65
18	29.67	29.4	30.3	32.52
19	27.26	27.32	27.49	27.06
20	28.44	28.72	29.68	29.46

Table 7.5: Comparison of lung V20 stratified according to dose calculation algorithms

References

[1] CRUK - Cancer mortality for common cancers. https://www.cancerresearchuk.org/health-professional/cancer-statistics/mortality/common-cancers-compared#heading-Zero, 2016. Accessed: 2018-12-06.

[2] CRUK - Lung cancer survival statistics. https://www.cancerresearchuk.org/health-professional/cancer-statistics/statistics-by-cancer-type/lung-cancer/survival#heading-Two, 2014. Accessed: 2018-12-06.

[3] J. Vansteenkiste, D. De Ruysscher, W. E. E. Eberhardt, E. Lim, S. Senan, E. Felip, S. Peters, and on behalf of the ESMO Guidelines Working Group. Early and locally advanced non-small-cell lung cancer (nsclc): Esmo clinical practice guidelines for diagnosis, treatment and follow-up†. Annals of Oncology, 24(suppl 6):vi89–vi98, 2013.

[4] A. G. Nicholson, K. Chansky, J. Crowley, R. Beyruti, K. Kubota, A. Turrisi, W. E. Eberhardt, J. van Meerbeeck, R. Rami-Porta, Staging, Advisory Boards Prognostic Factors Committee, Institutions Participating, Staging, Boards Prognostic Factors Committee Advisory, and Institutions Participating. The international association for the study of lung cancer lung cancer staging project: Proposals for the revision of the clinical and pathologic staging of small

cell lung cancer in the forthcoming eighth edition of the tnm classification for lung cancer. J Thorac Oncol, 11(3):300–11, 2016.

[5] W. J. Scott, J. Howington, S. Feigenberg, B. Movsas, K. Pisters, and Physicians American College of Chest. Treatment of non-small cell lung cancer stage i and stage ii: Accp evidence-based clinical practice guidelines (2nd edition). Chest, 132(3 Suppl):234S–242S, 2007.

[6] M. Guckenberger, N. Andratschke, H. Alheit, R. Holy, C. Moustakis, U. Nestle, O. Sauer, and Radioonkologie Deutschen Gesellschaft fur. Definition of stereotactic body radiotherapy: principles and practice for the treatment of stage i non-small cell lung cancer. Strahlenther Onkol, 190(1):26–33, 2014.

[7] R. Timmerman, R. McGarry, C. Yiannoutsos, L. Papiez, K. Tudor, J. DeLuca, M. Ewing, R. Abdulrahman, C. DesRosiers, M. Williams, and J. Fletcher. Excessive toxicity when treating central tumors in a phase ii study of stereotactic body radiation therapy for medically inoperable early-stage lung cancer. J Clin Oncol, 24(30):4833–9, 2006.

[8] S. Bral, T. Gevaert, N. Linthout, H. Versmessen, C. Collen, B. Engels, D. Verdries, H. Everaert, N. Christian, M. De Ridder, and G. Storme. Prospective, risk-adapted strategy of stereotactic body radiotherapy for early-stage non-small-cell lung cancer: results of a phase ii trial. Int J Radiat Oncol Biol Phys, 80(5):1343–9, 2011.

[9] M. N. Corradetti, A. R. Haas, and R. Rengan. Central-airway necrosis after stereotactic body-radiation therapy. N Engl J Med, 366(24):2327–9, 2012.

[10] A. A. Chaudhuri, C. Tang, M. S. Binkley, M. Jin, J. F. Wynne, R. von Eyben, W. Y. Hara, N. Trakul, Jr. Loo, B. W., and M. Diehn. Stereotactic ablative

radiotherapy (sabr) for treatment of central and ultra-central lung tumors. Lung Cancer, 89(1):50–6, 2015.

[11] A. Bezjak, R. Paulus, L. E. Gaspar, R. D. Timmerman, W. L. Straube, W. F. Ryan, Y. I. Garces, A. T. Pu, A. K. Singh, G. M. Videtic, R. C. McGarry, P. Iyengar, J. R. Pantarotto, J. J. Urbanic, A. Y. Sun, M. E. Daly, I. S. Grills, P. Sperduto, D. P. Normolle, J. D. Bradley, and H. Choy. Safety and efficacy of a five-fraction stereotactic body radiotherapy schedule for centrally located non-small-cell lung cancer: Nrg oncology/rtog 0813 trial. J Clin Oncol, 37(15):1316–1325, 2019.

[12] S. Adebahr, Y. Liu, S. Colette, C. Faivre-Finn, S. Ahmad, M. Ahmed, J. Belderbos, N. Andratschke, K. Franks, X. Geets, M. Guckenberger, K. Konopa, M. Lambrecht, V. Lewitzki, Y. Lievens, N. Pourel, D. De Ruysscher, R. Dziadziuszko, C. Fortpied, F. McDonald, H. Peulen, A. Grosu, C. Hurkmans, C. Le Pechoux, and U. Nestle. Oc-0061 eortc 22113-8113 lungtech trial on sbrt of central lung tumors. Radiotherapy and Oncology, 133:S24–S25, 2020/02/24 2019.

[13] Karin Lindberg, Per Bergström, Odd Terje Brustugun, Silke Engelholm, Vitali Grozman, Morten Hoyer, Kristin Karlsson, Azza Khalil, Charlotte Kristiansen, Ingmar Lax, Britta Löden, Jan Nyman, Gitte Persson, Lotte Rogg, Peter Wersäll, and Rolf Lewensohn. Oa24.05 the nordic hilus-trial - first report of a phase ii trial of sbrt of centrally located lung tumors. Journal of Thoracic Oncology, 12(1, Supplement):S340, 2017. Abstracts from the IASLC 17th World Conference on Lung Cancer.

[14] D. Georg, M. Hillbrand, M. Stock, K. Dieckmann, and R. Potter. Can protons improve sbrt for lung lesions? dosimetric considerations. Radiother Oncol, 88(3):368–75, 2008.

[15] N. Kadoya, Y. Obata, T. Kato, M. Kagiya, T. Nakamura, T. Tomoda, A. Takada, K. Takayama, and N. Fuwa. Dose-volume comparison of proton radiotherapy and stereotactic body radiotherapy for non-small-cell lung cancer. Int J Radiat Oncol Biol Phys, 79(4):1225–31, 2011.

[16] S. P. Register, X. Zhang, R. Mohan, and J. Y. Chang. Proton stereotactic body radiation therapy for clinically challenging cases of centrally and superiorly located stage i non-small-cell lung cancer. Int J Radiat Oncol Biol Phys, 80(4):1015–22, 2011.

[17] C. A. Perez, T. F. Pajak, P. Rubin, J. R. Simpson, M. Mohiuddin, L. W. Brady, R. Perez-Tamayo, and M. Rotman. Long-term observations of the patterns of failure in patients with unresectable non-oat cell carcinoma of the lung treated with definitive radiotherapy. report by the radiation therapy oncology group. Cancer, 59(11):1874–81, 1987.

[18] M. Machtay, K. Bae, B. Movsas, R. Paulus, E. M. Gore, R. Komaki, K. Albain, W. T. Sause, and W. J. Curran. Higher biologically effective dose of radiotherapy is associated with improved outcomes for locally advanced non-small cell lung carcinoma treated with chemoradiation: an analysis of the radiation therapy oncology group. Int J Radiat Oncol Biol Phys, 82(1):425–34, 2012.

[19] A. Auperin, C. Le Pechoux, E. Rolland, W. J. Curran, K. Furuse, P. Fournel, J. Belderbos, G. Clamon, H. C. Ulutin, R. Paulus, T. Yamanaka, M. C. Bozonnat, A. Uitterhoeve, X. Wang, L. Stewart, R. Arriagada, S. Burdett, and J. P. Pignon. Meta-analysis of concomitant versus sequential radiochemotherapy in locally advanced non-small-cell lung cancer. J Clin Oncol, 28(13):2181–90, 2010.

[20] J. D. Bradley, R. Paulus, R. Komaki, G. Masters, G. Blumenschein, S. Schild, J. Bogart, C. Hu, K. Forster, A. Magliocco, V. Kavadi, Y. I. Garces, S. Narayan,

P. Iyengar, C. Robinson, R. B. Wynn, C. Koprowski, J. Meng, J. Beitler, R. Gaur, Jr. Curran, W., and H. Choy. Standard-dose versus high-dose conformal radiotherapy with concurrent and consolidation carboplatin plus paclitaxel with or without cetuximab for patients with stage IIIA or IIIB non-small-cell lung cancer (RTOG 0617): a randomised, two-by-two factorial phase 3 study. Lancet Oncol, 16(2):187–99, 2015.

[21] S. C. Darby, M. Ewertz, P. McGale, A. M. Bennet, U. Blom-Goldman, D. Bronnum, C. Correa, D. Cutter, G. Gagliardi, B. Gigante, M. B. Jensen, A. Nisbet, R. Peto, K. Rahimi, C. Taylor, and P. Hall. Risk of ischemic heart disease in women after radiotherapy for breast cancer. N Engl J Med, 368(11):987–98, 2013.

[22] K. E. Henson, R. C. Reulen, D. L. Winter, C. J. Bright, M. M. Fidler, C. Frobisher, J. Guha, K. F. Wong, J. Kelly, A. B. Edgar, M. G. McCabe, J. Whelan, D. J. Cutter, S. C. Darby, and M. M. Hawkins. Cardiac mortality among 200 000 five-year survivors of cancer diagnosed at 15 to 39 years of age: The teenage and young adult cancer survivor study. Circulation, 134(20):1519–1531, 2016.

[23] S. G. Chun, C. Hu, H. Choy, R. U. Komaki, R. D. Timmerman, S. E. Schild, J. A. Bogart, M. C. Dobelbower, W. Bosch, J. M. Galvin, V. S. Kavadi, S. Narayan, P. Iyengar, C. G. Robinson, R. B. Wynn, A. Raben, M. E. Augspurger, R. M. MacRae, R. Paulus, and J. D. Bradley. Impact of intensity-modulated radiation therapy technique for locally advanced non-small-cell lung cancer: A secondary analysis of the nrg oncology rtog 0617 randomized clinical trial. J Clin Oncol, 35(1):56–62, 2017.

[24] T. W. Zhang, J. Snir, R. G. Boldt, G. B. Rodrigues, A. V. Louie, S. Gaede, R. C. McGarry, J. J. Urbanic, M. E. Daly, and D. A. Palma. Is the importance of heart

dose overstated in the treatment of non-small cell lung cancer? a systematic review of the literature. Int J Radiat Oncol Biol Phys, 104(3):582–589, 2019.

[25] M. D. Johnson, K. Sura, V. S. Mangona, A. Glick, M. Wallace, H. Ye, and I. S. Grills. Matched-pair analysis of high dose versus standard dose definitive chemoradiation for locally advanced non-small-cell lung cancer. Clin Lung Cancer, 18(2):149–155, 2017.

[26] Christina K. Speirs, Todd A. DeWees, Sana Rehman, Alerson Molotievschi, Maria A. Velez, Daniel Mullen, Sandra Fergus, Marco Trovo, Jeffrey D. Bradley, and Cliff G. Robinson. Heart dose is an independent dosimetric predictor of overall survival in locally advanced non–small cell lung cancer. Journal of Thoracic Oncology, 12(2):293 – 301, 2017.

[27] R. T. Dess, Y. Sun, M. M. Matuszak, G. Sun, P. D. Soni, L. Bazzi, V. L. Murthy, J. W. D. Hearn, F. M. Kong, G. P. Kalemkerian, J. A. Hayman, R. K. Ten Haken, T. S. Lawrence, M. J. Schipper, and S. Jolly. Cardiac events after radiation therapy: Combined analysis of prospective multicenter trials for locally advanced non-small-cell lung cancer. J Clin Oncol, 35(13):1395–1402, 2017.

[28] Kyle Wang, Michael J. Eblan, Allison M. Deal, Matthew Lipner, Timothy M. Zagar, Yue Wang, Panayiotis Mavroidis, Carrie B. Lee, Brian C. Jensen, Julian G. Rosenman, Mark A. Socinski, Thomas E. Stinchcombe, and Lawrence B. Marks. Cardiac Toxicity After Radiotherapy for Stage III Non–Small-Cell Lung Cancer: Pooled Analysis of Dose-Escalation Trials Delivering 70 to 90 Gy. Journal of Clinical Oncology, 35(13):1387–1394, 2017. PMID: 28113017.

[29] Amode R. Tembhekar, Cari L. Wright, and Megan E. Daly. Cardiac dose and

survival after stereotactic body radiotherapy for early-stage non–small-cell lung cancer. Clinical Lung Cancer, 18(3):293 – 298, 2017.

[30] S. C. Darby, D. J. Cutter, M. Boerma, L. S. Constine, L. F. Fajardo, K. Kodama, K. Mabuchi, L. B. Marks, F. A. Mettler, L. J. Pierce, K. R. Trott, E. T. Yeh, and R. E. Shore. Radiation-related heart disease: current knowledge and future prospects. Int J Radiat Oncol Biol Phys, 76(3):656–65, 2010.

[31] K. Wang, K. A. Pearlstein, N. D. Patchett, A. M. Deal, P. Mavroidis, B. C. Jensen, M. B. Lipner, T. M. Zagar, Y. Wang, C. B. Lee, M. J. Eblan, J. G. Rosenman, M. A. Socinski, T. E. Stinchcombe, and L. B. Marks. Heart dosimetric analysis of three types of cardiac toxicity in patients treated on dose-escalation trials for stage iii non-small-cell lung cancer. Radiother Oncol, 125(2):293–300, 2017.

[32] D. B. Landau, L. Hughes, A. Baker, A. T. Bates, M. C. Bayne, N. Counsell, A. Garcia-Alonso, S. V. Harden, J. D. Hicks, S. R. Hughes, M. C. Illsley, I. Khan, V. Laurence, Z. Malik, H. Mayles, W. P. M. Mayles, E. Miles, N. Mohammed, Y. Ngai, E. Parsons, J. Spicer, P. Wells, D. Wilkinson, and J. D. Fenwick. Ideal-crt: A phase 1/2 trial of isotoxic dose-escalated radiation therapy and concurrent chemotherapy in patients with stage ii/iii non-small cell lung cancer. Int J Radiat Oncol Biol Phys, 95(5):1367–1377, 2016.

[33] S. Vivekanandan, D. B. Landau, N. Counsell, D. R. Warren, A. Khwanda, S. D. Rosen, E. Parsons, Y. Ngai, L. Farrelly, L. Hughes, M. A. Hawkins, and J. D. Fenwick. The Impact of Cardiac Radiation Dosimetry on Survival After Radiation Therapy for Non-Small Cell Lung Cancer. International Journal of Radiation Oncology Biology Physics, 2017.

[34] A. McWilliam, J. Kennedy, C. Hodgson, E. Vasquez Osorio, C. Faivre-Finn,

and M. van Herk. Radiation dose to heart base linked with poorer survival in lung cancer patients. Eur J Cancer, 85:106–113, 2017.

[35] I. W. Gayed, H. H. Liu, X. Wei, Z. Liao, S. W. Yusuf, J. Y. Chang, R. Bassett, and R. Komaki. Patterns of cardiac perfusion abnormalities after chemoradiotherapy in patients with lung cancer. J Thorac Oncol, 4(2):179–84, 2009.

[36] C. B. Lee, T. E. Stinchcombe, D. T. Moore, D. E. Morris, D. N. Hayes, J. Halle, J. G. Rosenman, M. P. Rivera, and M. A. Socinski. Late complications of high-dose (¿/=66 gy) thoracic conformal radiation therapy in combined modality trials in unresectable stage iii non-small cell lung cancer. J Thorac Oncol, 4(1):74–9, 2009.

[37] T. Schytte, O. Hansen, T. Stolberg-Rohr, and C. Brink. Cardiac toxicity and radiation dose to the heart in definitive treated non-small cell lung cancer. Acta Oncol, 49(7):1058–60, 2010.

[38] M. S. Ning, L. Tang, D. R. Gomez, T. Xu, Y. Luo, J. Huo, E. Mouhayar, and Z. Liao. Incidence and predictors of pericardial effusion after chemoradiation therapy for locally advanced non-small cell lung cancer. Int J Radiat Oncol Biol Phys, 99(1):70–79, 2017.

[39] B. Stam, H. Peulen, M. Guckenberger, F. Mantel, A. Hope, M. Werner-Wasik, J. Belderbos, I. Grills, N. O'Connell, and J. J. Sonke. Dose to heart substructures is associated with non-cancer death after sbrt in stage i-ii nsclc patients. Radiother Oncol, 123(3):370–375, 2017.

[40] J. R. Niska, C. S. Thorpe, S. M. Allen, T. B. Daniels, W. G. Rule, S. E. Schild, C. E. Vargas, and F. Mookadam. Radiation and the heart: systematic review of dosimetry and cardiac endpoints. Expert Rev Cardiovasc Ther, 16(12):931–950, 2018.

[41] W. H. Bragg M.A. and R. Kleeman B.Sc. Xxxix. on the α particles of radium, and their loss of range in passing through various atoms and molecules. The London, Edinburgh, and Dublin Philosophical Magazine and Journal of Science, 10(57):318–340, 1905.

[42] A. Lomax. Intensity modulation methods for proton radiotherapy. Phys Med Biol, 44(1):185–205, 1999.

[43] A. J. Lomax. Intensity modulated proton therapy and its sensitivity to treatment uncertainties 1: the potential effects of calculational uncertainties. Phys Med Biol, 53(4):1027–42, 2008.

[44] M. van Herk. Errors and margins in radiotherapy. Semin Radiat Oncol, 14(1):52–64, 2004.

[45] M. F. Moyers, D. W. Miller, D. A. Bush, and J. D. Slater. Methodologies and tools for proton beam design for lung tumors. Int J Radiat Oncol Biol Phys, 49(5):1429–38, 2001.

[46] P. C. Park, X. R. Zhu, A. K. Lee, N. Sahoo, A. D. Melancon, L. Zhang, and L. Dong. A beam-specific planning target volume (ptv) design for proton therapy to account for setup and range uncertainties. Int J Radiat Oncol Biol Phys, 82(2):e329–36, 2012.

[47] F. Albertini, E. B. Hug, and A. J. Lomax. Is it necessary to plan with safety margins for actively scanned proton therapy? Phys Med Biol, 56(14):4399–413, 2011.

[48] J. Unkelbach, T. C. Chan, and T. Bortfeld. Accounting for range uncertainties in the optimization of intensity modulated proton therapy. Phys Med Biol, 52(10):2755–73, 2007.

[49] A. Trofimov, J. Unkelbach, T. F. DeLaney, and T. Bortfeld. Visualization of a variety of possible dosimetric outcomes in radiation therapy using dose-volume histogram bands. Pract Radiat Oncol, 2(3):164–171, 2012.

[50] M. Casiraghi, F. Albertini, and A. J. Lomax. Advantages and limitations of the 'worst case scenario' approach in impt treatment planning. Phys Med Biol, 58(5):1323–39, 2013.

[51] E. Engwall, L. Glimelius, and E. Hynning. Effectiveness of different rescanning techniques for scanned proton radiotherapy in lung cancer patients. Phys Med Biol, 63(9):095006, 2018.

[52] A. Krauss, S. Nill, M. Tacke, and U. Oelfke. Electromagnetic real-time tumor position monitoring and dynamic multileaf collimator tracking using a siemens 160 mlc: geometric and dosimetric accuracy of an integrated system. Int J Radiat Oncol Biol Phys, 79(2):579–87, 2011.

[53] S. Mori, S. Zenklusen, and A. C. Knopf. Current status and future prospects of multi-dimensional image-guided particle therapy. Radiol Phys Technol, 6(2):249–72, 2013.

[54] C. Grassberger, J. Daartz, S. Dowdell, T. Ruggieri, G. Sharp, and H. Paganetti. Quantification of proton dose calculation accuracy in the lung. International Journal of Radiation Oncology* Biology* Physics, 89(2):424–430, 2014.

[55] Y. Jia, C. Beltran, D.J. Indelicato, S. Flampouri, Z. Li, and T.E. Merchant. Proton therapy dose distribution comparison between monte carlo and a treatment planning system for pediatric patients with ependymomaa). Medical physics, 39(8):4742–4747, 2012.

[56] H. A. Bethe. Moliere's theory of multiple scattering. Phys. Rev., 89:1256–1266, Mar 1953.

[57] M. Soukup, M. Fippel, and M. Alber. A pencil beam algorithm for intensity modulated proton therapy derived from monte carlo simulations. Phys Med Biol, 50(21):5089–104, 2005.

[58] X. R. Zhu, F. Poenisch, M. Lii, G. O. Sawakuchi, U. Titt, M. Bues, X. Song, X. Zhang, Y. Li, G. Ciangaru, H. Li, M. B. Taylor, K. Suzuki, R. Mohan, M. T. Gillin, and N. Sahoo. Commissioning dose computation models for spot scanning proton beams in water for a commercially available treatment planning system. Med Phys, 40(4):041723, 2013.

[59] Francesca Fiorini, Niek Schreuder, and Frank Van den Heuvel. Technical Note: Defining cyclotron-based clinical scanning proton machines in a FLUKA Monte Carlo system. Medical Physics, 45(2):963–970, 2018.

[60] G Magro, S Molinelli, A Mairani, A Mirandola, D Panizza, S Russo, A Ferrari, F Valvo, Piero Fossati, and M Ciocca. Dosimetric accuracy of a treatment planning system for actively scanned proton beams and small target volumes: Monte carlo and experimental validation. Physics in medicine and biology, 60(17):6865, 2015.

[61] I. J. Chetty, B. Curran, J. E. Cygler, J. J. DeMarco, G. Ezzell, B. A. Faddegon, I. Kawrakow, P. J. Keall, H. Liu, C. M. Ma, D. W. Rogers, J. Seuntjens, D. Sheikh-Bagheri, and J. V. Siebers. Report of the aapm task group no. 105: Issues associated with clinical implementation of monte carlo-based photon and electron external beam treatment planning. Med Phys, 34(12):4818–53, 2007.

[62] H. Paganetti. Range uncertainties in proton therapy and the role of monte carlo simulations. Phys Med Biol, 57(11):R99–117, 2012.

[63] RaySearch Laboratories AB. RAYSTATION 7.0 Reference Manual. 2017.

[64] Jatinder Saini, Dominic Maes, Alexander Egan, Stephen R Bowen, Sara St James, Martin Janson, Tony Wong, and Charles Bloch. Dosimetric evaluation of a commercial proton spot scanning monte-carlo dose algorithm: comparisons against measurements and simulations. Physics in Medicine & Biology, 62(19):7659, 2017.

[65] P. A. Taylor, S. F. Kry, and D. S. Followill. Pencil beam algorithms are unsuitable for proton dose calculations in lung. Int J Radiat Oncol Biol Phys, 99(3):750–756, 2017.

[66] X. Liang, Z. Li, D. Zheng, J.A. Bradley, M. Rutenberg, and N. Mendenhall. A comprehensive dosimetric study of Monte Carlo and pencil-beam algorithms on intensity-modulated proton therapy for breast cancer. Journal of Applied Clinical Medical Physics, 2018.

[67] X. Zhang, Y. Li, X. Pan, L. Xiaoqiang, R. Mohan, R. Komaki, J. D. Cox, and J. Y. Chang. Intensity-modulated proton therapy reduces the dose to normal tissue compared with intensity-modulated radiation therapy or passive scattering proton therapy and enables individualized radical radiotherapy for extensive stage iiib non-small-cell lung cancer: a virtual clinical study. Int J Radiat Oncol Biol Phys, 77(2):357–66, 2010.

[68] R. C. Nichols, S. N. Huh, R. H. Henderson, N. P. Mendenhall, S. Flampouri, Z. Li, H. J. D'Agostino, J. D. Cury, D. C. Pham, and B. S. Hoppe. Proton radiation therapy offers reduced normal lung and bone marrow exposure for patients receiving dose-escalated radiation therapy for unresectable stage iii non-small-cell lung cancer: a dosimetric study. Clin Lung Cancer, 12(4):252–7, 2011.

[69] E. Roelofs, M. Engelsman, C. Rasch, L. Persoon, S. Qamhiyeh, D. de Ruyss-

cher, F. Verhaegen, M. Pijls-Johannesma, P. Lambin, and Rococo Consortium. Results of a multicentric in silico clinical trial (rococo): comparing radiotherapy with photons and protons for non-small cell lung cancer. J Thorac Oncol, 7(1):165–76, 2012.

[70] M. Stuschke, A. Kaiser, C. Pöttgen, W. Lübcke, and J. Farr. Potentials of robust intensity modulated scanning proton plans for locally advanced lung cancer in comparison to intensity modulated photon plans. Radiotherapy and Oncology, 104(1):45–51, 2012. cited By 51.

[71] E. Roelofs, M. Engelsman, C. Rasch, L. Persoon, S. Qamhiyeh, D. de Ruysscher, F. Verhaegen, M. Pijls-Johannesma, P. Lambin, and Rococo Consortium. Results of a multicentric in silico clinical trial (rococo): comparing radiotherapy with photons and protons for non-small cell lung cancer. J Thorac Oncol, 7(1):165–76, 2012.

[72] T. Inoue, J. Widder, L. V. van Dijk, H. Takegawa, M. Koizumi, M. Takashina, K. Usui, C. Kurokawa, S. Sugimoto, A. I. Saito, K. Sasai, A. A. Van't Veld, J. A. Langendijk, and E. W. Korevaar. Limited Impact of Setup and Range Uncertainties, Breathing Motion, and Interplay Effects in Robustly Optimized Intensity Modulated Proton Therapy for Stage III Non-small Cell Lung Cancer. Int J Radiat Oncol Biol Phys, 96(3):661–9, 2016.

[73] S. Teoh, F. Fiorini, B. George, K.A. Vallis, and F. Van den Heuvel. Ep-2062: Probabilistic scenarios for assessing setup uncertainty in vmat and impt plans for lung cancer. Radiotherapy and Oncology, 127:S1130 – S1131, 2018. ESTRO 37, April 20-24, 2018, Barcelona, Spain.

[74] Z. Liao, J. J. Lee, R. Komaki, D. R. Gomez, M. S. O'Reilly, F. V. Fossella, Jr. Blumenschein, G. R., J. V. Heymach, A. A. Vaporciyan, S. G. Swisher,

P. K. Allen, N. C. Choi, T. F. DeLaney, S. M. Hahn, J. D. Cox, C. S. Lu, and R. Mohan. Bayesian adaptive randomization trial of passive scattering proton therapy and intensity-modulated photon radiotherapy for locally advanced non-small-cell lung cancer. J Clin Oncol, 36(18):1813–1822, 2018.

[75] J. A. Langendijk, P. Lambin, D. De Ruysscher, J. Widder, M. Bos, and M. Verheij. Selection of patients for radiotherapy with protons aiming at reduction of side effects: the model-based approach. Radiother Oncol, 107(3):267–73, 2013.

[76] L. B. Marks, E. D. Yorke, A. Jackson, R. K. Ten Haken, L. S. Constine, A. Eisbruch, S. M. Bentzen, J. Nam, and J. O. Deasy. Use of normal tissue complication probability models in the clinic. Int J Radiat Oncol Biol Phys, 76(3 Suppl):S10–9, 2010.

[77] Ane L. Appelt, Ivan R. Vogelius, Katherina P. Farr, Azza A. Khalil, and Soren M. Bentzen. Towards individualized dose constraints: Adjusting the QUANTEC radiation pneumonitis model for clinical risk factors. Acta Oncologica, 2014.

[78] Ada G.T.M. Egelmeer, E. Rios Velazquez, Jos M.A. de Jong, Cary Oberije, Yasmyne Geussens, Sandra Nuyts, Bernd Kremer, Derek Rietveld, C. René Leemans, Monique C. de Jong, Coen Rasch, Frank Hoebers, Jarrod Homer, Nick Slevin, Catharine West, and Philippe Lambin. Development and validation of a nomogram for prediction of survival and local control in laryngeal carcinoma patients treated with radiotherapy alone: A cohort study based on 994 patients. Radiotherapy and Oncology, 100(1):108 – 115, 2011.

[79] D. A. Bush, G. Cheek, S. Zaheer, J. Wallen, H. Mirshahidi, A. Katerelos, R. Grove, and J. D. Slater. High-dose hypofractionated proton beam radiation therapy is safe and effective for central and peripheral early-stage non-small cell

lung cancer: results of a 12-year experience at loma linda university medical center. Int J Radiat Oncol Biol Phys, 86(5):964–8, 2013.

[80] M. Hata, K. Tokuuye, K. Kagei, S. Sugahara, H. Nakayama, N. Fukumitsu, T. Hashimoto, M. Mizumoto, K. Ohara, and Y. Akine. Hypofractionated high-dose proton beam therapy for stage i non-small-cell lung cancer: preliminary results of a phase i/ii clinical study. Int J Radiat Oncol Biol Phys, 68(3):786–93, 2007.

[81] S. J. Antonia, A. Villegas, D. Daniel, D. Vicente, S. Murakami, R. Hui, T. Kurata, A. Chiappori, K. H. Lee, M. de Wit, B. C. Cho, M. Bourhaba, X. Quantin, T. Tokito, T. Mekhail, D. Planchard, Y. C. Kim, C. S. Karapetis, S. Hiret, G. Ostoros, K. Kubota, J. E. Gray, L. Paz-Ares, J. de Castro Carpeno, C. Faivre-Finn, M. Reck, J. Vansteenkiste, D. R. Spigel, C. Wadsworth, G. Melillo, M. Taboada, P. A. Dennis, M. Ozguroglu, and Pacific Investigators. Overall survival with durvalumab after chemoradiotherapy in stage iii nsclc. N Engl J Med, 379(24):2342–2350, 2018.

[82] K. A. Higgins, K. O'Connell, Y. Liu, T. W. Gillespie, M. W. McDonald, R. N. Pillai, K. R. Patel, P. R. Patel, C. G. Robinson, 2nd Simone, C. B., T. K. Owonikoko, C. P. Belani, F. R. Khuri, W. J. Curran, S. S. Ramalingam, and M. Behera. National cancer database analysis of proton versus photon radiation therapy in non-small cell lung cancer. Int J Radiat Oncol Biol Phys, 97(1):128–137, 2017.

[83] J. Y. Chang, V. Verma, M. Li, W. Zhang, R. Komaki, C. Lu, P. K. Allen, Z. Liao, J. Welsh, S. H. Lin, D. Gomez, M. Jeter, M. O'Reilly, R. X. Zhu, X. Zhang, H. Li, R. Mohan, J. V. Heymach, A. A. Vaporciyan, S. Hahn, and J. D. Cox. Proton Beam Radiotherapy and Concurrent Chemotherapy for Un-

resectable Stage III Non-Small Cell Lung Cancer: Final Results of a Phase 2 Study. JAMA Oncol, 3(8):e172032, 2017.

[84] T. Ono, T. Nakamura, H. Yamaguchi, Y. Azami, K. Takayama, M. Suzuki, H. Wada, Y. Kikuchi, M. Murakami, and K. Nemoto. Clinical results of proton beam therapy for elderly patients with non-small cell lung cancer. Radiat Oncol, 13(1):19, 2018.

[85] B. S. Hoppe, S. Flampouri, R. H. Henderson, D. Pham, A. A. Bajwa, H. D'Agostino, S. N. Huh, Z. Li, N. P. Mendenhall, and R. C. Nichols. Proton therapy with concurrent chemotherapy for non-small-cell lung cancer: technique and early results. Clin Lung Cancer, 13(5):352–8, 2012.

[86] J. Y. Chang, R. Komaki, C. Lu, H. Y. Wen, P. K. Allen, A. Tsao, M. Gillin, R. Mohan, and J. D. Cox. Phase 2 study of high-dose proton therapy with concurrent chemotherapy for unresectable stage III nonsmall cell lung cancer. Cancer, 117(20):4707–13, 2011.

[87] B. S. Hoppe, R. Henderson, D. Pham, J. D. Cury, A. Bajwa, C. G. Morris, Jr. D'Agostino, H., S. Flampouri, S. Huh, Z. Li, B. McCook, and Jr. Nichols, R. C. A Phase 2 Trial of Concurrent Chemotherapy and Proton Therapy for Stage III Non-Small Cell Lung Cancer: Results and Reflections Following Early Closure of a Single-Institution Study. Int J Radiat Oncol Biol Phys, 95(1):517–22, 2016.

[88] Q. N. Nguyen, N. B. Ly, R. Komaki, L. B. Levy, D. R. Gomez, J. Y. Chang, P. K. Allen, R. J. Mehran, C. Lu, M. Gillin, Z. Liao, and J. D. Cox. Long-term outcomes after proton therapy, with concurrent chemotherapy, for stage II-III inoperable non-small cell lung cancer. Radiother Oncol, 115(3):367–72, 2015.

[89] C. Tang, D. R. Gomez, H. Wang, L. B. Levy, Y. Zhuang, T. Xu, Q. Nguyen, R. Komaki, and Z. Liao. Association between white blood cell count following

radiation therapy with radiation pneumonitis in non-small cell lung cancer. Int J Radiat Oncol Biol Phys, 88(2):319–25, 2014.

[90] H. Harada, H. Fuji, A. Ono, H. Kenmotsu, T. Naito, H. Yamashita, H. Asakura, T. Nishimura, T. Takahashi, and S. Murayama. Dose escalation study of proton beam therapy with concurrent chemotherapy for stage III non-small cell lung cancer. Cancer Sci, 107(7):1018–21, 2016.

[91] Y. Oshiro, T. Okumura, K. Kurishima, S. Homma, M. Mizumoto, H. Ishikawa, M. Onizuka, M. Sakai, Y. Goto, N. Hizawa, Y. Sato, and H. Sakurai. High-dose concurrent chemo-proton therapy for Stage III NSCLC: preliminary results of a Phase II study. J Radiat Res, 55(5):959–65, 2014.

[92] Y. Oshiro, M. Mizumoto, T. Okumura, T. Hashimoto, N. Fukumitsu, A. Ohkawa, A. Kanemoto, H. Hashii, T. Ohno, T. Sakae, K. Tsuboi, and H. Sakurai. Results of proton beam therapy without concurrent chemotherapy for patients with unresectable stage III non-small cell lung cancer, journal = J Thorac Oncol. 7(2):370–5, 2012.

[93] Y. Hatayama, T. Nakamura, M. Suzuki, Y. Azami, T. Ono, H. Yamaguchi, Y. Hayashi, I. Tsukiyama, M. Hareyama, Y. Kikuchi, and Y. Takai. Preliminary results of proton-beam therapy for stage III non-small-cell lung cancer. Curr Oncol, 22(5):e370–5, 2015.

[94] H. Paganetti. Relative biological effectiveness (rbe) values for proton beam therapy. variations as a function of biological endpoint, dose, and linear energy transfer. Phys Med Biol, 59(22):R419–72, 2014.

[95] Geoffrey D Hugo, Elisabeth Weiss, William C Sleeman, Salim Balik, Paul J Keall, Jun Lu, and Jeffrey F Williamson. A longitudinal four-dimensional computed tomography and cone beam computed tomography dataset for image-

guided radiation therapy research in lung cancer. Med Phys, 44(2):762–771, Feb 2017.

[96] Kenneth Clark, Bruce Vendt, Kirk Smith, John Freymann, Justin Kirby, Paul Koppel, Stephen Moore, Stanley Phillips, David Maffitt, Michael Pringle, Lawrence Tarbox, and Fred Prior. The cancer imaging archive (tcia): maintaining and operating a public information repository. J Digit Imaging, 26(6):1045–57, Dec 2013.

[97] RTOG1308 protocol, version 2105/05/15. https://www.rtog.org/ClinicalTrials/ProtocolTable/StudyDetails.aspx?study=1308, 2015.

[98] T. Giaddui, W. Chen, J. Yu, L. Lin, 2nd Simone, C. B., L. Yuan, Y. U. Gong, Q. J. Wu, R. Mohan, X. Zhang, J. B. Bluett, M. Gillin, K. Moore, E. O'Meara, J. Presley, J. D. Bradley, Z. Liao, J. Galvin, and Y. Xiao. Establishing the feasibility of the dosimetric compliance criteria of rtog 1308: phase iii randomized trial comparing overall survival after photon versus proton radiochemotherapy for inoperable stage ii-iiib nsclc. Radiat Oncol, 11:66, 2016.

[99] On target: ensuring geometric accuracy in radiotherapy. https://www.rcr.ac.uk/system/files/publication/field_publication_files/BFCO%2808%295_On_target.pdf, 2008.

[100] RTOG 1106 OAR Atlas. https://www.rtog.org/CoreLab/ContouringAtlases/LungAtlas.aspx. Accessed: 2018-12-05.

[101] A. Fredriksson, A. Forsgren, and B. Hardemark. Minimax optimization for handling range and setup uncertainties in proton therapy. Med Phys, 38(3):1672–84, 2011.

[102] J. Y. Chang, X. Zhang, A. Knopf, H. Li, S. Mori, L. Dong, H. M. Lu, W. Liu, S. N. Badiyan, S. Both, A. Meijers, L. Lin, S. Flampouri, Z. Li, K. Umegaki,

2nd Simone, C. B., and X. R. Zhu. Consensus guidelines for implementing pencil-beam scanning proton therapy for thoracic malignancies on behalf of the ptcog thoracic and lymphoma subcommittee. Int J Radiat Oncol Biol Phys, 99(1):41–50, 2017.

[103] M. van Herk. Errors and margins in radiotherapy. Semin Radiat Oncol, 14(1):52–64, 2004.

[104] J. M. Bland and D. G. Altman. Statistical methods for assessing agreement between two methods of clinical measurement. Lancet, 1(8476):307–10, 1986.

[105] O. Weistrand and S. Svensson. The anaconda algorithm for deformable image registration in radiotherapy. Med Phys, 42(1):40–53, 2015.

[106] K. K. Brock, S. Mutic, T. R. McNutt, H. Li, and M. L. Kessler. Use of image registration and fusion algorithms and techniques in radiotherapy: Report of the aapm radiation therapy committee task group no. 132. Med Phys, 44(7):e43–e76, 2017.

[107] D. A. Low, W. B. Harms, S. Mutic, and J. A. Purdy. A technique for the quantitative evaluation of dose distributions. Med Phys, 25(5):656–61, 1998.

[108] Expert Panel on Detection, Evaluation, , and Treatment of High Blood Cholesterol in Adults. Executive summary of the third report of the national cholesterol education program (ncep) expert panel on detection, evaluation, and treatment of high blood cholesterol in adults (adult treatment panel iii). JAMA, 285(19):2486–2497, 2001.

[109] D. Pflugfelder, J. J. Wilkens, and U. Oelfke. Worst case optimization: a method to account for uncertainties in the optimization of intensity modulated proton therapy. Phys Med Biol, 53(6):1689–700, 2008.

[110] W. Liu, X. Zhang, Y. Li, and R. Mohan. Robust optimization of intensity modulated proton therapy. Med Phys, 39(2):1079–91, 2012.

[111] Sebastian van der Voort, Steven van de Water, Zoltán Perkó, Ben Heijmen, Danny Lathouwers, and Mischa Hoogeman. Robustness recipes for minimax robust optimization in intensity modulated proton therapy for oropharyngeal cancer patients. International Journal of Radiation Oncology*Biology*Physics, 95(1):163 – 170, 2016. Particle Therapy Special Edition.

[112] S Teoh, B George, F Fiorini, K Vallis, and F Van den Heuvel. Robustness assessment using probabilistic scenarios of intensity modulated proton therapy and volumetric arc therapy in non-small-cell lung cancer: an in-silico radiotherapy planning study. The Lancet, 389, Supplement 1:S94, 2017.

[113] S. E. McGowan, F. Albertini, S. J. Thomas, and A. J. Lomax. Defining robustness protocols: a method to include and evaluate robustness in clinical plans. Phys Med Biol, 60(7):2671–84, 2015.

[114] J. Wolfelschneider, T. Friedrich, R. Luchtenborg, K. Zink, M. Scholz, L. Dong, M. Durante, and C. Bert. Impact of fractionation and number of fields on dose homogeneity for intra-fractionally moving lung tumors using scanned carbon ion treatment. Radiother Oncol, 118(3):498–503, 2016.

[115] M. Lowe, F. Albertini, A. Aitkenhead, A. J. Lomax, and R. I. MacKay. Incorporating the effect of fractionation in the evaluation of proton plan robustness to setup errors. Phys Med Biol, 61(1):413–29, 2016.

[116] J. Gorgisyan, P. Munck Af Rosenschold, R. Perrin, G. F. Persson, M. Josipovic, M. F. Belosi, S. A. Engelholm, D. C. Weber, and A. J. Lomax. Feasibility of pencil beam scanned intensity modulated proton therapy in breath-hold for

locally advanced non-small cell lung cancer. Int J Radiat Oncol Biol Phys, 99(5):1121–1128, 2017.

[117] K. Stutzer, A. Lin, M. Kirk, and L. Lin. Superiority in robustness of multifield optimization over single-field optimization for pencil-beam proton therapy for oropharynx carcinoma: An enhanced robustness analysis. Int J Radiat Oncol Biol Phys, 99(3):738–749, 2017.

[118] MV. Mishra, S. Aggarwal, SM. Bentzen, N. Knight, MP. Mehta, and WF. Regine. Establishing evidence-based indications for proton therapy: An overview of current clinical trials. International Journal of Radiation Oncology*Biology*Physics, 97(2):228 – 235, 2017.

[119] J. Doyen, AF. Tuan, F. Floquet, J. Hérault, and JM. Hannoun-Levi. Proton beams in cancer treatments: Clinical outcomes and dosimetric comparisons with photon therapy. Cancer Treatment Reviews, 43:104 – 112, 2016.

[120] M. Soukup and M. Alber. Influence of dose engine accuracy on the optimum dose distribution in intensity-modulated proton therapy treatment plans. Phys Med Biol, 52(3):725–40, 2007.

[121] J. Schuemann, D. Giantsoudi, C. Grassberger, M. Moteabbed, C. H. Min, and H. Paganetti. Assessing the clinical impact of approximations in analytical dose calculations for proton therapy. Int J Radiat Oncol Biol Phys, 92(5):1157–1164, 2015.

[122] B. Bednarz, J. Daartz, and H. Paganetti. Dosimetric accuracy of planning and delivering small proton therapy fields. Phys Med Biol, 55(24):7425–38, 2010.

[123] L. Widesott, S. Lorentini, F. Fracchiolla, P. Farace, and M. Schwarz. Improvements in pencil beam scanning proton therapy dose calculation accuracy in

brain tumor cases with a commercial monte carlo algorithm. Phys Med Biol, 63(14):145016, 2018.

[124] Dominic Maes, Jatinder Saini, Jing Zeng, Ramesh Rengan, Tony Wong, and Stephen R. Bowen. Advanced proton beam dosimetry part ii: Monte carlo vs . pencil beam-based planning for lung cancer. Translational Lung Cancer Research, 7(2), 2018.

[125] P. Yepes, A. Adair, D. Grosshans, D. Mirkovic, F. Poenisch, U. Titt, Q. Wang, and R. Mohan. Comparison of monte carlo and analytical dose computations for intensity modulated proton therapy. Phys Med Biol, 63(4):045003, 2018.

[126] S. Teoh, F. Fiorini, B. George, K.A. Vallis, and F. Van den Heuvel. Proton vs photon: A model-based approach to patient selection for reduction of cardiac toxicity in locally advanced lung cancer. Radiotherapy and Oncology, 2019.

[127] F. Tommasino, F. Fellin, S. Lorentini, and P. Farace. Impact of dose engine algorithm in pencil beam scanning proton therapy for breast cancer. Phys Med, 50:7–12, 2018.

[128] C. Winterhalter, S. Zepter, S. Shim, G. Meier, A. Bolsi, A. Fredh, J. Hrbacek, D. Oxley, Y. Zhang, D. C. Weber, A. Lomax, and S. Safai. Evaluation of the ray-casting analytical algorithm for pencil beam scanning proton therapy. Phys Med Biol, 64(6):065021, 2019.

[129] Uwe Titt, Martin Sell, Jan Unkelbach, Mark Bangert, Dragan Mirkovic, Uwe Oelfke, and Radhe Mohan. Degradation of proton depth dose distributions attributable to microstructures in lung-equivalent material. Medical Physics, 42(11):6425–6432, 11 2015.

[130] Corinne Faivre-Finn. Dose escalation in lung cancer: have we gone full circle? The Lancet Oncology, 16(2):125–127, 2018/10/26 2015.

[131] Shawn S. Groth, Natasha M. Rueth, James S. Hodges, Elizabeth B. Habermann, Rafael S. Andrade, Jonathan D'Cunha, and Michael A. Maddaus. Conditional cancer-specific versus cardiovascular-specific survival after lobectomy for stage i non-small cell lung cancer. The Annals of Thoracic Surgery, 90(2):375 – 382, 2010.

[132] T. G. Clark, M. F. Murphy, K. Hey, M. Drury, K. K. Cheng, and P. Aveyard. Does smoking influence survival in cancer patients through effects on respiratory and vascular disease? Eur J Cancer Prev, 15(1):87–90, 2006.

[133] G. Ghobadi, S. van der Veen, B. Bartelds, R. A. de Boer, M. G. Dickinson, J. R. de Jong, H. Faber, M. Niemantsverdriet, S. Brandenburg, R. M. Berger, J. A. Langendijk, R. P. Coppes, and P. van Luijk. Physiological interaction of heart and lung in thoracic irradiation. International Journal of Radiation Oncology*Biology*Physics, 84(5):e639 – e646, 2012.

[134] E. X. Huang, A. J. Hope, P. E. Lindsay, M. Trovo, I. El Naqa, J. O. Deasy, and J. D. Bradley. Heart irradiation as a risk factor for radiation pneumonitis. Acta Oncologica, 50(1):51–60, 2011.

[135] R. Wijsman, Fjwm Dankers, E. G. C. Troost, A. L. Hoffmann, Ehfm van der Heijden, L. F. de Geus-Oei, and J. Bussink. Inclusion of incidental radiation dose to the cardiac atria and ventricles does not improve the prediction of radiation pneumonitis in advanced-stage non-small cell lung cancer patients treated with intensity modulated radiation therapy. International Journal of Radiation Oncology*Biology*Physics, 99(2):434 – 441, 2017.

[136] S. L. Tucker, Z. Liao, J. Dinh, S. X. Bian, R. Mohan, M. K. Martel, and D. R. Grosshans. Is there an impact of heart exposure on the incidence of radiation

pneumonitis? analysis of data from a large clinical cohort. Acta Oncologica, 53(5):590–596, 2014. PMID: 23992110.

[137] A. Carabe, S. Espana, C. Grassberger, and H. Paganetti. Clinical consequences of relative biological effectiveness variations in proton radiotherapy of the prostate, brain and liver. Phys Med Biol, 58(7):2103–17, 2013.

[138] M. C. Frese, J. J. Wilkens, P. E. Huber, A. D. Jensen, U. Oelfke, and Z. Taheri-Kadkhoda. Application of constant vs. variable relative biological effectiveness in treatment planning of intensity-modulated proton therapy. Int J Radiat Oncol Biol Phys, 79(1):80–8, 2011.